INTEGRATING EXPERIMENT AND THEORY IN ELECTROCHEMICAL SURFACE SCIENCE: STUDIES ON THE MOLECULAR ADSORPTION ON NOBLE-METAL ELECTRODE SURFACES BY DENSITY FUNCTIONAL THEORY, ELECTRON SPECTROSCOPY, AND ELECTROCHEMISTRY

A Dissertation

by

ALNALD CAINTIC JAVIER

Submitted to the Office of Graduate Studies of
Texas A&M University
in partial fulfillment of the requirements for the degree of

DOCTOR OF PHILOSOPHY

Chair of Committee,	Manuel P. Soriaga
Co-Chair of Committee,	Perla B. Balbuena
Committee Members,	James D. Batteas
	Sergio Capareda
	Gyula Vigh
Head of Department,	David H. Russell

August 2013

Major Subject: Chemistry

ABSTRACT

Computational techniques based on density functional theory (DFT) and experimental methods based on electrochemistry (EC), electrochemical scanning tunneling microscopy (EC-STM), and high-resolution electron energy loss spectroscopy (HREELS) were employed to study the adsorption of (i) sulfuric acid on Pd(111), (ii) benzene on Pd(111), (iii) hydroquinone/benzoquinone on Pd(111), (iv) hydroquinone sulfonate/benzoquinone sulfonate on Pd(111), (v) 2,3-dimethylhydroquinone/2,3-dimethylbenzoquinone on Pd(111) and polycrystalline Pd, (vi) hydrogen on 1-6 monolayers (ML) of Pd deposited on a Pt(111) substrate, and (vii) a thiolated iron hydrogenase model complex on polycrystalline Au.

In situ EC-STM and DFT investigations of sulfuric acid on a Pd(111) surface indicated that two layers of water molecules and hydronium ions are assembled, non-co-planar with one another, between the rows of surface-coordinated sulfate anions; the layer that is slightly elevated is composed of hydronium counter cations.

The STM images of benzene chemisorbed on a Pd(111) electrode surface were simulated and the results suggested that, when the potential of the Pd electrode is held at 0.3 V, benzene is chemisorbed on a 3-fold site; while at 0.55 V, the molecule is adsorbed on a position between a 3-fold and a 2-fold site.

Computational and experimental results implied that at low concentrations, hydroquinone sulfonate undergoes oxidative chemisorption forming benzoquinone sulfonate (BQS) on the Pd(111) surface, BQS adopts a flat orientation in which the

quinone ring is centered over a 2-fold site, and the C–H and C–S bonds are no longer co-planar with the quinone ring and are slightly tilted, directed away from the surface.

At very dilute concentrations, when hydroquinone (H_2Q) undergoes oxidative chemisorption producing benzoquinone oriented flat, albeit with a slight tilt, on the Pd(111) surface, the flat-adsorbed quinone ring is centered on a bridge site where the C_2 axis is rotated 30^o from the [110] direction of the metal substrate, the *p*-oxygen atoms are located above two-fold sites, and the ring is slightly puckered with the C–H bonds tilted away from the surface at approximately 20^o.

When 2,3-dimethylH_2Q is chemisorbed on the Pd surface, at low concentrations, 2,3-dimethylH_2Q is oxidatively chemisorbed producing 2,3-dimethyl-1,4-benzoquinone oriented flat on the surface, the flat-adsorbed rings are centered above 2-fold sites wherein the C=O bonds are pointing 30^o from the [110] direction of the substrate, the para-oxygen atoms are located above bridge sites, the peripheral bonds are tilted away from the surface at *ca.* 20^o, and at higher concentrations, oxidative chemisorption occurs through activation of the ring's C–H bonds yielding edge-oriented 2,3-dimethylH_2Q.

Electrochemistry and DFT results also implied that at 1-2 ML of Pd on Pt(111), hydrogen is only adsorbed on a hollow site while at 3 ML of Pd or more, atomic hydrogen may be chemisorbed on the 3-fold site or absorbed in the octahedral hole underneath the hollow site.

Using Au electrodes, an unbound iron hydrogenase analogue complex studied was found to slightly catalyze the H_2 evolution process. However, when the complex was immobilized unto the Au surface, the electrocatalytic activity was greatly improved.

ACKNOWLEDGMENTS

I wish to express my sincere gratitude to my research advisors, Dr. Manuel P. Soriaga and Dr. Perla B. Balbuena, for their continued guidance throughout my graduate career.

I also would like to thank my committee members, Dr. James D. Batteas, Dr. Sergio Capareda, Dr. Christian Hilty, and Dr. Gyula Vigh, for their aid and valuable comments.

I am forever grateful to all former members of Dr. Soriaga's research group, Juan, Kyle, Akhtar, Ding, Jack, Jean, and Joy for their advice, mentoring, and friendship.

I would like to acknowledge Dr. Lisa Perez and the Laboratory for Molecular Simulation (LMS) for all the countless calculations.

I really appreciate all the joy and laughter from my friends in College Station that made my time at Texas A&M an unforgettable experience.

I am greatly indebted to my wife, Jesselyn, and to my family not only for their unwavering love and support but for their encouragement and prayers as well.

TABLE OF CONTENTS

Page

LIST OF FIGURES

Page

LIST OF TABLES

Page

1. INTRODUCTION

Noble metals have been found to have unique properties such as resistance to bulk oxidation and high catalytic activity on various heterogeneous reactions [1-3]. Surfaces of such metals allow certain industrially significant chemical reactions to occur. Hence, they are used in various technological applications such as in fuel cells, petroleum processing, electrocatalysis, electronics, batteries, and chemical synthesis.

Studying palladium, a noble metal, is a very interesting realm because of the metal's unique properties such as the ability to adsorb and absorb hydrogen [4,5] and the capacity to form chemical bonds with adsorbed molecules due to its anomalously weak intermetallic bonds [6]. These properties provide great interest from various scientists whose aims are to utilize and manipulate these functions for a wide array of novel applications.

Palladium has also been known for its catalytic properties. A good metal catalyst must have considerable interaction with reactant molecules. Since Pd has low dissociation and atomization enthalpies, it has weak Pd-Pd bonds making it interact more with the solution species [2,7].

Gold is also used as a heterogeneous catalyst. Generally, although its catalytic activity is not as prominent as those of Pd and Pt, it is the most inert among the noble metals and is the most resistant against corrosion and catalyst poisoning. At certain reactions though (i.e. oxygen reduction in alkaline media), Au is the better catalyst [8].

1.1 Modification of Interfacial Properties

The interaction between molecules and metal surfaces is very important in the field of surface science because this dictates the physical and chemical properties of the interface [2,9] and the product distributions of electrocatalytic reactions of these molecules [10]. The presence of molecules on surfaces alters the properties of the interface, which becomes the basis for the functionalization of electrode and nanoparticle surfaces.

Alloy formation, which involves fusing two or more metals together, is also a different way of altering the properties of a metal surface. This method is accomplished by electrodeposition and thermal treatment [11,12]. Oftentimes, the resulting properties of the surface manifest hybrid features of the components or unique attributes not observed in the constituent metals.

Another way of modifying surface properties is the formation of ultrathin films. In contrast to classical thin films, which have micrometer thickness, ultrathin films correspond to a single to several atomic layers or full monolayer (ML) coverages with thickness in the order of Å to a few nm. The number of studies involving ultrathin films is increasing due to the possibility of modifying these films into nanometer-scale structures that manifest size-dependent functions [13,14].

Systematic introduction of various elements onto the surfaces of metal catalysts is used in a combinatorial method in discovering promising bimetallic catalysts and in understanding the reason behind such catalytic performance or modification thereof [15]. Hence, a multitude of metals have been deposited on platinum-group metal surfaces with

aims such as (i) finding the ideal electrode for fuel cells [16,17], (ii) discovering novel materials for advanced applications [18-20], and (iii) understanding the electrocatalytic process [21,22].

In this study, the adsorption of various molecular and ionic species on Pd(111) surfaces, ultrathin Pd films deposited on Pt(111) surfaces, and complexes immobilized on polycrystalline Au surfaces were investigated.

1.2 Adsorption on Noble-Metal Surfaces

Knowledge of the electrode/solution interfacial chemistry is very important because this is the basis for our understanding on heterogeneous reactions and other processes, which find various applications such as in electrocatalysis, corrosion, fuel cells, batteries, sensors, and synthesis [2]. In this realm, it is worthwhile to study the adsorption of different species on metal surfaces to gain various insights of the processes that occur on the surface.

In this work, the structures of ionic and molecular species adsorbed on metal surfaces are investigated since this is an essential step in gaining knowledge or elucidating mechanisms of various interfacial processes or reactions and in determining structure-composition-function relationships. For instance, the degree of anodic oxidation of chemisorbed molecules was observed to be strongly dependent on their initial structural orientation on the metal surface [23].

1.3 Sulfuric Acid on Pd(111)

The role of electrolyte anions in reactions that occur at the electrode surface is of great importance in electrochemical surface science. The observation that the current-potential curve of Pt(111) with perchloric acid as the supporting electrolyte is noticeably different than that with sulfuric acid is a familiar example [24].

The extensive use of sulfuric acid as an "inert" supporting electrolyte has led to various studies on its interaction with the noble-metal electrodes [24-36]. A number of experimental methods that included electrochemical scanning tunneling microscopy (EC-STM), cyclic voltammetry (CV), chronocoulometry, radiotracer measurements and optical spectroscopy have been used; computational techniques were also employed. Although results from different studies on the interfacial coverages and reactivities agree well with one another, the nature, identity, or structure of the adsorbed anion has not been unambiguously established. Essential concepts from inorganic chemistry were used to make a case that only sulfate ions would exist on the electrode surface: if HSO_4^- were surface-coordinated through the oxygen electron lone pairs, the inductive effect due to the pull of electron density away from the sulfur atom and towards the more electronegative coordinated-oxygen atoms weakens the O–H bond since the decreased negative-charge density on sulfur would withdraw electron density from the O–H functional group [24]. As a result, when HSO_4^- binds to a transition-metal center, whether in homogeneous or heterogeneous complexes, the enhanced acidity of the O–H group will most likely produce SO_4^{2-} anions in the compact layer or coordination sphere.

In an earlier study, electrochemical STM studies on the interfacial structure of a Pd(111) electrode surface in 0.05 M H_2SO_4 revealed that when the Pd electrode is immersed in a dilute sulfuric acid solution, a well-ordered ($\sqrt{3} \times \sqrt{7}$) adlattice is formed on the Pd(111) surface [24]. This interfacial structure is similar to those found in EC-STM investigations on Au(111) [25,26], Pt(111) [27,28], Rh(111) [29], Cu(111) [30-33], and Ir(111) [34,35] in dilute sulfuric acid solutions. The STM images showed rows of bright spots, which are believed to be the adsorbed anions, and dim rows, which are formed from the hydrogen-bonded chains of water molecules [26,29,33,34] and hydronium cations [24,27,28,35,36].

Examination of the STM images showed essential structural information: (i) the adsorbed sulfate is trigonally coordinated on the Pd(111) surface in such a way that the ion is directly above a 3-fold hollow site, and (ii) two layers of water molecules and hydronium cations are formed between the anionic rows and the layers, however, are not co-planar. Two real-space structures were proposed; however, EC-STM was not able to ascertain which of the two geometries is the actual structure. It was in this regard that the EC-STM results have been revisited and computationally examined.

The two aims in the investigation were to determine (i) the nature or structure of the two co-adsorbed but non-co-planar layers of water molecules and hydronium cations, and (ii) the most probable structure of the interfacial ensemble. The computational work was based on density functional theory (DFT). The dissection of structural nuances was achieved by geometry-optimization calculations. The identification of the most favorable

real-space structure was accomplished by total-energy calculations and STM-image simulations.

1.4 Benzene on Pd(111)

In electrochemical surface science, it is of great significance to identify the structure of molecules chemisorbed on electrocatalyst surfaces. A surface-sensitive method that can be employed for this purpose is EC-STM. However, interpretation of STM images is not straightforward since these images do not always unambiguously reveal the actual positions of the atoms; instead, the electronic states on the surface near the substrate Fermi energy level are displayed [37]. Fortunately, STM profiles can be calculated or simulated by computational techniques such as those based on DFT. By comparing experimental and computational STM results, elucidation and identification of certain structural attributes such as adsorbate orientation and adsorption site can be attained.

The chemisorption of aromatic molecules such as benzene on Pt(111) surfaces has been investigated by STM. The images of benzene molecules on the metal surface were found to be dependent on the molecular adsorption site [38]. With the aid of STM-image simulation based on the electron scattering quantum chemical (ESQC) method, the following results were obtained: (i) when benzene is chemisorbed parallel to the surface at a 3-fold hollow site, the molecule appears to be triangular with three lobes at each vertex of the triangle; (ii) if the molecule is centered on a 2-fold bridge site, the molecular images appear to be a single elongated bump; and (iii) a ring-like structure

with six lobes is observed only when the center of the molecule (C_6 axis) is on an atop site [37,39,40].

Simulation of STM profiles of benzene chemisorbed on Pd(111) surfaces has also been done previously [41]. In that theoretical study, extended Hückel molecular orbital theory (EHT) was used in the calculations. The resulting images were found to be similar with those obtained with Pt(111) [37,39,40].

Several EC-STM images in a previous work showed benzene adsorbed, at certain potentials, on Pd(111) electrode surfaces [42]. The resulting images suggested that, when the potential of the Pd electrode is held at 0.3 V (vs. RHE), benzene is chemisorbed or centered on a hollow site in a Pd(111)-(3×3)-C_6H_6 adlattice. However, at 0.55 V (vs. RHE), the aromatic molecule is located on a spot between a 3-fold hollow and a 2-fold bridge site as a Pd(111)-c(2√3×3)-*rect*-C_6H_6 adlayer. To confirm these scenarios, STM profiles of benzene at various adsorption sites on a Pd(111) surface were simulated or calculated using DFT and the computational results were then compared with the experimental images [42].

1.5 Hydroquinone Sulfonate and Benzoquinone Sulfonate on Pd(111)

Previous investigations based on the combination of electrochemistry (EC), high-resolution electron-energy loss spectroscopy (HREELS), Auger electron spectroscopy (AES) and STM studied the chemisorption of substituted *p*-diphenols from aqueous solutions unto well-defined Pd(111) and Pd(100) electrode surfaces [43,44]. The EC and HREELS measurements revealed that at very dilute concentrations, whether the solution

initially contained the diphenol or its oxidized (quinone) form, the species ultimately present on the surface was the quinone. For instance, when 1,4-dihydroxybenzene (hydroquinone, H_2Q) was chemisorbed on Pt surfaces, it underwent oxidation producing benzoquinone (Q) on the interface; identical HREELS spectra were observed for both species. 2,5-Dihydroxybenzenesulfonate (hydroquinone sulfonate, H_2QS) was later explored and consistent with earlier studies on unsubstituted diphenols, it was likewise indicated from HREELS spectra that H_2QS underwent oxidative chemisorption forming benzoquinone sulfonate (BQS).

An EC-STM experiment was also undertaken for H_2QS/BQS [43,44]. At 0.1 mM, the flat orientation of the quinone group was evident on the images and indicated a surface chemical bond that involves the π-electron system of the quinone double bonds. A *completely* parallel orientation would, however, be hindered by the presence of the bulky sulfonate group so a slight tilt was surmised on the molecule. A possibility also exists that, in the chemisorbed state, the quinone ring may undergo slight distortions such that the peripheral (C–S, C–S and C–O) bonds are no longer co-planar with the quinone moiety.

Based from the EC-STM images, two real-space structures of the adlattice were proposed. Unfortunately, it was not possible to determine which of the two probable geometries is the actual one from EC-STM images only.

To aid in resolving the issues as to (i) whether or not the quinone ring undergoes distortions from planarity, and (ii) which of the two probable arrangements is more stable or favorable, insights from computational studies would definitely be beneficial. It

is in this context that this computational work, based on DFT, was undertaken.

Density functional calculations have been employed to study the adsorption geometries of various aromatic compounds on different metal surfaces [45-48]. In some studies, computations were used to validate assertions or resolve conflicting ideas that arise from different experimental measurements. The chemisorption of benzene on Pt(111), Pd(111) and Rh(111) surfaces has therefore been investigated by first-principles DFT; the results from the energy calculations were then correlated with measurements from a host of surface-characterization methods such as infrared absorption-reflection spectroscopy (IRAS), HREELS, low-energy electron diffraction (LEED) and STM [47,48]. In this research, DFT calculations were similarly employed not only to optimize the adsorbed-molecule structure of BQS on Pd(111) but also to ascertain which of the possible adsorption sites would be most favored.

1.6 Hydroquinone and Benzoquinone on Pd(111)

Direct interaction between the electrode surface and the organic molecule always occurs during electrocatalytic processes. Thus, if substantial advances are to be obtained in fuel-cell and other related technologies or applications that depend on electrochemical catalysis, the nature of such interactions must be well-understood [3,49-50]. It is for this purpose that the structure, composition, and reactivity of a wide variety of organic molecules at well-defined noble-metal electrode surfaces are explored [23,42-44,51-53]. Studies on the chemisorption of diphenols on Pd(*hkl*) surfaces based on EC, HREELS, and EC-STM were described earlier [23,42-44,51-53] and revealed that, when a well-

defined Pd(111) electrode is immersed in a dilute aqueous solution of hydroquinone (H_2Q), an immediate chemisorption reaction occurs in which the surface-coordinated H_2Q molecule undergoes spontaneous oxidation to benzoquinone (Q) on the Pd surface [23,51] and forms a Pd(111)-(3 x 3)-Q adlayer structure. Detailed analysis of the EC-STM measurements implied that, when Q is chemisorbed parallel to the Pd(111) surface: (i) it adopts an essentially flat orientation *albeit* with a slight tilt, and (ii) the quinone ring is centered on a two-fold bridge site with two possible structures. Unfortunately, it was not possible to identify from the EC-STM images alone which of the two probable geometries is the actual structure.

In this work, DFT total-energy calculations were utilized to determine the most plausible interfacial structure of the Pd(111)-(3 × 3)-Q adlayer. In addition, surface-vibrational frequencies of the chemisorbed Q was calculated by DFT and comparison of the calculated results with the experimental HREELS data helped (i) ascertain the geometry of the chemisorbed molecule, and (ii) determine which of the two structures proposed is more probable.

1.7 2,3-Dimethyhydroquinone and 2,3-Dimethylbenzoquinone on Pd(111)

Fundamental studies exploring organic compounds chemisorbed on electrode surfaces are very important because the presence of these molecules alters the chemical properties of the metal surface [2,9] especially in electrocatalysis [10]. Even the adsorbed-molecule orientation affects certain electrocatalytic reactions [23].

Thin-layer electrochemistry (TLE) was earlier used to identify the orientation of chemisorbed hydroquinone (H_2Q) and benzoquinone (Q) on smooth polycrystalline palladium electrodes [23]. By determining the coverage or the surface concentration (Γ) of the chemisorbed molecule, the molecular cross section (σ) can be approximated. Comparison of the measured molecular cross sections with the calculated surface area occupied by a single adsorbed molecule for each possible orientation led to the identification of the adsorbed-molecule orientation. That investigation suggested that at low aqueous-solution concentrations, H_2Q is chemisorbed oxidatively yielding surface-coordinated benzoquinone with an orientation parallel to the surface (η^6-Q) and at high concentrations, oxidative chemisorption generates edge-oriented diphenolic species (η^2). This orientational transition is evident on the TLE-generated chemisorption isotherm, which shows a change of coverage (Γ) at various solution concentrations. In a separate report, high-resolution electron energy loss spectroscopy (HREELS) was used to generate a chemisorption isotherm by plotting the normalized C–H bending vibrational peak intensity as a function of quinone concentration [5]. The resulting isotherm resembled that of TLE; hence, both HREELS and TLE indicate an orientational transition of the quinone molecule from parallel to the surface at low concentrations to edgewise or perpendicular to the surface at high concentrations. To ascertain this behavior on 2,3-dimethylhydroquinone on Pd, this work was conducted.

Experimental HREELS and electrochemical scanning tunneling microscopy (EC-STM) together with computational results based on density functional theory (DFT) can be used to determine the adsorbed-molecule structure of aromatic compounds on the

Pd(111) surface. Hence, TLE, HREELS, and DFT were employed in this investigation to identify the structure of 2,3-dimethylhydroquinone chemisorbed on Pd surfaces at various aqueous-solution concentrations. In particular, the experimental cross section of the chemisorbed molecule on the Pd surface at various concentrations was determined from the TLE- and HREELS-generated chemisorption isotherms and was compared to the calculated molecular cross sections at various orientations on the surface to identify the molecular orientation. Computational vibrational spectra from DFT were obtained and compared with the experimental HREELS spectra to ascertain the molecular orientation on the surface. DFT total-energy calculations were also performed to identify the most plausible adsorption geometry and site.

1.8 Hydrogen on Ultrathin Pd Films Deposited on Pt(111)

Electrochemistry (EC) was used to deposit and characterize ultrathin Pd films, from submonolayer to multilayer coverages, unto well-defined Pt(111) surfaces [54]. In the EC measurements, underpotential deposition of hydrogen (H_{UPD}) is notably a thin-film phenomenon because for bulk Pd, the high hydrogen uptake makes adsorption indistinguishable from absorption. Hence, H_{UPD} peaks in voltammetric scans are only visible when a thin Pd film is used instead of bulk Pd. The emergence of bulk-like properties of the films was identified by the disappearance of the voltammetric H_{UPD} desorption-adsorption peaks for the surface terrace sites. The earlier experimental results indicated that the Pd films begin to show bulk-like properties at 3 ML after EC annealing.

To ascertain the ultrathin-film-to-bulk transition of Pd electrodeposited on Pt(111) substrates, insights from computational studies are indeed important. In this regard, the current computational work based on density functional theory (DFT) was conducted.

Density functional theory has been used extensively to study the adsorption or absorption of different molecules on Pd and Pt surfaces [55-60]. In this research, DFT was also used to optimize the adsorption or absorption structure of H on Pd deposited on a Pt(111) substrate, calculate the adsorption or absorption energies, and determine the most stable site for atomic hydrogen on the surface by comparing the calculated energies.

1.9 Iron Hydrogenase Model Complex on Au

Dinuclear iron complexes (μ-pdt)[$Fe(CO)_2L]_2$ (pdt = $–SCH_2CH_2CH_2S–$; L = PMe_3, $CN^–$, and CO), which are structural and functional analogues of iron hydrogenase, have been found to act as electrocatalysts for the production of H_2 [61-64]. If these complexes can be chemisorbed unto metal surfaces, changes in electrocatalytic activity between free and immobilized species can be studied.

Compounds containing thiol functional groups are among the many types of molecules that are easily chemisorbed on metal surfaces especially on Au surfaces since these compounds readily form –S– bonds to Au and produce self-assembled monolayers (SAM) on Au surfaces [65]. Therefore, if the iron hydrogenase analogues are thiolated,

these complexes can be attached on Au surfaces and consequently be used as surface-modified electrodes.

The electrochemistry of (μ-pdt)[$Fe(CO)_3$][$Fe(CO)_2L$] (pdt = –$SCH_2CH_2CH_2S$–; L = $P(Ph)_3$) iron hydrogenase model complex using a glassy carbon electrode and acetic acid (HOAc) as the proton source has been investigated previously [66]. Electrochemical responses characteristic of electrocatalysis were observed at very negative potentials at –2.05 V (vs. Fc/Fc^+). Similar to other iron hydrogenase analogues, there were two reduction processes that occur during the negative potential scan: $Fe^IFe^I \rightarrow Fe^IFe^0$ and $Fe^IFe^0 \rightarrow Fe^0Fe^0$. Although the former process was not catalytically active, hydrogen gas was produced catalytically on the latter process [61-64,66].

To evaluate the electrocatalysis of H_2 formation by the (μ-pdt)[$Fe(CO)_3$][$Fe(CO)_2L$] (pdt = –$SCH_2CH_2CH_2S$–; L = $P(Ph)_3$) complex (**I**) using Au electrodes, this study was carried out. In addition, the effect of immobilizing the complex on the Au surface using (μ-pdt)[$Fe(CO)_3$][$Fe(CO)_2L$] (pdt = –$SCH_2CH_2CH_2S$–; L = $P(Ph)_2CH_2CH_2SH$) (**II**) through a thiol functional group on electrocatalysis was investigated.

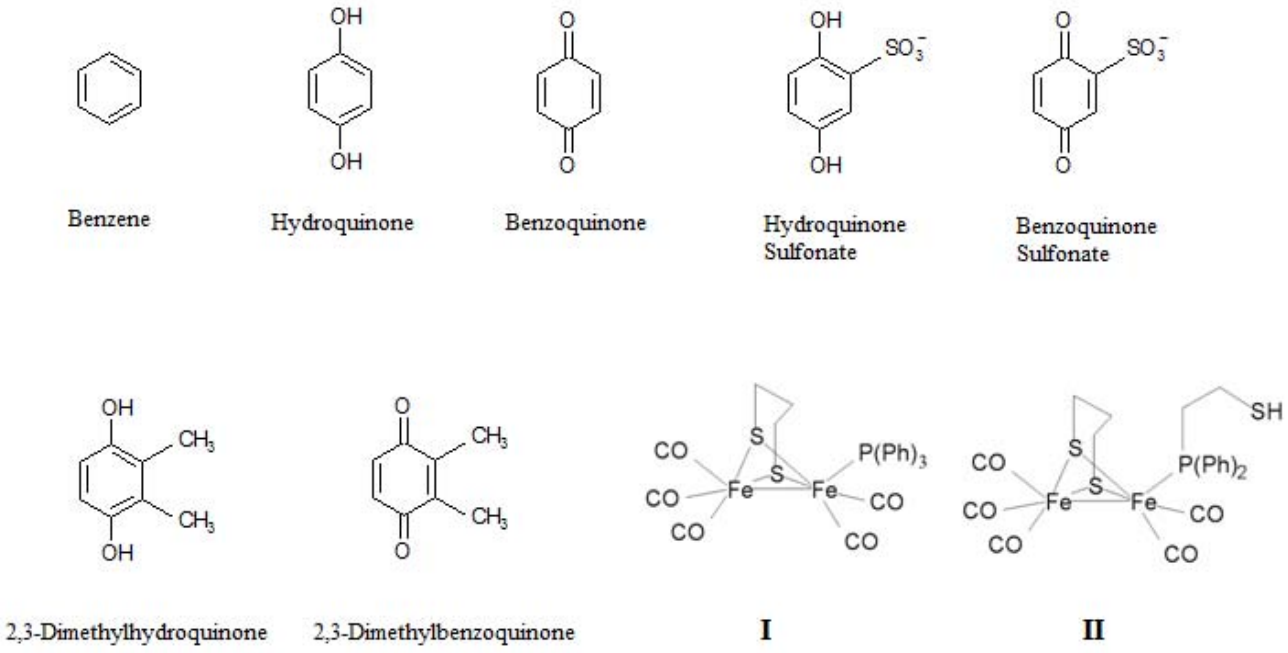

Figure 1. Structures of the compounds investigated in the study.

1.10 Objectives

The study mainly aimed to investigate the adsorption of various compounds on noble-metal surfaces using computational techniques based on DFT and experimental methods such as EC, EC-STM, AES, LEED, and HREELS in an attempt to determine structure, composition, and reactivity relationships that provide significant advancement of surface science concepts for a variety of technological applications. Specifically, this work intended to:

(i) determine the structure of the interfacial ensemble of the Pd(111) surface immersed in a sulfuric acid solution,

(ii) identify the adsorption site of benzene on the Pd(111) surface held at certain potentials,

(iii) ascertain the adsorption structure and site of hydroquinone sulfonate chemisorbed on the Pd(111) surface,

(iv) confirm the adsorption site and structure of hydroquinone on a Pd(111) surface,

(v) elucidate the adsorbed molecular structure and site of 2,3-dimethylhydroquinone chemisorbed on Pd(111) surfaces at various concentrations,

(vi) determine the adsorption site of atomic hydrogen on 1-6 ML of Pd deposited on a Pt(111) substrate and validate thin-film-to-bulk transition of Pd ultrathin films, and

(vii) evaluate the electrocatalysis of H_2 production by unadsorbed and chemisorbed (immobilized) iron hydrogenase model complexes on polycrystalline Au surfaces.

2. METHODOLOGY

2.1 Density Functional Theory

Aside from first-principles (ab initio) methods, density functional theory (DFT) is also an alternative way in solving the time-independent Schrödinger equation $\hat{H}\psi = E\psi$. Instead of decomposing the true wave function of a system into various single electron wave functions, which may lead into a huge number of variables and a multitude of parameters that must be optimized for the ab initio methods, DFT simplifies this problem by approximating the ground-state electron density (ρ) in the Hohenberg-Kohn formulation to solve the approximate ground-state wave function, molecular energy, and all the other properties of the system [67].

The Thomas Fermi (TF) theory was the first concept to calculate the electronic energy from electron density distributions. It provided equations involving interacting electrons moving in an external potential (υ) and relates υ with electron density (ρ). However, it did not predict bonding in molecules and in this theory, it was uncertain if there really is a definite relation between the density distribution and the potential. This problem was solved using the concepts by Hohenberg and Kohn, which imply that the external potential (υ) of a system of interacting electrons is determined uniquely by the ground-state electron density (ρ) and thus suggest that all properties of a system derived from solving the Schrödinger equation can be determined using ρ [68].

Since the external potential is dependent on a number of variables such as atomic positions and lattice parameters, minimization of the system's energy with respect to

these variables gives ground-state molecular structures or geometries, lattice constants, and etc. By studying the change in energy as a function of these variables, phonon spectra and vibrational frequencies can also be calculated. Furthermore, comparing the total energies of molecules with those of their constituent atoms yields dissociation energies.

The total energy of the system can therefore be calculated from the electron density distribution and this energy can be minimized to determine the ground-state energy and wave function. Thus, the ground-state total energy (E_t) may be expressed as:

$$E_t[\rho] = T[\rho] + U[\rho] + V[\rho] + E_{XC}[\rho] \quad (1)$$

where $T[\rho]$ is the kinetic energy from non-interacting particles, $U[\rho]$ is the potential energy from Coulombic interactions, $V[\rho]$ is the potential energy from an external potential (υ), and $E_{XC}[\rho]$ is the exchange and correlation energy arising from many-body contributions [69,70]. The Kohn-Sham approach introduces unique single-particle wave functions to treat the various energy terms and ultimately calculates the energies by solving the Kohn-Sham equations self-consistently [71].

The total kinetic energy ($T[\rho]$) is simply the sum of the kinetic energies of the non-interacting particles. The potential energy arising from electronic interactions, $U[\rho]$, can be approximated by the Hartree energy or the classical electrostatic interaction. The external potential (υ), the basis for $V[\rho]$, is derived from the electrostatic potential of the nuclei that is treated to be fixed in space according to the Born-Oppenheimer approximation. Lastly, the exchange-correlation energy ($E_{XC}[\rho]$) is composed of the kinetic correlation energy (the difference in the kinetic energy for the molecule and the

reference system of non-interacting particles), exchange energy (the energy lowering due to the antisymmetry requirement such as the tendency of same-spin electrons to avoid each other), correlation energy (the lowering in energy associated with the repulsion of interacting electrons), and the self-interaction correction (SIC) since an electron does not interact with itself [67].

The total energy can only be calculated or minimized once a suitable approximation for $E_{XC}[\rho]$ can be obtained. The local density approximation (LDA) estimates this exchange-correlation energy term by assuming that the electron density varies slowly with position and apply locally the results for a homogeneous system to a non-homogeneous system. This approximation is based on the uniform-electron-gas model and is only appropriate for systems where the density distribution varies slowly with position. The generalized gradient approximation (GGA) is a huge improvement in which it accounts for the variation in ρ with position. Some of the widely used GGAs are the Perdew-Wang (PW), Perdew-Burke-Ernzerhof (PBE), and the Becke-Lee-Yang-Parr (BLYP) exchange and correlation functionals [67].

Generally, GGAs only depend on the electron density and its first derivatives (with respect to position). Another way to improve this approximation is to utilize functionals that also depend on second derivatives of ρ and on a term called kinetic-energy density. These new improvements led to meta-GGA and hybrid functionals, which are commonly used today. Some of the more popular functionals used in this category are the B3LYP and B3PW91 [67].

2.1.1 *Computational Method*

The Cambridge Sequential Total Energy Package (CASTEP), a DFT code in the Material Studio 5.0 computational software distributed by Accelrys Inc., was used in all computations [72]. The generalized gradient approximation (GGA) [73] and the Perdew-Wang exchange-correlation functional, PW91 [74], were used to approximate contributions from exchange and correlation effects. The single-particle wave functions were obtained from the plane-wave basis set and norm-conserving pseudopotentials were employed to represent the periodic system and to perform calculations at lower cutoff energies.

In various commercial simulation modules, knowing the derivative of the total energy (E_t) with respect to changes in geometry is essential since it permits one to identify the structure with the lowest energy during geometry optimization calculations. This would therefore allow the determination of the most probable or the actual chemical structure.

During structural optimization, the cutoff energy was set to 300-450 eV and the energy minimization algorithm was chosen to be the Broyden-Fletcher-Goldfarb-Shanno (BFGS) method. The Monkhorst-Pack grid (k-point set) and Fermi smearing were selected to be 3 × 3 × 1 and 0.1 eV, respectively. As the criteria for convergence, the tolerance in energy, force, and displacement were 1.0 x 10^{-5} eV/atom, 0.03 eV/Å, and 0.001 Å, respectively. These parameters were sufficient enough in obtaining a reasonable convergence in the computation for the total energy and the determination of the optimized structure [46,47].

In order to model the various adsorption structures, applicable supercells (i.e. 1 x 1, 3 x 3 or 5 x 5) were used in the computations. The (111) metal surfaces were represented by a metal slab consisting of layers of Pd or Pt atoms and only the upper two layers were allowed to relax. A vacuum space of *ca.* 15 Å was placed to isolate the metal surface vertically from its periodic images[20] and the adsorbed species were positioned in this vacuum space. The slab model was utilized instead of the cluster model since the former solves many of the difficulties encountered by the latter (i.e. maintaining the symmetry of the crystal surface) [75,76].

The adsorption energy (E_{ads}) is calculated to determine the relative stabilities of the adsorption structures and is defined as:

$$E_{ads} = E_{M\text{-}A} - E_A - E_M \qquad (2)$$

where $E_{M\text{-}A}$, E_A and E_M represent the total energies of the interfacial system where the species are adsorbed on the metal surface, the unadsorbed species, and the clean (111) metal surface, respectively. It can be inferred that the lower (more negative) the adsorption energy, the stronger (more stable) the adsorption.

Frequencies from various molecular vibrational modes can be calculated from the Hessian matrix (matrix of Cartesian second derivatives) of a molecular or periodic system [77]. In this work, the finite displacement method was used in calculating the vibrational frequencies and in determining the vibrational modes in the interfacial system.

To simulate scanning tunneling microscopy (STM) images, DFT was used to calculate the energy levels of the system and the Tersoff-Hamann method [78] was

utilized to show a 2D plot of the electron density isosurface, which corresponds to the surface local density of states (LDOS), produced by certain electronic states at a particular energy relative to the Fermi energy level. In an actual experiment, the energy difference relative to the Fermi level is controlled by the bias applied on the STM tip. In these simulations, a theoretical tip bias can be applied to display the LDOS and hence obtain a simulated STM image. A hypothetical tip potential of approximately 0.100 V was employed to reproduce the conditions used in the actual EC-STM experiments.

2.2 Ultrahigh Vacuum (UHV) Surface Analysis

Most molecular-level studies on species adsorbed on metal surfaces prefer the use of single crystal surfaces as substrates to fully elucidate the interfacial structure and understand the resulting properties. However, before any experiment can be performed on the surface, the initial structure and composition must be determined or well-defined. This would allow a direct comparison between modified and unmodified surfaces and would aid in understanding various processes or properties of the interface. Surface investigations are accomplished by utilizing electron spectroscopy that uses electrons to probe the surface. The penetration depth of the incident low-energy electrons can easily be modified such that only the topmost surface layer can be examined. This leads to an increased surface sensitivity of the techniques. Based from the Universal Curve proposed by Seah and Dench as presented in Figure 2, by changing the electron beam energy, the inelastic mean free path of the electrons can be altered; hence, the region from the surface to be studied can be controlled [2].

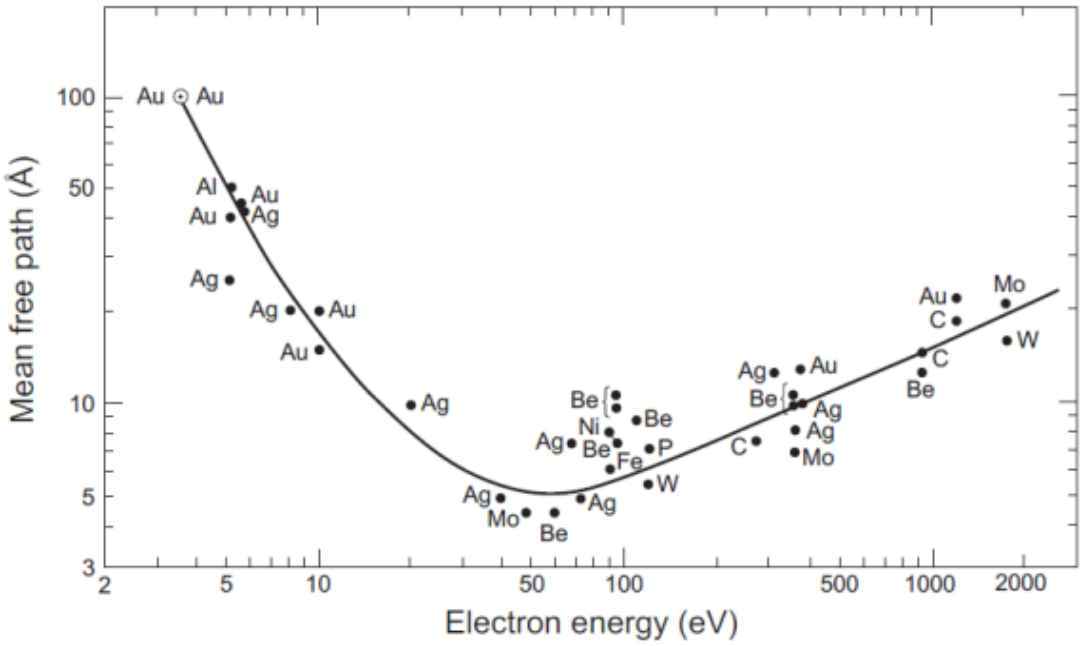

Figure 2. The "Universal Curve" of electron mean free path in solids as a function of electron kinetic energy [2]. This figure is reproduced with permission from G.A. Somorjai, Y. Li, Introduction to Surface Chemistry and Catalysis, Wiley, New York, New York, 2010. Copyright John Wiley & Sons, Inc.

The experiments must also be done at an ultrahigh vacuum (UHV) environment to guarantee that the signals represent those only from the surface and not from processes due to electronic collisions with gaseous species in the atmosphere after the electrons escape from the surface [2].

Pressures used in UHV experiments generally are $\leq 10^{-9}$ torr. These conditions substantially increase the mean free path of residual gases in the system to minimize collisions with electrons used to study the surface as well as decrease the rate at which the surface is bombarded with these gases. Even under high-vacuum conditions ($\sim 10^{-6}$ torr), a "clean" surface would immediately be covered by species from residual gases in the system. For example, at 300 K, it takes approximately 2.6 s to form a monolayer of CO on a metal surface at 10^{-6} torr while 7.3 hours is needed to produce such a layer at 10^{-9} torr [79].

All surface science techniques used in the experimental portion of the study are discussed in the following sections.

2.2.1 *Low Energy Electron Diffraction (LEED)*

Low energy electron diffraction (LEED) is generally used to determine the long-range surface order of single-crystal surfaces or probe the two-dimensional surface lattice. This technique relies on the elastic backscattering of electrons and the interference of these electrons is based on the de Broglie equation $\lambda = h/mv$. Constructive interference occurs if the path differences of scattered waves from adjacent lattice points are multiples of λ [79].

The interference of the elastically scattered electrons causes the intensity to rely on the electron energy and direction. Identification of the directions of the interference maxima is fulfilled by inspecting the LEED pattern. Eventually, application of the simple geometric theory of diffraction to the pattern gives the dimension of the unit cell of the periodic structure at the surface [79].

All LEED experiments were done using the PE 15-120 LEED Optics and PE 11-020 LEED Electronics system (Perkin-Elmer, Eden Prairie, MN). Figure 3 presents a schematic diagram of a LEED display system. The electron gun directs a monoenergetic electron beam to the grounded single-crystal electrode. The diffracted electrons are then backscattered unto the concentric grids. In this process, the grids are biased such that only the elastically backscattered electrons are able to reach the fluorescent collector screen.

The diffraction pattern from LEED such as that presented in Figure 4 corresponds directly to the reciprocal-space lattice of the surface. Employment of the geometrical theory of diffraction yields the real-space lattice dimensions of the surface [79].

Aside from the determination of the lattice structure of the surface, LEED patterns are also useful in qualitatively identifying the overall surface morphology. For instance, a diffuse background would imply a disordered adlayer while the presence of sharp signals would indicate large ordered surface domains [80].

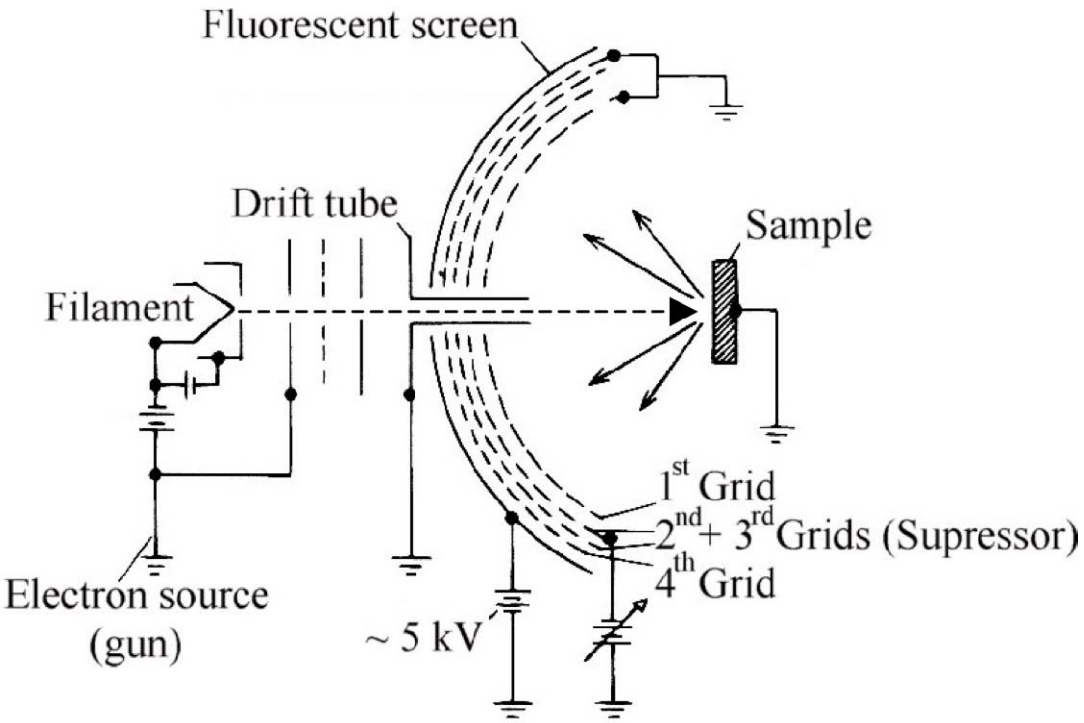

Figure 3. Schematic diagram of a LEED display system [79]. This figure is reproduced with permission from G. Ertl, J. Kuppers, Low Energy Electrons and Surface Chemistry, VCH, Boca Raton, Florida, 1985. Copyright Wiley-VCH Verlag GmbH & Co. KGaA.

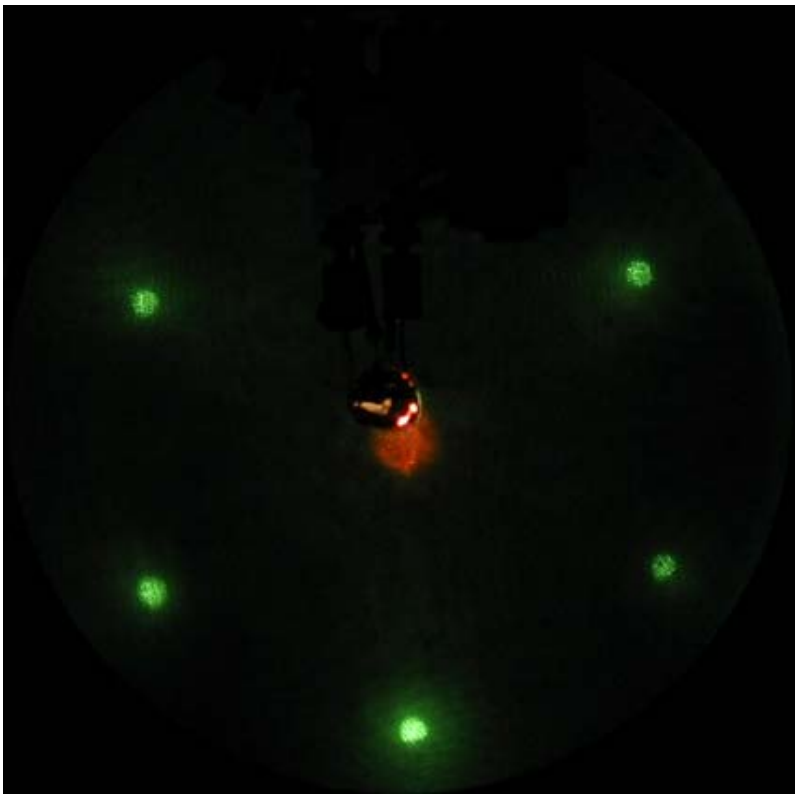

Figure 4. LEED pattern of a clean well-ordered Pd(111) single-crystal surface.

After the pressure was brought down to UHV levels and the crystal positioned opposite the fluorescent screen, the LEED measurements were conducted with a beam current of 2 μA above the background to obtain the images.

2.2.2 *Auger Electron Spectroscopy (AES)*

When an inner core electron is excited and ejected from the atom, the electronic ground state can be achieved through one of the two following processes as presented in Figure 5: (i) an electron in a higher energy level relaxes unto the core "hole" thereby releasing energy as a photoemitted x-ray radiation and (ii) when the core "hole" is filled by the upper-level electron, the energy released ejects another electron with a kinetic energy characteristic to the particular atom in a radiationless process called Auger effect [79].

Using the KLL transition shown in Figure 5 as an example, the kinetic energy of the ejected electron called the Auger electron can be calculated by:

$$E_{Kin} = [E_K - E_{LI}] - E_{LIII} - \varphi \qquad (3)$$

where $[E_K - E_{LI}]$ represents the energy released as the L_I-shell electron relaxes unto the K-shell core "hole" or the energy available to eject the Auger electron, E_{LIII} corresponds to the binding energy of the electron to be ejected at the L_{III} shell, and φ is the work function of the instrument. Both E_{LIII} and φ correspond to the total energy required for the electron to be ejected into the vacuum.

Auger electron spectroscopy (AES) can therefore be used to determine the elemental composition of various surfaces since the kinetic energy of the Auger electron

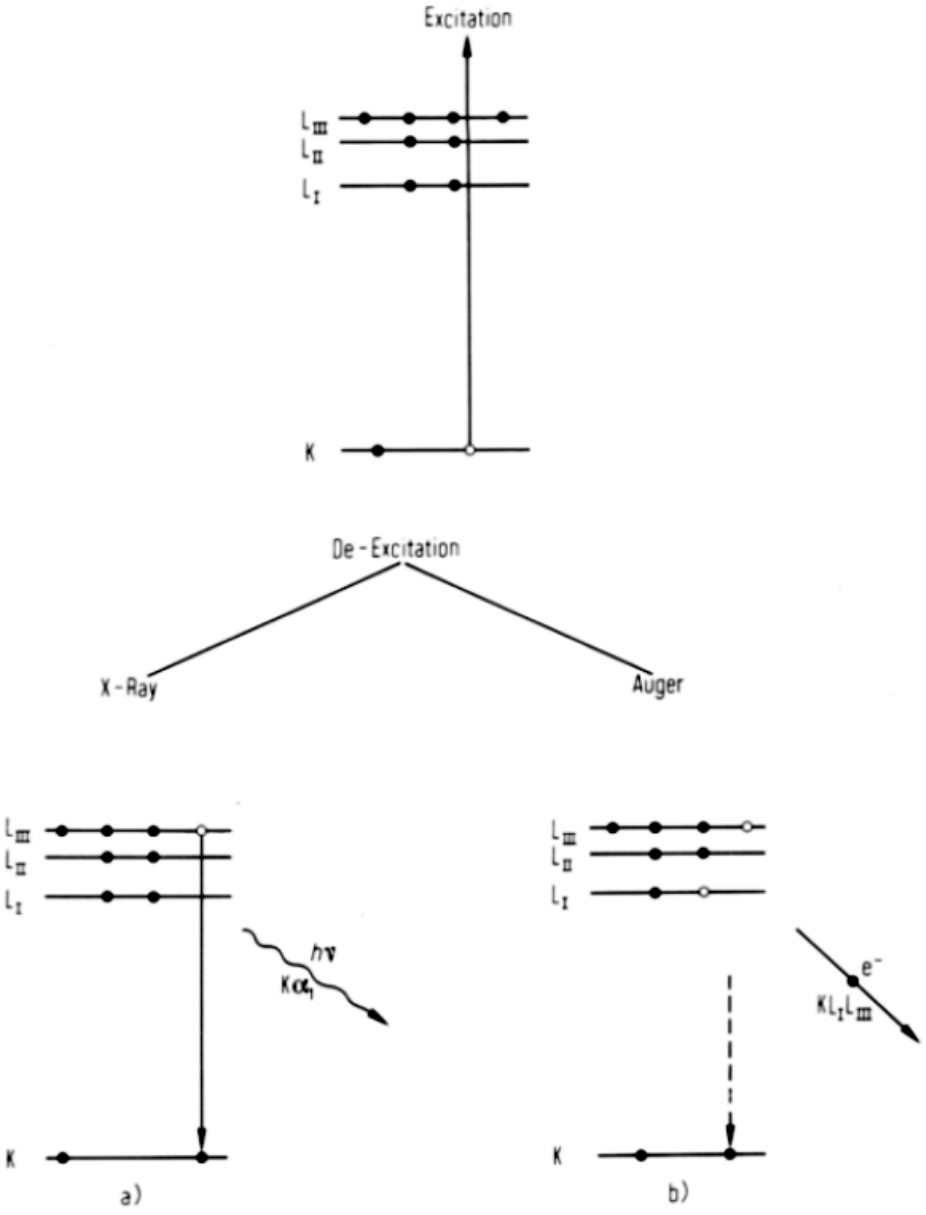

Figure 5. Electronic relaxation processes of atomic core holes through (a) x-ray radiation emission and (b) Auger electron emission [79]. This figure is reproduced with permission from G. Ertl, J. Kuppers, Low Energy Electrons and Surface Chemistry, VCH, Boca Raton, Florida, 1985. Copyright Wiley-VCH Verlag GmbH & Co. KGaA.

is characteristic to a particular element. In this study, the PE AES system (Perkin Elmer, Eden Prairie, MN), which is composed of the PE 10-155 Cylindrical Auger-Electron Optics, PE 32-150 Digital AES Control, PE 32-100 Electron Multiplier Supply, PE 11-010 Electron Gun Control, and PE 96B V/f Preamplifier, was used.

An electron beam with a typical primary energy of 2 keV from an electron gun is directed to the single-crystal electrode. The scattered electrons enter a cylindrical mirror analyzer (CMA) as shown in Figure 6 to separate the Auger electrons from the rest of the secondary electrons. The outer cylinder is held at a negative potential relative to the inner cylinder in order to deflect the electrons to the exit slit located at the inner cylinder. In this process, the voltages of the cylinders are carefully controlled such that only those electrons with a specific kinetic energy can pass through the exit slit at a particular instant and hence, reach the detector, which is usually an electron multiplier [79].

The Auger signal is electronically differentiated to address a difficulty in peak identification due to a large sloping background to produce a derivative spectrum of the electron energy distribution. An AES spectrum of a clean Pd(111) single-crystal surface and the positions where characteristic peaks from various common elemental impurities would appear are presented in Figure 7. Since various elements have their unique AES peaks, the presence (or absence) of such peaks would simply imply the presence (or absence) of such elements on the surface.

The AES measurements used in this study were conducted with a 1.5 kV electron gun voltage in verifying the cleanliness of the surface.

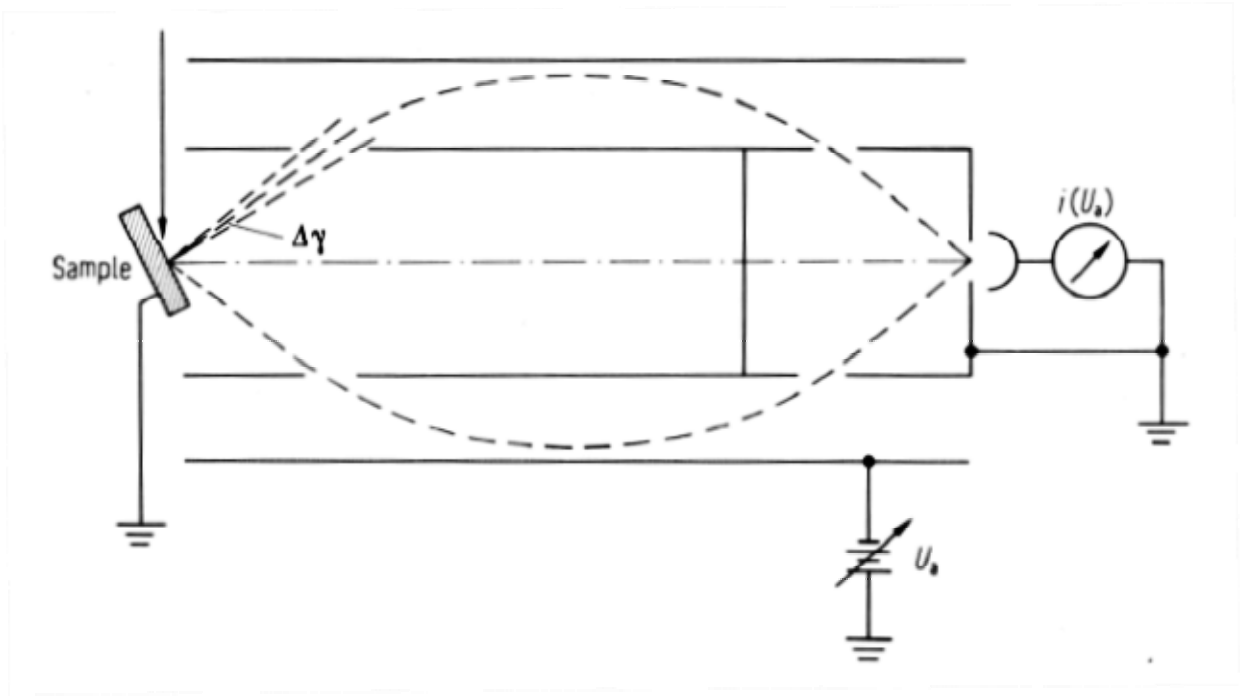

Figure 6. Schematic diagram of a cylindrical mirror analyzer [79]. This figure is reproduced with permission from G. Ertl, J. Kuppers, Low Energy Electrons and Surface Chemistry, VCH, Boca Raton, Florida, 1985. Copyright Wiley-VCH Verlag GmbH & Co. KGaA.

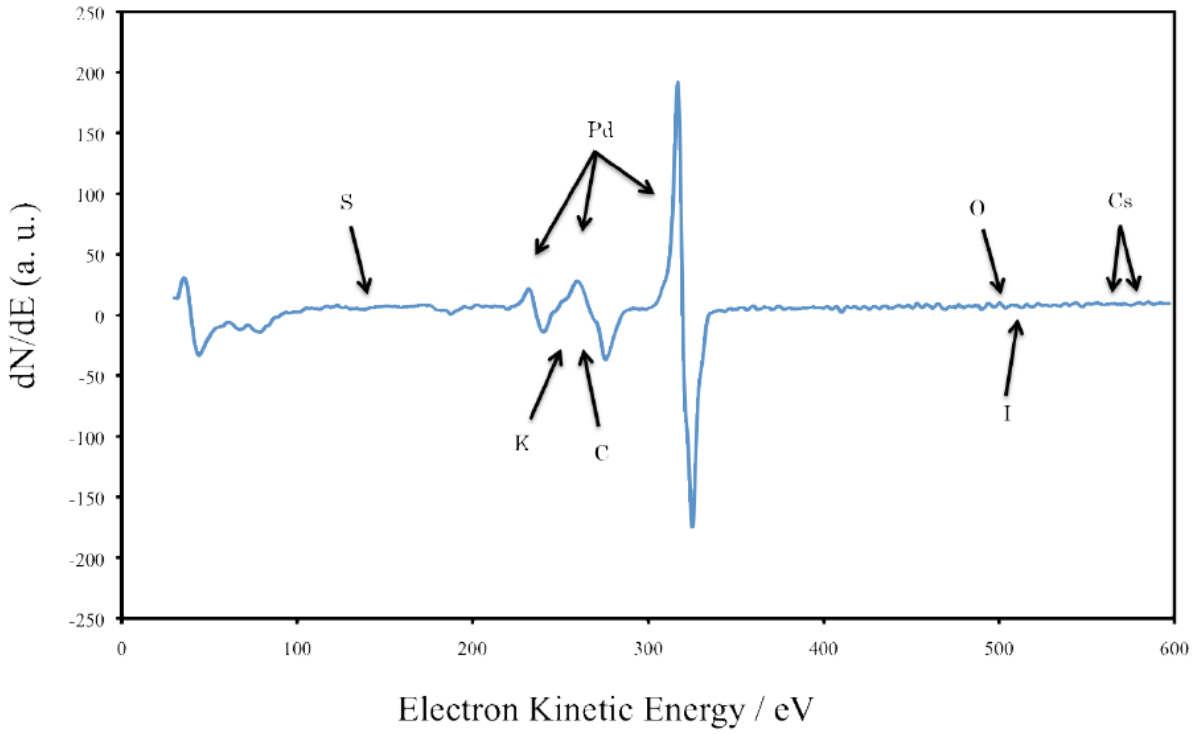

Figure 7. AES spectrum of a clean Pd(111) surface.

2.2.3 *High-Resolution Electron Energy Loss Spectroscopy (HREELS)*

Many of the electrons from the incident electron beam that impinge into the surface are inelastically backscattered causing them to have lower kinetic energies than the primary energy. These electrons would correspond to various peaks, which are referred to as electron energy loss peaks, in the energy distribution spectrum. Since inelastic events due to vibrational interactions only cause a small decrease in energy, the corresponding loss peaks can only be observed if the measurements are performed at high resolution [82].

There are two main mechanisms that explain the presence of the electron energy loss peaks: (i) dipole scattering and (ii) impact scattering [2,79,83-85]. In dipole scattering, the electron impinging into the surface interacts with the electric dipole moment caused by molecular vibrations on the surface. As presented in Figure 8, if the vibration is parallel to the surface, its dynamic dipole moment is cancelled by that of its image dipole at the surface thereby leading to a zero net dynamic dipole moment. However, if the vibration is perpendicular to the surface, the dipole moment is not cancelled by its image dipole thus producing a non-zero dynamic dipole moment. Therefore, only those vibrations with a component perpendicular to the surface can yield energy loss peaks. This principle is similar to that for infrared reflection-absorption spectroscopy (IRAS) [86-89]. In addition, energy loss peaks due to dipole scattering can only be observed when the backscattered electrons are measured at the specular direction; they vanish at off-specular angles. In impact scattering, the incident electron penetrates into the surface-adsorbed molecule and transfers some of its energy to a

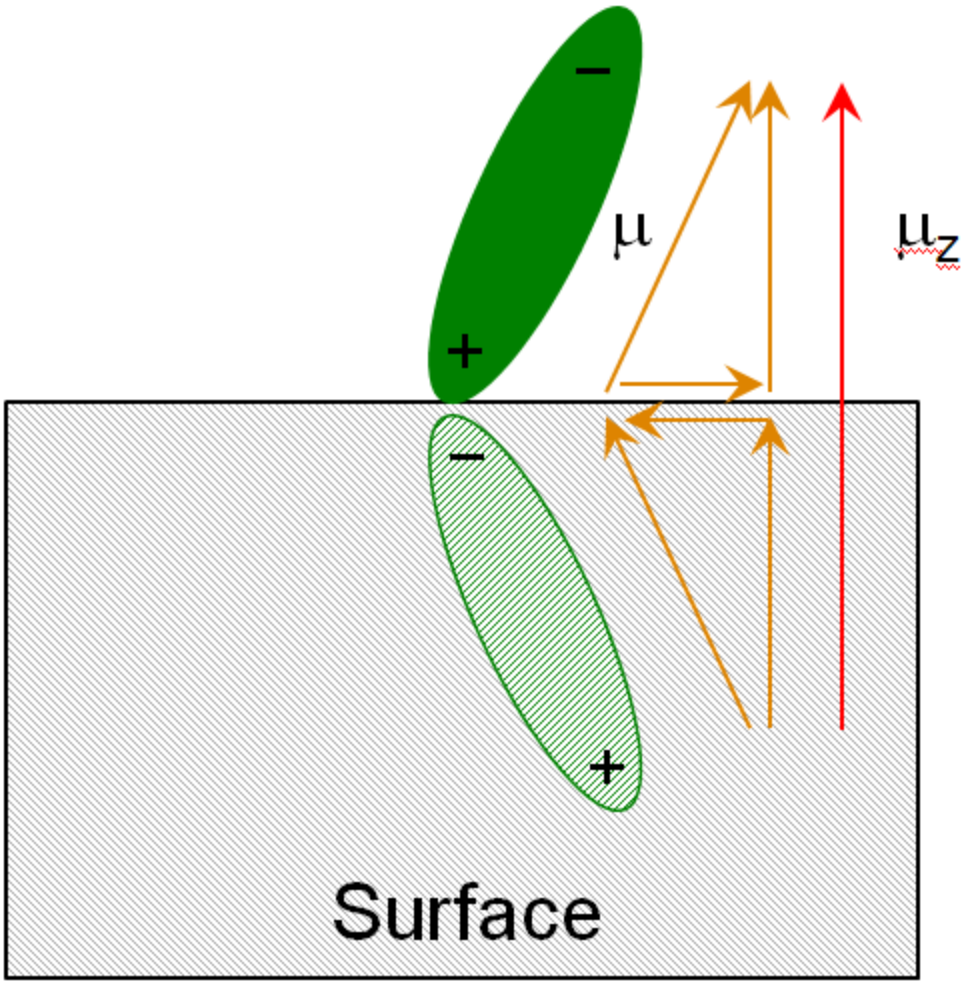

Figure 8. The dynamic dipole moment of surface and image dipoles oriented parallel and perpendicular to the surface.

vibrational mode. This mechanism is rather complex and is treated quantum mechanically [84]. Moreover, the selection rules from dipole scattering however, do not apply with impact scattering. It was also observed that impact scattering disappears at the specular direction but is more significant at higher vibrational energies. Furthermore, oscillations that interact more in the impact scattering mechanism have low dipole scattering interactions (and vice versa) [84].

High-resolution electron energy loss spectroscopy (HREELS) can therefore be utilized to identify molecular vibrational modes and frequencies on surfaces. In this investigation, the LK 2000 HREEL spectrometer (L.K. Technologies Inc., Bloomington, IN) was used. As presented in Figure 9, this instrument is composed of a LaB_6-filament electron gun, two-stage monochromator, energy analyzer, and a channeltron detector. The energy range of the incident electron beam from the electron gun is narrowed down from 300 meV to *ca.* 1 meV by the two-stage monochromator, which uses a 127^o cylindrical deflection analyzer (CDA), and the intermediate lens system. The monoenergetic beam of low-energy electrons, which is usually 1-10 eV, is then focused unto the sample using a zoom lens system. The inelastically scattered electrons are subsequently focused into the energy analyzer, which also uses a 127^o CDA and only allows electrons with a certain energy to pass through at a certain moment, using a second set of zoom lenses. The electrons are finally collected and detected using a channel electron multiplier (channeltron) and the resulting signal is supplied to a preamplifier for further processing.

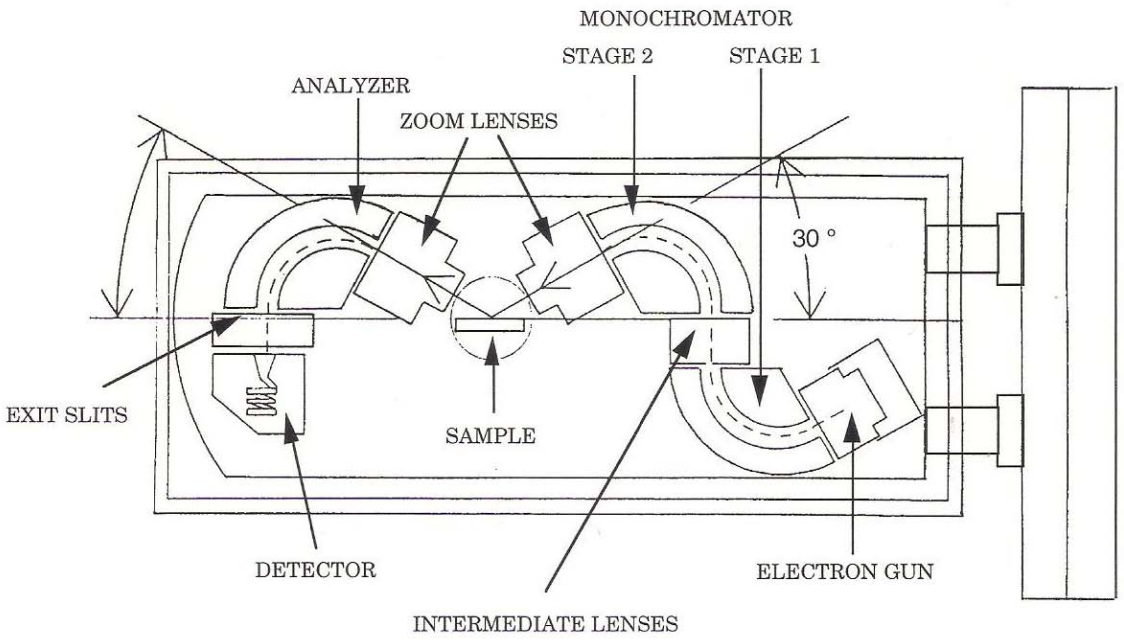

Figure 9. HREEL spectrometer schematic diagram.

Adsorption of molecules unto the Pd(111) surface was accomplished by immersing the single-crystal electrode unto the analyte solution containing 10 mM H_2SO_4 as the supporting electrolyte in a custom-built EC cell at open-circuit potential (OCP) for several minutes. After multiple rinses of supporting electrolyte to remove unadsorbed species on the surface, the electrode was allowed to dry in N_2 atmosphere before the pressure in the EC chamber was lowered down to UHV conditions for surface analysis measurements.

The HREELS experiments were performed with a beam energy of *ca.* 4 eV, elastic beam rate of 1.7 x 10^5 cps, and a resolution of 4.8 meV (38 cm^{-1}). In this study, all spectra were collected only in the specular direction (62° from the surface normal).

The vibrational assignment of the HREELS peaks was accomplished by comparing the HREELS frequencies with the characteristic IR frequencies of various functional groups [90]. Moreover, since the frequency of a molecular vibration may shift if the molecule is chemically bonded to a metal surface, it is also significant to compare the vibrational frequencies with those of organometallic complexes where ligands are bonded to metal centers [91].

Normalization of the HREEL spectra was performed by matching the intensities of the background region of all spectra [92]. To attain this, a clean Pd spectrum was obtained and its elastic peak count rate was set to 2.5×10^5 cps, the maximum obtainable count. Each spectrum for the adsorbed organic species was then multiplied by a constant to normalize the background of the spectrum (2100~2700 cm^{-1}) to that of the clean Pd spectrum.

The HREELS-based chemisorption isotherm was generated by integrating the specific normalized HREELS peak to obtain the peak intensity and plotting the integrated values against the logarithm of the adsorbate aqueous-solution concentrations.

2.3 Ultrahigh Vacuum–Electrochemistry (UHV-EC) Instrumentation

In order to preserve the cleanliness of single-crystal electrodes, the experiments must have to be conducted at ultrahigh vacuum conditions. In this work, ultrahigh vacuum–electrochemistry (UHV-EC) experiments were carried out using a stainless steel assembly (Figure 10) (Perkin-Elmer, Eden Prairie, MN), which is composed of an electrochemistry (EC) chamber, where adsorption and electrochemistry experiments are done, a surface analysis (SA) chamber that can be isolated from the electrochemistry chamber by a gate valve (MDC Vacuum Products, Hayward, CA), and a valve-isolable ion pump well. An X-Y-Z manipulator (Huntington Laboratories, Mountain View, CA) that is mounted on a twin-rail positioning table (Lintech, Mountain View, CA) controls the rotational and vertical movement of the electrode inside the UHV chamber.

An electrochemical cell built for UHV-EC studies as shown in Figure 11 can be used to introduce various solutions into the EC chamber through another gate valve. This cell is made up of two compartments: one that contains the Ag/AgCl (1 mM NaCl) reference electrode and a Pt auxiliary electrode and another that accommodates the Pd(111) working electrode. A fine glass frit separates these two compartments and a long tube connected to the working electrode compartment introduces (or withdraws) various solutions to (or from) this compartment.

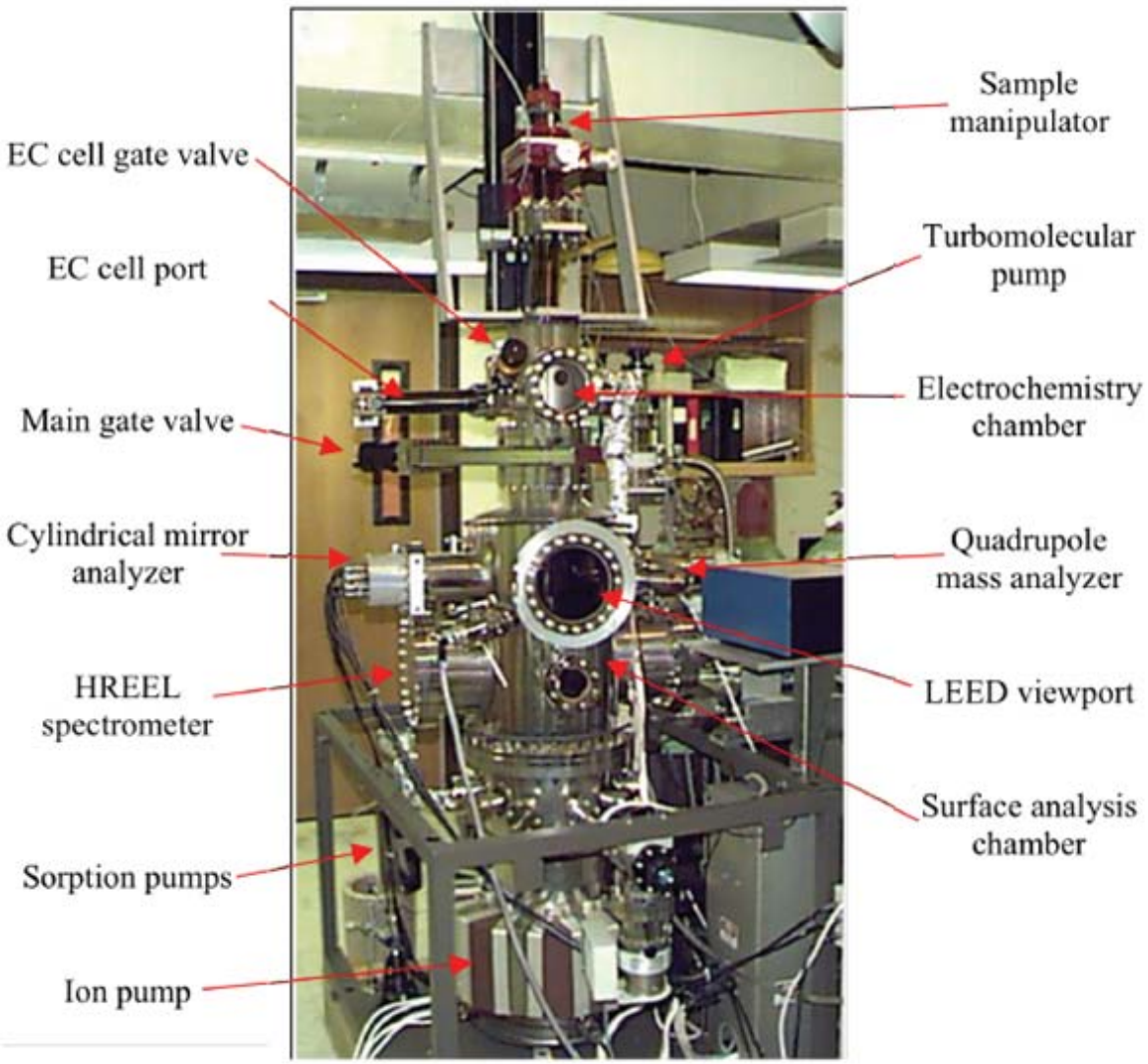

Figure 10. The UHV-EC system used in the ultrahigh vacuum surface studies.

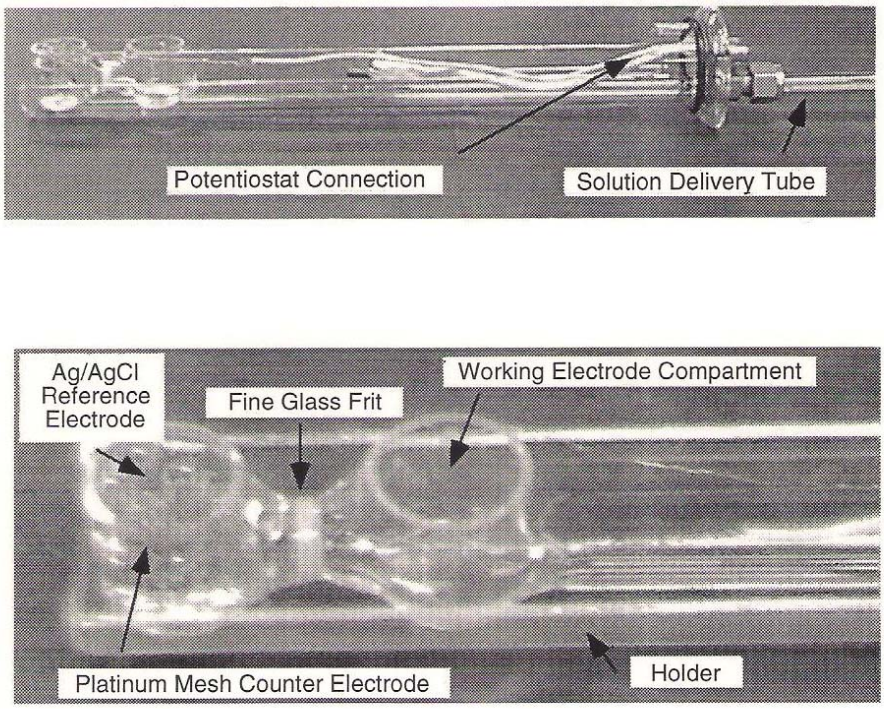

Figure 11. The electrochemical cell employed in the UHV-EC experiments.

The SA chamber houses the (i) LEED optics for surface structure analysis, (ii) AES optics for surface elemental analysis, (iii) HREELS module for surface vibrational analysis, (iv) quadrupole mass analyzer (UTI Instrument Company, Sunyvale, CA) for residual gas analysis, (v) ion cage (LVC Engineering, Santa Barbara, CA) for argon-ion bombardment, and (vi) two separate variable leak valves (Varian, Lexington, MA) to introduce oxygen (for thermal annealing) and argon (for argon bombardment).

Typical surface analysis experiments are performed in the following manner: (i) The crystal is raised to the EC chamber and is isolated from the SA chamber by closing the main gate valve. (ii) The pressure in the upper chamber is increased to ambient levels using N_2 so adsorption or electrochemistry experiments can be done using the EC cell inserted in the cell port. (iii) The pressure inside the UHV chamber is then reduced using a 3-stage process. Two sorption pumps cooled by liquid nitrogen first remove the gas that is in the EC chamber after an electrochemical experiment, which is done at ambient pressures. Once the pressure is lowered down to about 10^{-3} torr, a 56 L/s turbomolecular pump (Balzers, NH) is employed to further reduce the pressure to 10^{-7} torr. Final pressure reduction to 10^{-10} torr, is attained using a TNB-X Series 500 ion pump (Perkin Elmer, Eden Prairie, MN) and a liquid-nitrogen-cooled titanium sublimation pump after the main gate valve is opened. (iv) When the pressure is reduced down to UHV levels after an experiment, the single-crystal electrode can be lowered to the SA chamber for characterization. Additionally, if the base pressure exceeds 10^{-9} torr, a 4-day bake-out at 200^{o}C of the UHV-EC system is performed.

2.3.1 *Well-Defined Working Electrodes*

For the UHV studies, commercially polished 99.999% Pd(111) (Aremco Products, Ossining, NY) circular disk electrodes were employed. The diameter of the electrode was 0.9 cm with a thickness of 0.3 cm. Two 0.5 mm Pt or Pd wires (99.99% purity, Johnson-Matthey Inc., Seabrook, NH) were spot-welded to the disk electrode edge and were connected to the X-Y-Z manipulator. Two Pt(10%)-Rh(90%) thermocouple wires were also spot-welded to the upper disc edge of the suspended Pd(111) single crystal for resistive heating during cleaning cycles using a crystal temperature controller (Omega Engineering).

To clean the single-crystal electrodes before an experiment, the surface was subjected to multiple cycles of Ar^+-ion bombardment (10^{-5} torr Ar) and thermal oxidation at 550^{o}C (10^{-6} torr O_2). Thermal annealing at 750^{o}C was also conducted to restore surface order. Eventually, the order and purity of the Pd(111) surface were ascertained by LEED and AES, respectively.

2.4 Electrochemical Scanning Tunneling Microscopy (EC-STM)

Scanning tunneling microscopy (STM) is one among the most widely used surface imaging and analysis techniques since it produces three-dimensional real-space images of surfaces with atomic resolution [94]. When a very sharp metal tip is placed at a very short distance to the surface (*ca.* 5-50 Å) and a low bias is applied between the surface and the tip, electrons tunnel across the barrier between the two materials. The

resulting tunneling current is dependent on the distance between the tip and the surface; hence, this technique can image atoms as well as molecules on various surfaces.

An STM measurement can be performed using a constant current or constant height mode while making the applied bias constant. In the constant current technique, a feedback mechanism is used such that there is a constant tip-sample distance thus producing a uniform tunneling current. In this mode, the vertical position of the tip needs to be varied throughout the scan in order to make the tip-sample distance constant. The variation of the tip height is recorded and corresponds to the constant charge density contour of the surface. In the constant height mode, the vertical position of the tip is held constant; thus, the variation in the tunneling current corresponds to the charge density isosurface.

When STM is used to study electrode-electrolyte interfaces at ambient conditions, it can be used as an *in situ* technique and is referred to as *in situ* STM or electrochemical STM (EC-STM). A bipotentiostat is employed in EC-STM to independently control the potential of the substrate, which is the working electrode (WE), relative to a reference electrode (RE) and the potential of the STM tip. The Faradaic current in the substrate and in the counter electrode (CE) is collected by the current follower, whereas the tunneling current is recorded by the tunneling current amplifier. The interference between the faradaic current and the tunneling current, which is a problem in earlier models, is prevented by this schematic, which is shown in Figure 12.

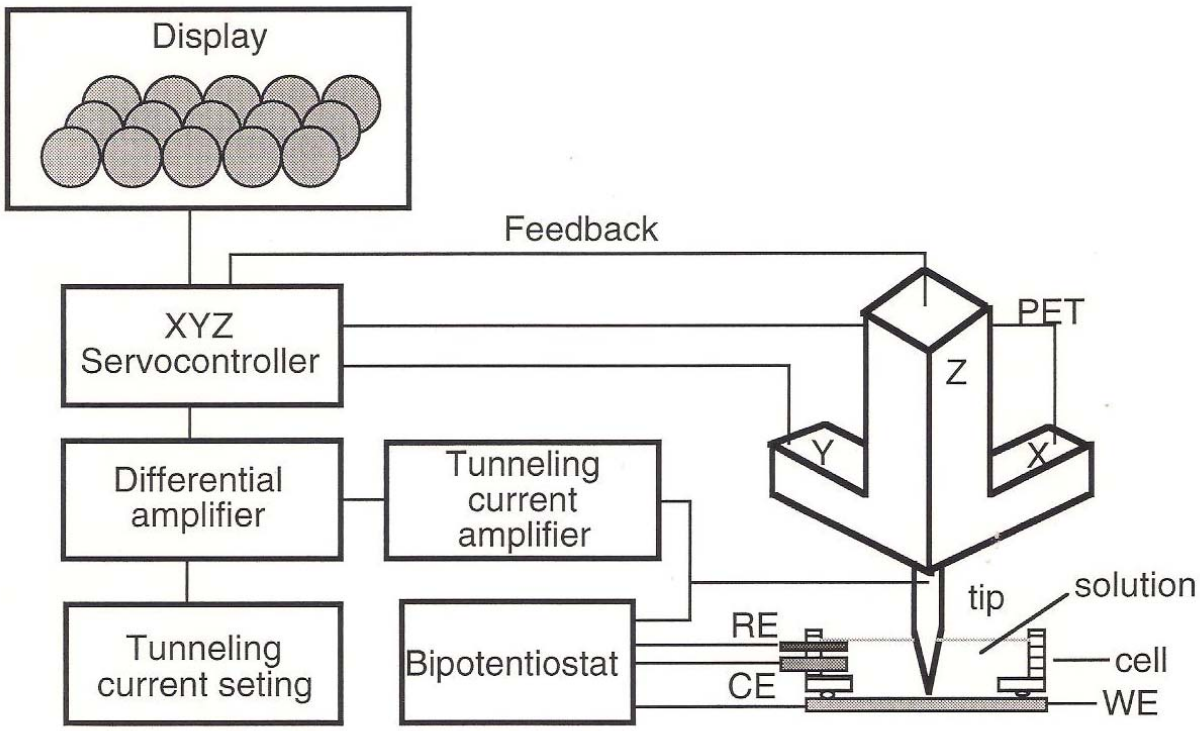

Figure 12. Schematic diagram of the EC-STM.

The Nanoscope III scanning probe microscope (Digital instruments, Santa Barbara, CA) and a custom-built Kel-F electrochemical cell in a four-electrode system were used in the experiments. Pt wires were used for the auxiliary electrode and for the quasi-reference electrode. A Pd bead was used as a working electrode and was secured using a conductive plate and an O-ring seal.

The Pd bead was prepared using the Clavilier method [95,96]. A 0.8-mm Pd wire (99.995% purity, Aldrich, Milwaukee, WI) was melted using an oxygen-hydrogen flame to form a bead (3 mm in diameter) with various single-crystal facets oriented at various planes. One (111) facet was selected and used as the working electrode surface for the EC-STM measurements. To clean the surface, the bead was flame-annealed at *ca.* 800^{o}C for 15-30 minutes, cooled slowly in an Ar stream, and immersed in Milli-Q Plus water saturated with hydrogen. A drop of water was allowed to adhere on the surface of the Pd bead as the electrode was transferred to the EC cell to protect the surface from contamination in the air.

The tunneling tips were prepared by electrochemical etching of a 0.25-mm tungsten wire (99.995% purity, Aldrich, Milwaukee, WI) in 1 M KOH at 15 V AC. The resulting tip was further coated with a very thin film of transparent nail polish to reduce any faradaic current interference [97].

All EC-STM measurements were performed by Dr. Y.-G. Kim.

2.5 Electrochemistry (EC)

Electrochemical measurements for the diiron (μ-pdt)[$Fe(CO)_3$][$Fe(CO)_2PPh_3$] (pdt = 1,3-propanedithiolate) complex (**I**) were made using an eDAQ EA161 potentiostat (eDAQ Inc., Colorado Springs, CO). All voltammograms were obtained using a gas-tight three-electrode H-type electrolysis cell under nitrogen atmosphere at room temperature. The polycrystalline Au bead (0.51 cm^2) working electrode was cleaned electrochemically in a 1.0 M H_2SO_4 solution prior to any experiment. The glassy carbon (0.071 cm^2) working electrode, on the other hand, was polished with a 1-μm diamond paste and sonicated in water for 15 min. prior to use. The supporting electrolyte was 0.1 M *n*-Bu_4NBF_4 (TBA-BF_4) in CH_3CN. A platinum wire was used as the counter electrode. The reference was a Ag/Ag^+ electrode, prepared by anodizing a silver wire in a 0.01 M $AgNO_3$ / 0.1 M *n*-Bu_4NBF_4 solution in CH_3CN. The electrocatalytic experiments were carried out using *ca.* 10 mL CH_3CN solutions containing 0.5 mM of the diiron complexes and 0.1 M in *n*-Bu_4NBF_4. Increments of glacial acetic acid were added using a micropipette and the potentials were reported relative to Fc^+/Fc as an internal standard.

A CH_3CN solution containing 0.5 mM of the diiron complex **I** in 0.1 M *n*-Bu_4NBF_4 was prepared. Cyclic voltammograms (CV) using a Au-bead electrode were then collected as 10-µL portions of glacial acetic acid (1.75 x 10^{-4} moles HOAc) were added.

The polycrystalline Au electrode was also immersed in a solution of complex **II** containing 0.1 M *n*-Bu_4NBF_4 in CH_3CN for several hours at OCP in order for

chemisorption to occur and induce the formation of a self-assembled monolayer of the diiron complex on the surface. After several rinses of the supporting electrolyte, CVs using the Au(pc)-bead electrode were obtained as increments of glacial HOAc were added.

2.5.1 *Cyclic Voltammetry (CV)*

Voltammetry is a technique in electrochemistry wherein the current is measured as a function of the applied potential. The electrode potential is generally swept from an initial value to a final potential at a specific scan rate. When the potential scan is terminated at a final voltage different from the initial potential, this method is referred to as linear sweep voltammetry. Furthermore, when the scan is returned back to the initial potential value, this corresponds to a technique called cyclic voltammetry (CV). The latter is used in various inorganic electrochemical experiments to characterize reduction-oxidation processes of different species in a solution and in this investigation, a scan rate of 200 mV/s is employed to study the redox processes of the diiron complexes in CH_3CN solution at various concentrations of acetic acid.

2.5.2 *Thin Layer Electrochemistry (TLE)*

Thin layer electrochemistry (TLE) is a technique used to (i) minimize diffusion since the analyte is isolated in a thin-layer solution with < 50-μm thickness, (ii) reduce contamination since only a small volume is introduced into the cavity, and (iii) increase sensitivity due to a high surface-area-to-volume ratio [23].

The TLE set-up is shown in Figure 13. The working electrode compartment was separated from the reference electrode compartment using a porous glass frit in an H-cell. A Pt-wire counter electrode was used. The Pd billet working electrode was inserted inside a cavity and the distance from the metal surface to the glass cavity wall is less than 50 μm. The analyte solution then fills the cavity space with capillary effect as the tip of the electrode was immersed into the solution. The surface area of the Pd billet was calculated to be 1.19 cm^2 and the cavity volume was found to be 3.60 μL.

All TLE measurements were performed by Dr. J. Cruz.

2.5.3 *Surface Coverage*

The surface concentration or surface coverage (Γ) of molecules adsorbed on electrode surfaces can be measured using TLE using the following equation:

$$\Gamma = (Q_x - Q_b)/nFA \quad (4)$$

where Q_x is the electrolytic charge obtained in pure supporting electrolyte solution (blank) after the species are chemisorbed unto the surface, Q_b is the background electrolytic charge, n is the number of electrons transferred in the reaction, F is the Faraday constant, and A is the surface area of the electrode [23].

If Γ is known, the molecular cross section (σ) can be calculated using the following equation:

$$\sigma = 10^{16} / N_A\Gamma \quad (5)$$

where N_A is the Avogadro's number.

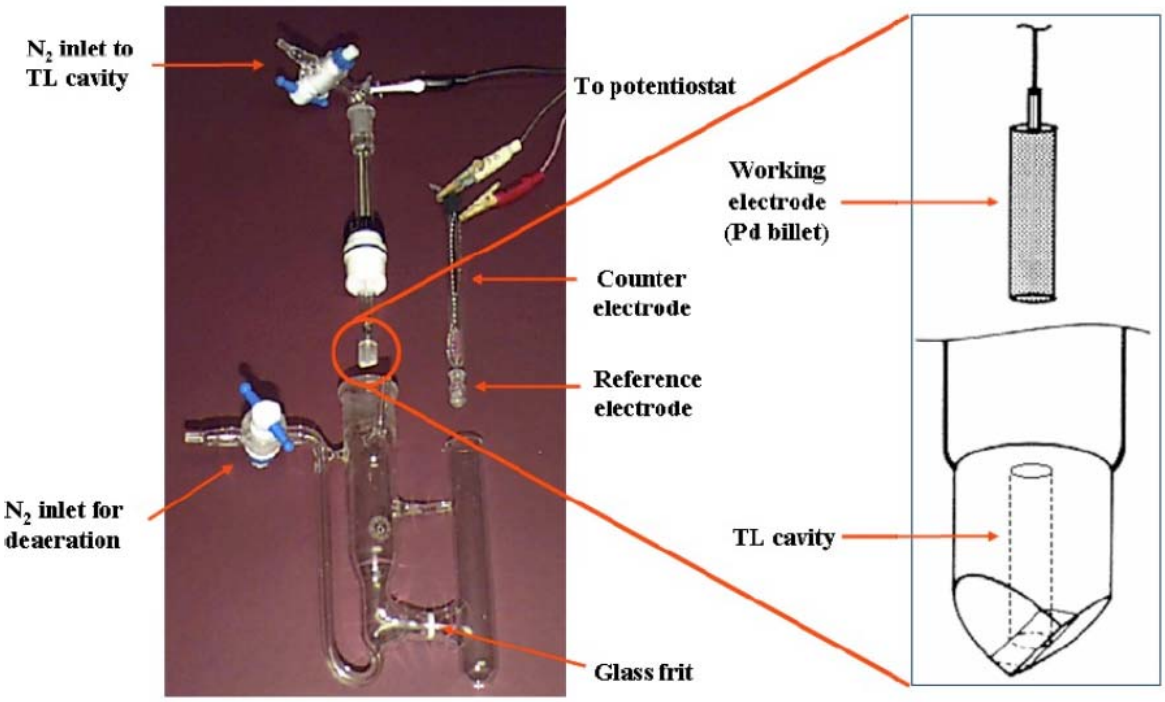

Figure 13. The thin layer electrochemical cell.

The adsorbed-molecule orientation can therefore be deduced by comparing the measured molecular cross section with those calculated for all possible orientations (σ_{calc}) based on covalent and van der Waals radii [9,23,109-112] as shown in Figure 14.

2.6 Reagents and Gases

Chromic acid (3% $K_2Cr_2O_7$ in 10 M H_2SO_4) was used to clean all glassware. The 1.0 M and 10 mM H_2SO_4 solutions for the EC experiments and UHV studies were prepared from fuming H_2SO_4 (Aldrich Chemicals, Milwaukee, WI). 2,3-Dimethylhydroquinone was purchased from Aldrich and was used as received. All aqueous solutions were prepared using 18.2 Ω Millipore water (Millipore Systems, Houston, TX). High-purity Ar (BOTCO, Bryan, TX), O_2 (Proxair, Danbury, CT), and N_2 (BOTCO, Bryan, TX) gases were also used.

The (μ-pdt)[$Fe(CO)_3$][$Fe(CO)_2$L] (pdt = –$SCH_2CH_2CH_2S$–; L = $P(Ph)_3$) (**I**) and (μ-pdt)[$Fe(CO)_3$][$Fe(CO)_2$L] (pdt = –$SCH_2CH_2CH_2S$–; L = $P(Ph)_2CH_2CH_2SH$) (**II**) complexes were synthesized using published procedures [98]. $AgNO_3$ crystals and *n*-Bu_4NBF_4 were purchased from Aldrich and CH_3CN (EMD, Gibbstown, NJ) was used to prepare the non-aqueous solutions.

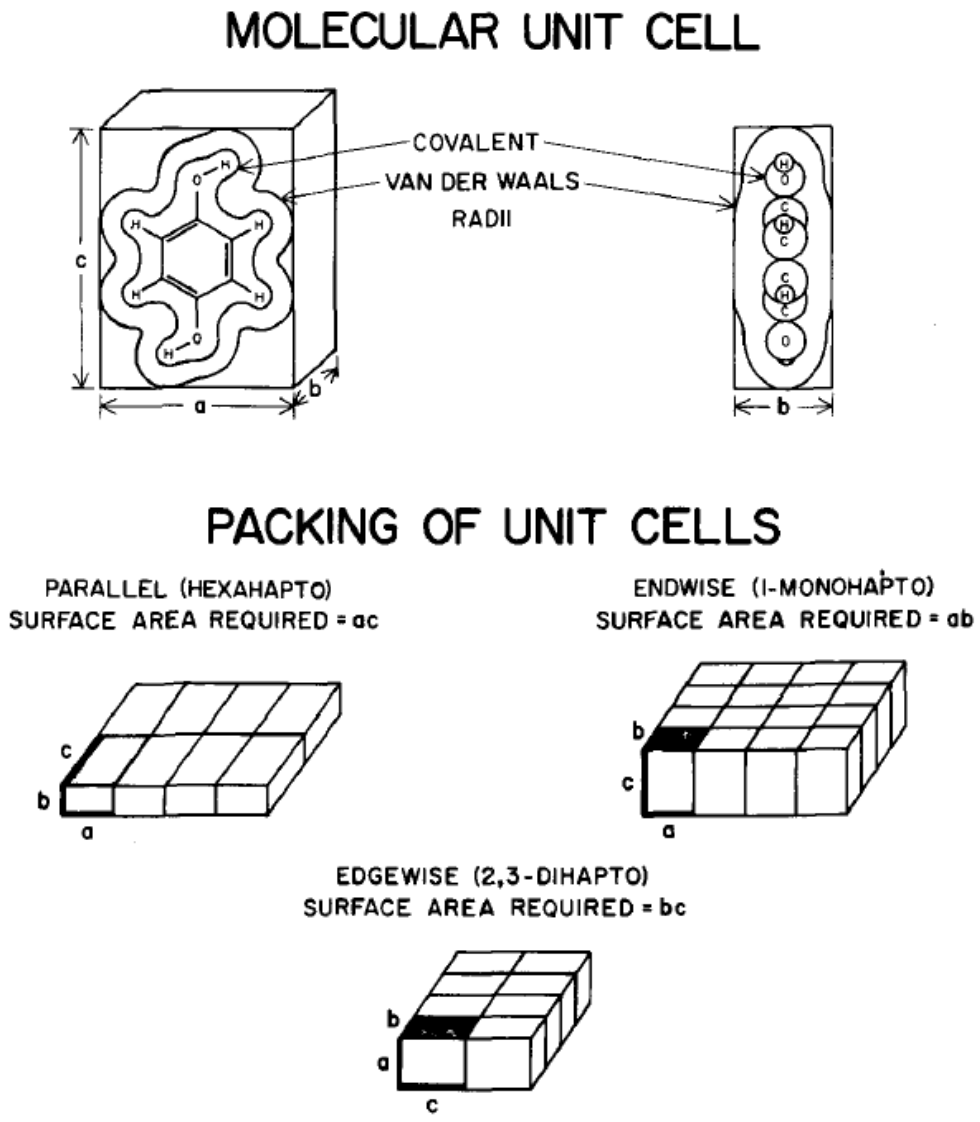

Figure 14. Molecular unit cells used in estimating σ_{calc} [109]. This figure is reproduced with permission from M.P. Soriaga, A.T. Hubbard, J. Electroanal. Chem. 167 (1984) 79. Copyright Elsevier.

3. RESULTS AND DISCUSSION

The underlying subject of this research is the employment of computational methods based on DFT and experimental techniques such as STM, HREELS, and EC to study the adsorption of various species on noble-metal surfaces. The first section describes the use of the computational and experimental techniques to determine the interfacial structure of a Pd(111) surface immersed in a sulfuric acid solution [99]. The second part utilizes the tandem technique in identifying the adsorption site of benzene on the Pd(111) electrode surface at different potentials [100]. The third segment presents the determination of the adsorption site and structure of hydroquinone sulfonate on the Pd(111) surface [101]. The fourth section describes the employment of STM and HREELS as well as vibrational-spectra calculation and total-energy calculation to obtain knowledge on the adsorption structure and site of hydroquinone on the Pd(111) surface [102]. The fifth part is a discussion on the chemisorption of 2,3-dimethylhydroquinone on the Pd(111) surface. The sixth portion presents the use of EC and total-energy calculation to study the adsorption and absorption of atomic hydrogen on ultrathin films (a few monolayers) of Pd deposited on Pt(111) substrates. Lastly, the final section demonstrates the use of electrochemical methods to measure the changes in electrocatalytic activity of hydrogen production by iron hydrogenase model complexes immobilized on Au surfaces.

3.1 Sulfuric Acid on Pd(111)

Electrochemical STM investigations on the interfacial structure of a Pd(111) surface in 0.05 M H_2SO_4 revealed that, when a Pd(111) electrode is immersed in a dilute sulfuric acid solution, a well-ordered ($\sqrt{3} \times \sqrt{7}$) adlayer is formed on the Pd surface as shown in Figure 15 [24]. The rows of bright spots are believed to represent the adsorbed anions, while the dim rows correspond to the hydrogen-bonded chains of water molecules [26,29,33,34] and hydronium cations [24,27,28,35,36].

Further examination of the three-dimensional and zoomed-in images of the ($\sqrt{3} \times \sqrt{7}$) adlattice structures (Figures 16A and 16B) uncover several significant structural information: (i) the adsorbed sulfate ion is trigonally coordinated on the Pd(111) surface such that the anion is directly above a 3-fold hollow site, and (ii) two layers of water molecules and hydronium cations are formed between the anionic chain; the layers, though, are non-co-planar and the slightly elevated layer is composed of hydronium counter-cations. Two real-space structures were proposed and are shown in Figure 17. The main differences between the two structures lie in the spatial orientations and the adsorption-site locations of the molecular and cationic species. Unfortunately, EC-STM was not able to identify the actual structure. Hence, the EC-STM results have been revisited and computationally scrutinized.

The top and the side views of the optimized geometry of Structure (a) in Figure 17 are presented in Figures 18A and 18B, respectively. The original model in Figure 17 was observed to closely resemble the optimized structure except that the O–H bonds of water are pointing towards the metal surface for the latter.

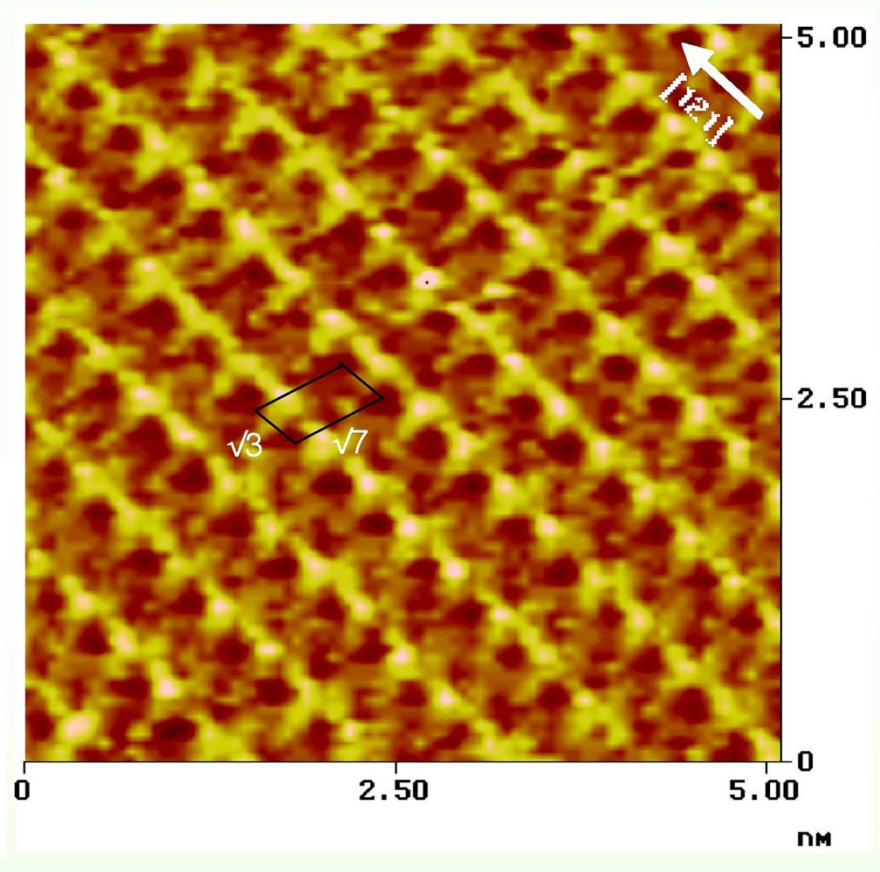

Figure 15. EC-STM image of a Pd(111) electrode surface in 0.05 M H_2SO_4 at 0.4 V that shows a ($\sqrt{3} \times \sqrt{7}$) adlattice structure. Tunneling current = 20 nA [24]. This figure is reproduced with permission from Y.-G. Kim, J. Soriaga, G. Vigh, M.P. Soriaga, J. Colloid Interface Sci. 227 (2000) 505. Copyright Elsevier.

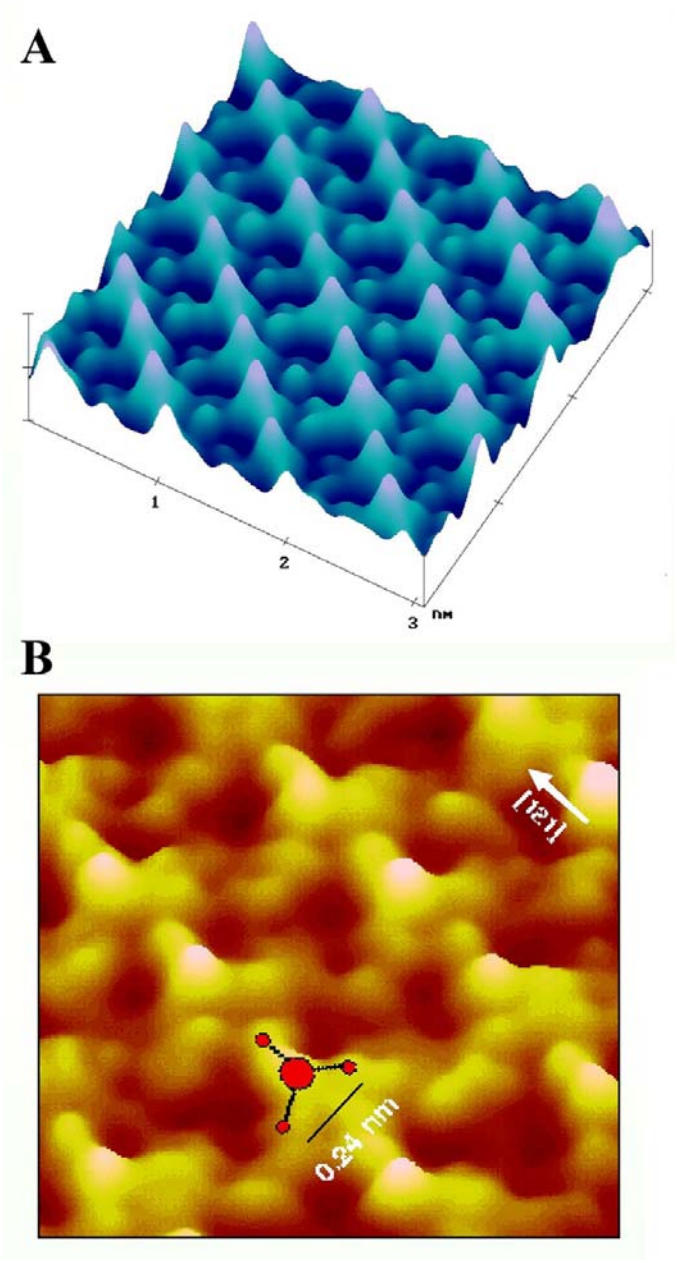

Figure 16. A: Three-dimensional plot of the ($\sqrt{3} \times \sqrt{7}$) adlattice on the Pd(111) surface in 0.05 M H_2SO_4 at 0.4 V. B: Zoomed-in high-quality EC-STM image of the same adlayer [24]. This figure is reproduced with permission from Y.-G. Kim, J. Soriaga, G. Vigh, M.P. Soriaga, J. Colloid Interface Sci. 227 (2000) 505. Copyright Elsevier.

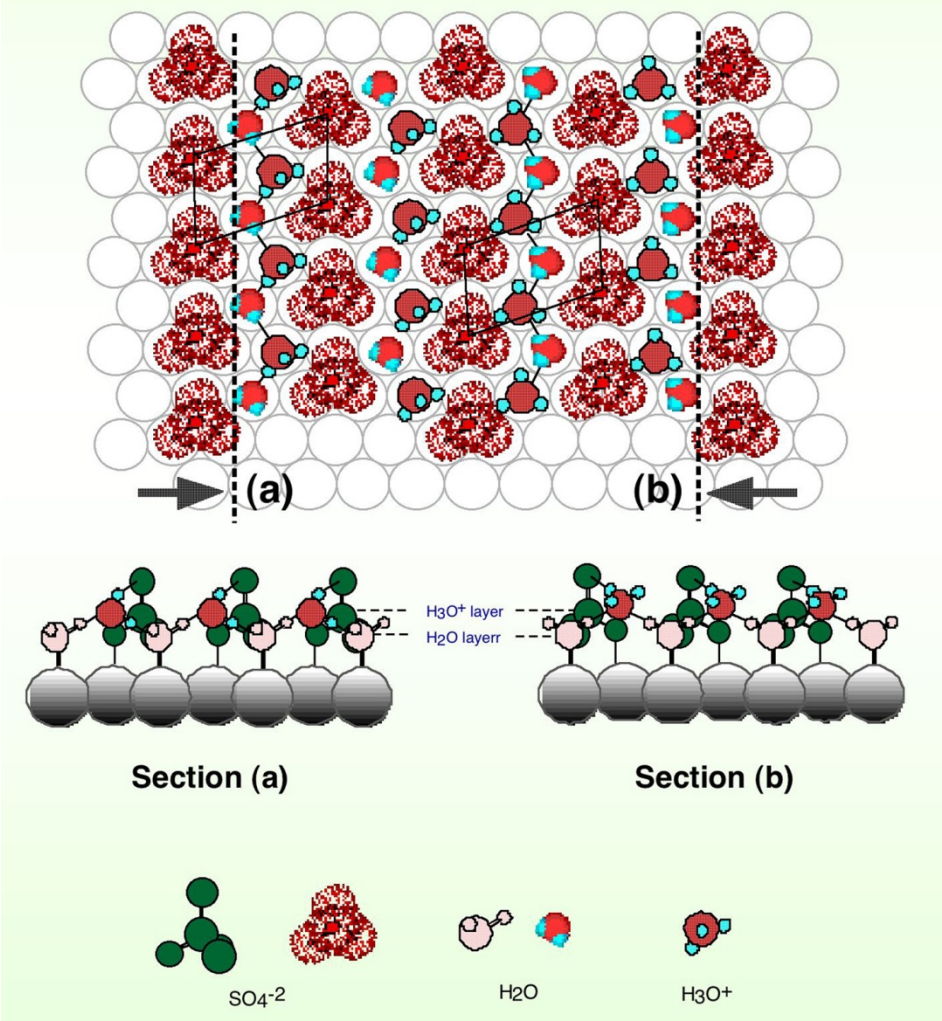

Figure 17. Two possible real-space structures of the Pd(111)-($\sqrt{3} \times \sqrt{7}$)-SO_4^{2-}-H_3O^+-H_2O adlattice [24]. This figure is reproduced with permission from Y.-G. Kim, J. Soriaga, G. Vigh, M.P. Soriaga, J. Colloid Interface Sci. 227 (2000) 505. Copyright Elsevier.

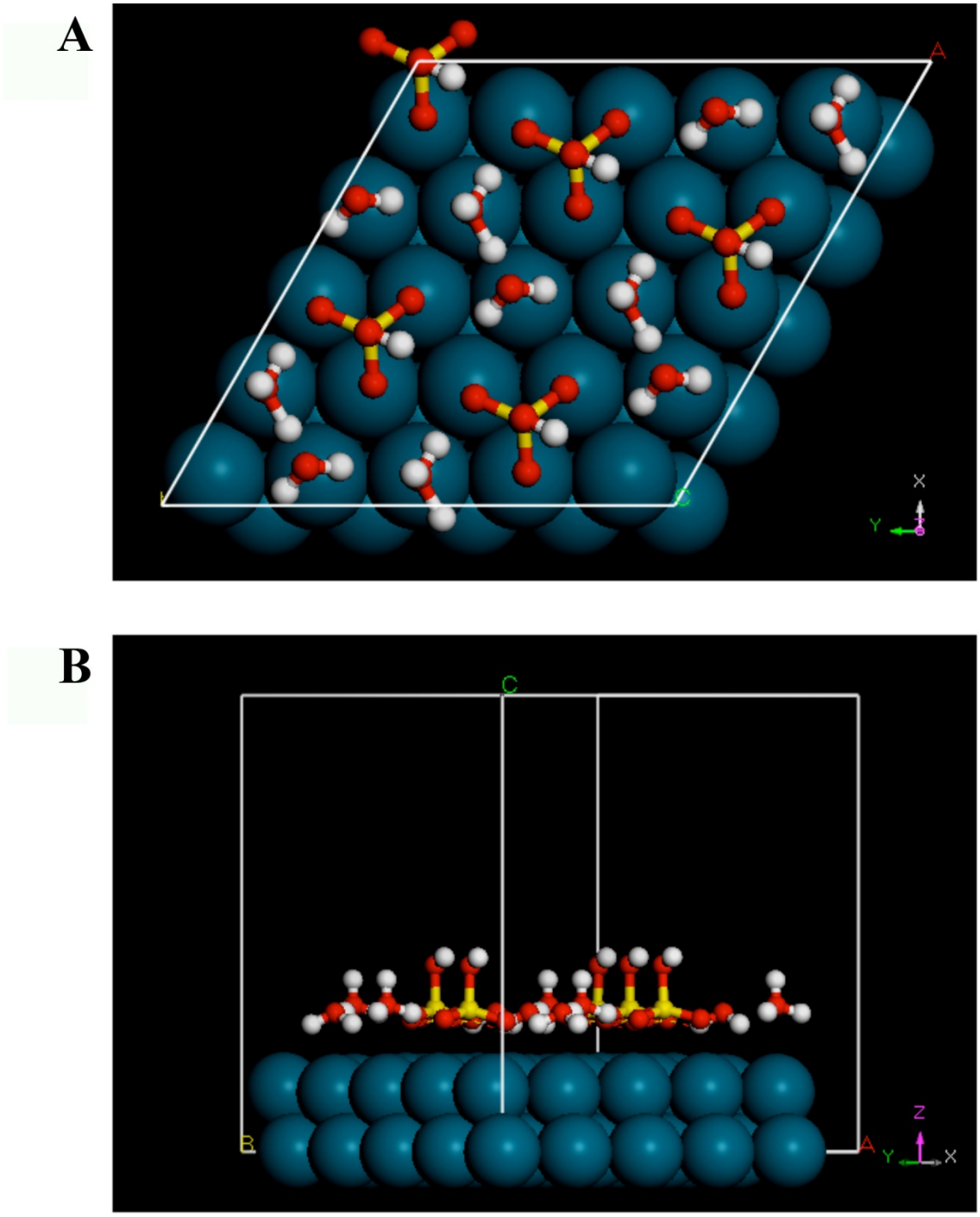

Figure 18. Top view (A) and side view (B) of the optimized geometry of structure (a) in Figure 17.

Figures 19A and 19B display the top and the side views, respectively, of the optimized geometry of Structure (b) in Figure 17. The optimized structure differs from the model in Figure 17 mainly on the spatial orientation of the water molecules and the hydronium ions.

It is indeed remarkable to observe that, on both structures, two layers of adsorbed species are formed between the sulfate rows in which water molecules compose the lower layer while the hydronium cations constitute the upper layer. This computational result validates the findings acquired from the EC-STM measurements [24].

Structures of a variety of chemical systems have been identified based on total energy calculations [45-48]. In a similar manner, in an attempt to determine the more stable interfacial structure, the total energies of the two proposed structural models in Figure 17 were calculated. Structure (b) was found to be more stable than Structure (a) by 0.073 eV per sulfate anion. Since the difference is small, the more favorable structure cannot be identified with absolute certainty based on total energy calculations alone. However, comparison of the experimental EC-STM images with the optimized structures may provide essential insights. Since the hydronium-ion layer is situated above the layer of water molecules, the regions in the STM image (Figure 16B) where these cations are located should show enhanced brightness. By comparing Figures 16B and 18B, the regions where the hydronium ions are positioned in Figure 18B were observed to correspond to empty areas in Figure 16B. This implies that Structure (a) is not likely the correct structure. On the other hand, the location of the hydronium ions in

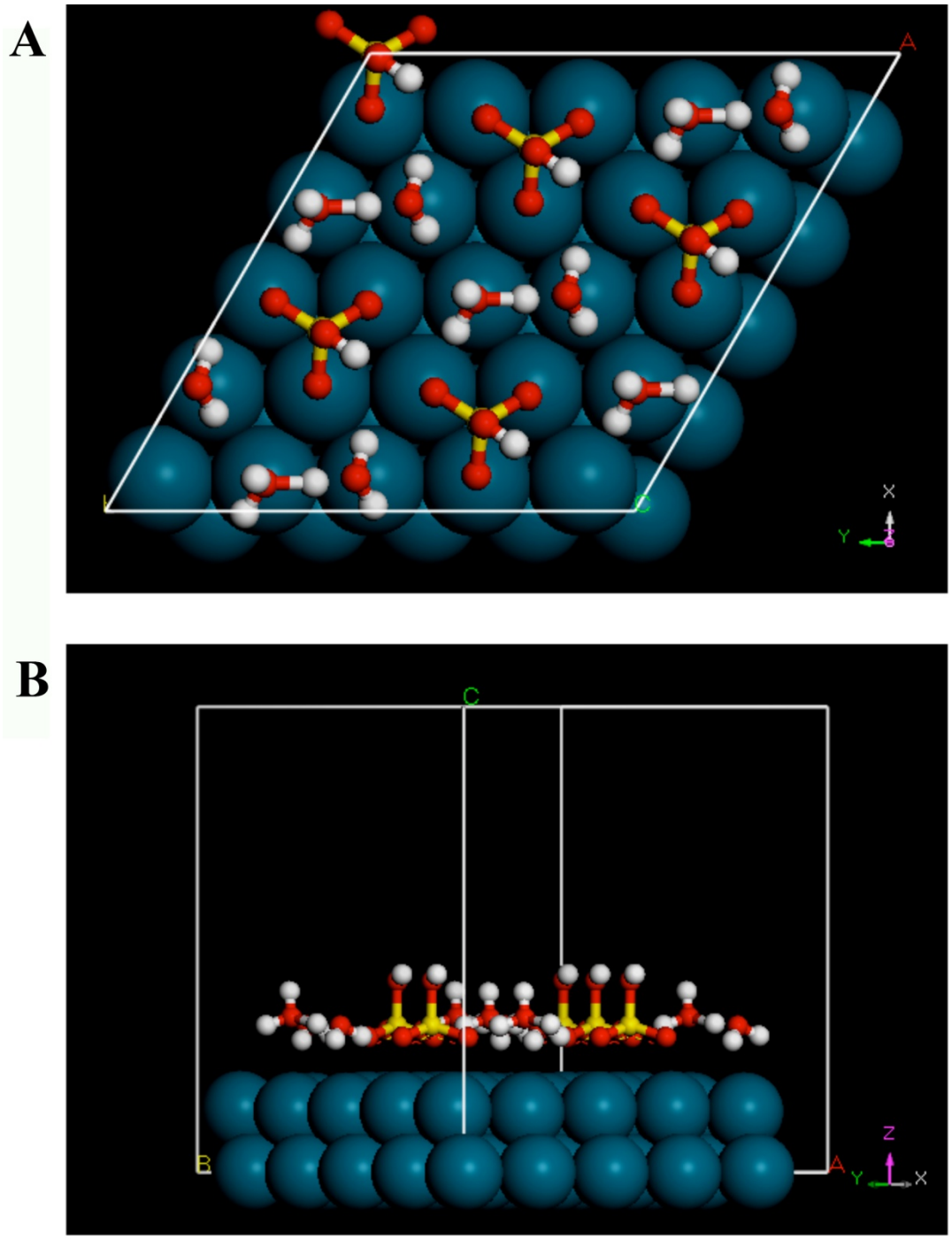

Figure 19. Top view (A) and side view (B) of the optimized geometry of structure (b) in Figure 17.

Figure 19B appears to be bright in Figure 16B, indicating that Structure (b) most certainly is the true real-space structure.

In order to prove the argument mentioned above, simulated STM images of Structures (a) and (b) were obtained and are shown in Figures 20A and 20B, respectively. It is apparent that Figure 16B closely resembles Figure 20B more than 20A since the bright spots between the sulfate rows in the actual EC-STM image (Figure 16B) coincide with the (round) elevated protrusions in the simulated STM image in Figure 20B. This signifies that Structure (b) most likely is the prevalent structure.

3.2 Benzene on Pd(111)

Unlike the ESQC method, which calculates the actual tunneling current obtained from the scattering matrix for the electrons on the tunnel gap [39], or the EHT-based approach, which uses the semi-empirical Hückel method in calculating the energy levels [41], the STM-simulation method adopted in this research relies on DFT to calculate and determine the energy levels of various electronic states, and the Tersoff-Hamann method [78] to display the electron density isosurface as the STM profile.

Figure 21A shows the adsorption geometry of benzene chemisorbed on a 3-fold hollow site on a Pd(111) surface. The corresponding simulated STM image is displayed in Figure 21B. Based from the simulated profile, it is apparent that benzene in this adsorption site adopts a triangular shape with three humps at each vertex of the triangle. These humps are believed to correspond to the three bright spots observed in the ESQC-

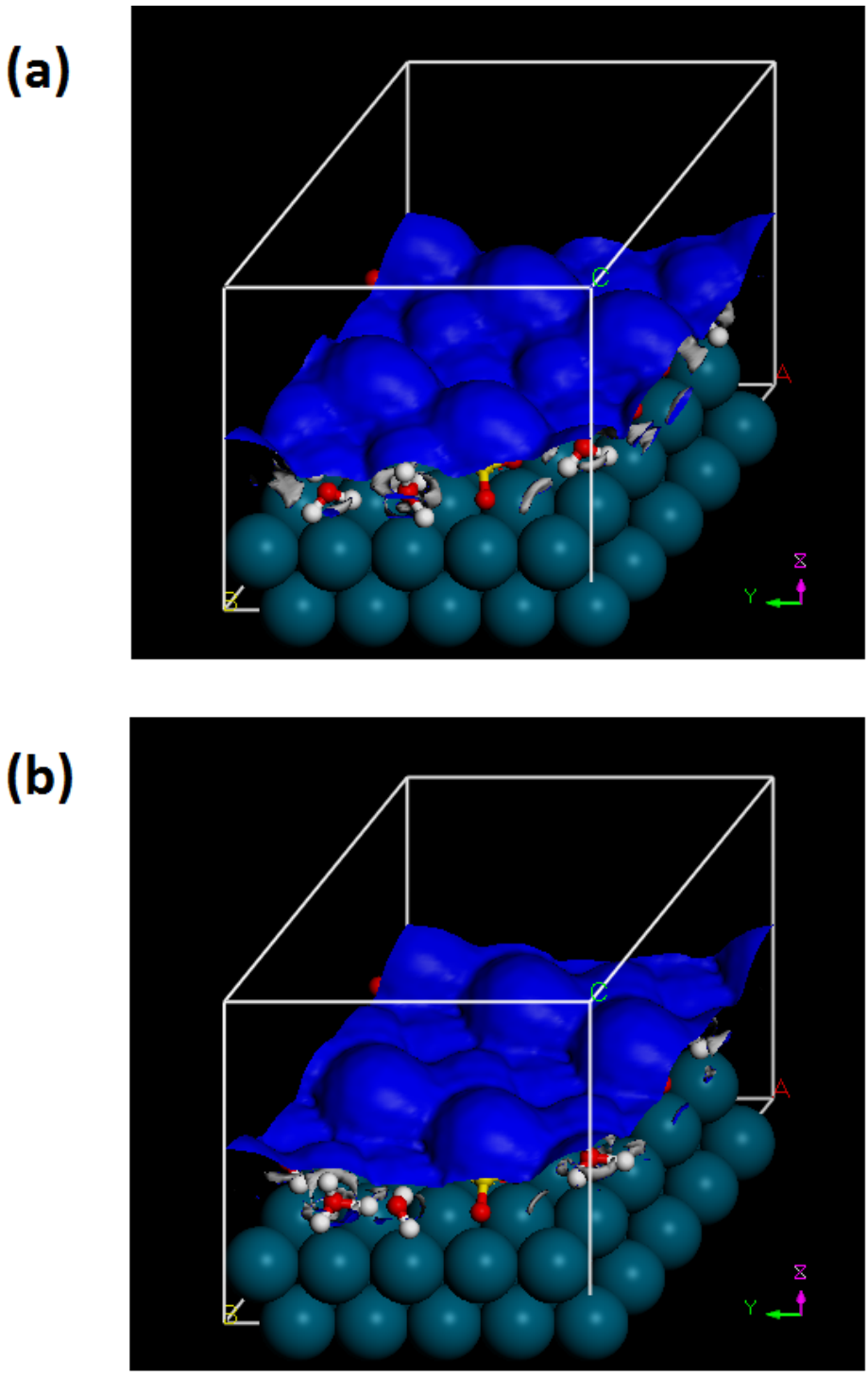

Figure 20. Simulated STM image of the optimized geometry of structures (a) and (b) in Figure 17.

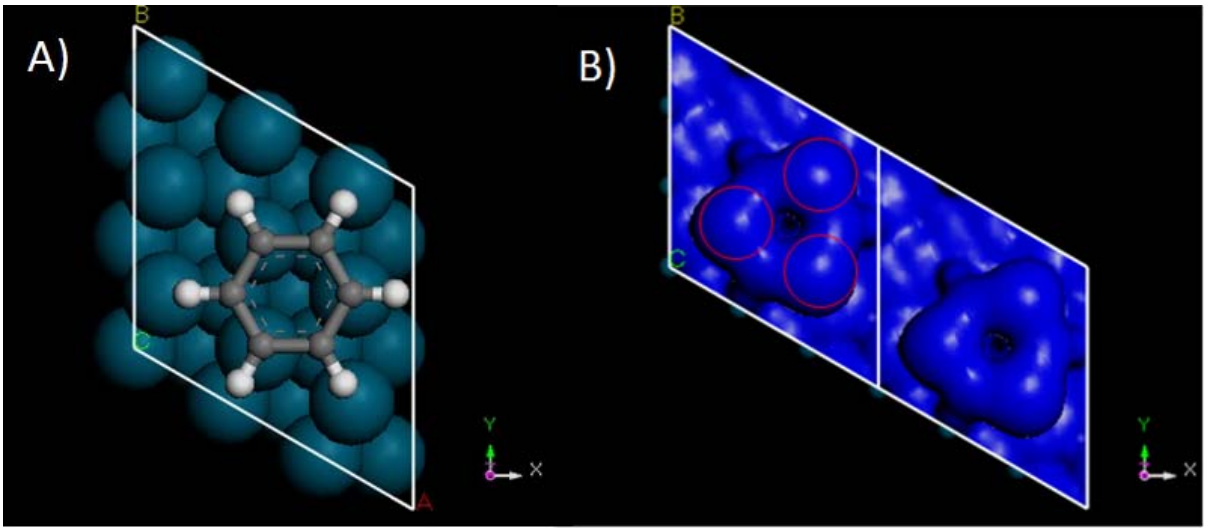

Figure 21. (A) Adsorption geometry of benzene adsorbed on a 3-fold hollow site on a Pd(111) surface. (B) Simulated STM images of the surface in (A).

based and EHT-based simulated STM images of benzene adsorbed on the hollow sites of Pt(111) [39] and Pd(111) [41] surfaces, respectively.

Figure 22A displays a Pd(111) surface with benzene on a 2-fold bridge site and its simulated STM profile is presented in Figure 22B. In this image and in this adsorption site, benzene conforms an oval-shaped figure, which is quite similar to the form observed in the ESQC-based [39] and EHT-based [41] STM simulations.

The adsorption configuration of benzene chemisorbed on an atop site on a Pd(111) surface is shown in Figure 23A. Based on its DFT-based STM profile as presented in Figure 23B, six humps or protrusions can be observed on the ring. This corresponds perfectly well with the six bright spots or lobes observed in the simulation on the Pt(111) surface using a similar adsorption structure [39].

The dependence of the molecular STM image on the adsorption site originates from the specific interactions between the electronic states of the adsorbed molecule and those of the surface metal atoms directly below it. Individual adsorbate molecular orbitals will have varying contributions to the perturbation of the surface electronic structure at different adsorption sites since the symmetries of the orbitals and of the sites are different [39].

The difference in the simulated STM profiles of benzene on various adsorption sites on a Pd(111) surface may be utilized to identify the molecule's site of adsorption on several experimental EC-STM images of Pd(111) single-crystal electrodes immersed in dilute solutions of benzene. Figure 24 shows the EC-STM image of benzene on a Pd(111) electrode surface at an applied potential of 0.3 V. It is apparent that the

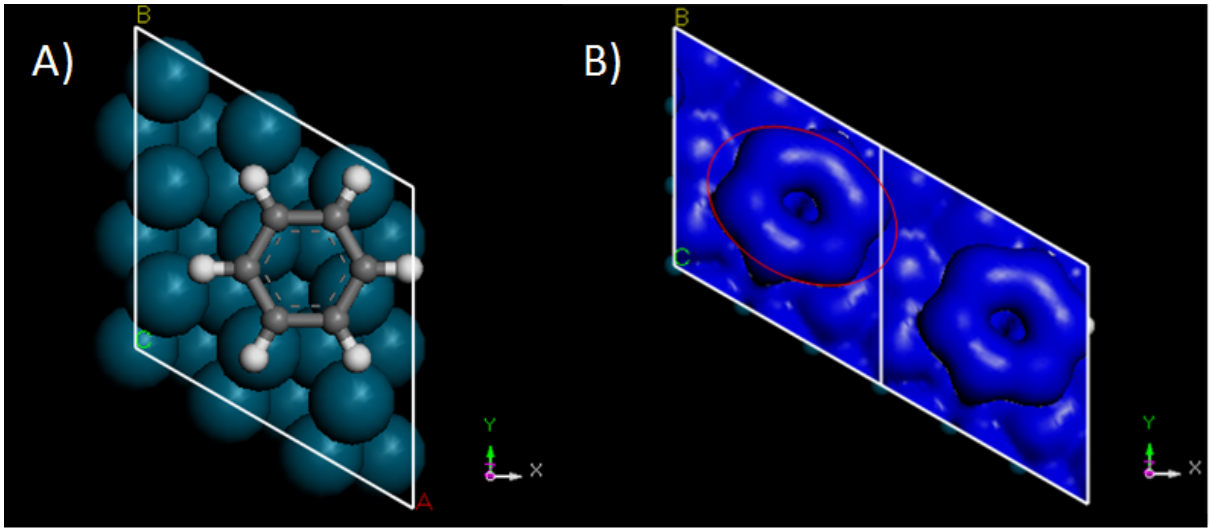

Figure 22. (A) Adsorption geometry and (B) simulated STM images of benzene chemisorbed on a 2-fold bridge site on a Pd(111) surface.

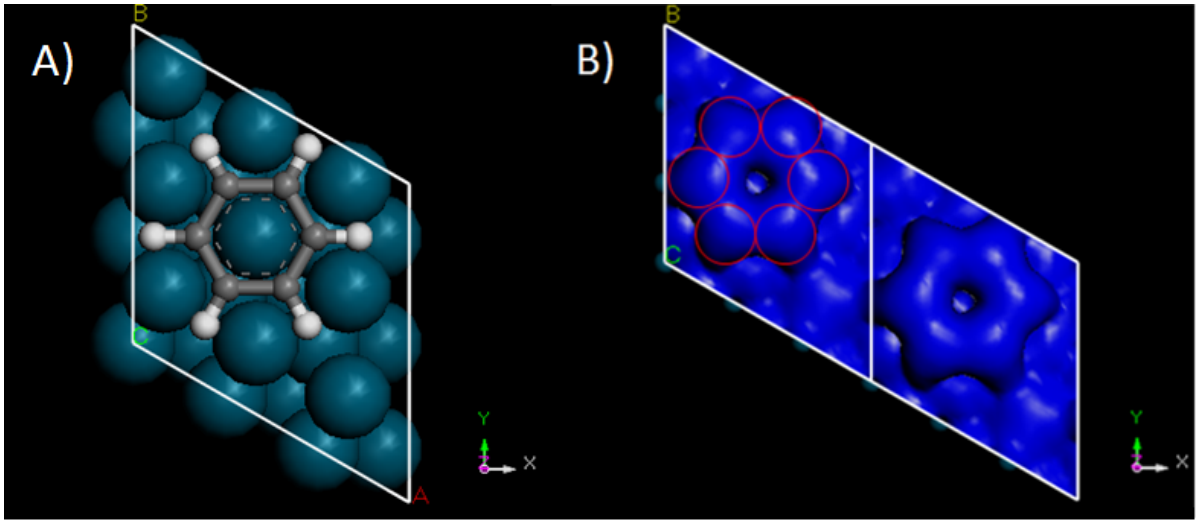

Figure 23. (A) Adsorption configuration of benzene adsorbed on a top site on a Pd(111) surface. (B) Simulated STM images of the Pd(111) surface with benzene on a top site.

molecule is composed of three spots since the fourth and faintest spot is considered to be due to a co-adsorbed water molecule [42,103]. Upon comparison of this STM image with those in Figures 21-23, it is clear that at 0.3 V, benzene is chemisorbed on a 3-fold hollow site as shown in Figure 21A. This confirms the previous findings obtained in an earlier investigation [42].

Figure 25 shows the EC-STM image of benzene on a Pd(111) surface held at 0.55 V. It is significant to note that in this STM image, the benzene molecule can be perceived as composed of two spots with one spot larger than the other to form a semi-triangular shape. Obviously, this does not correspond to any of the STM images in Figures 21-23. However, when benzene is on a position between a 3-fold hollow and a 2-fold bridge site as shown in Figure 26A, an STM profile that shows a wide and a narrow hill or lobe is obtained (Figure 26B). This simulated STM profile clearly resembles the adsorbate images in Figure 25. This validates the results proposed previously [42].

3.3 Hydroquinone Sulfonate and Benzoquinone Sulfonate on Pd(111)

The HREELS measurements in an earlier investigation indicated that at 0.1 mM, whether the solution initially contained the diphenol or its oxidized (quinone) form the species present on the surface was invariably the quinone; identical HREELS spectra were found for both species (Figure 27) [43,44]. 2,5-Dihydroxybenzenesulfonate [hydroquinone sulfonate (H_2QS)] underwent oxidative chemisorption to benzoquinone sulfonate (BQS).

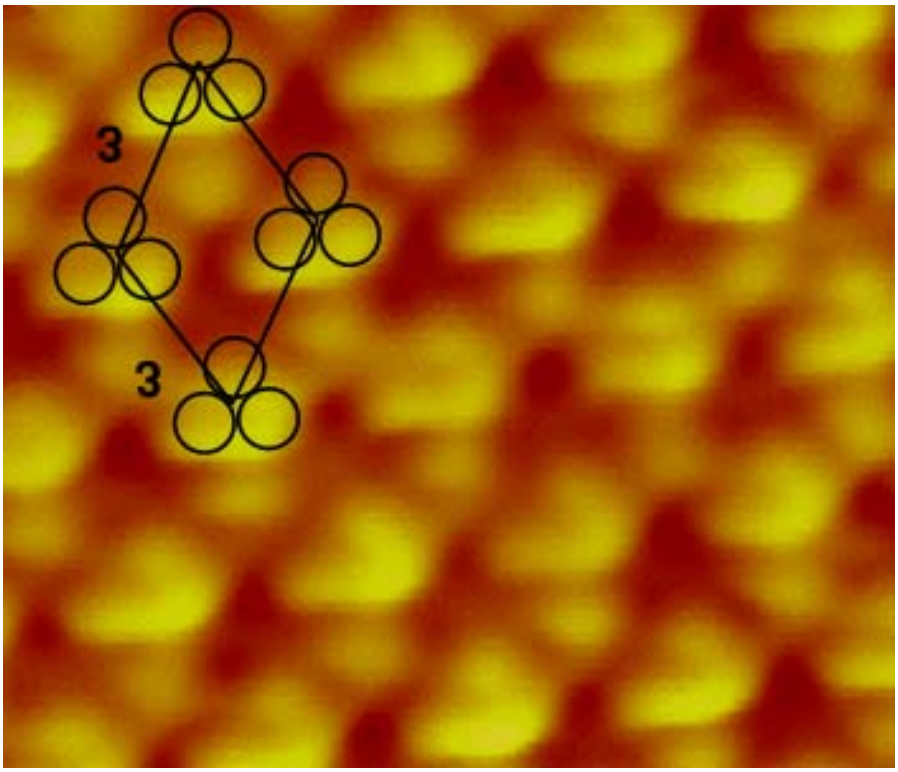

Figure 24. High-resolution EC-STM image of the Pd(111)-(3 x 3)-C_6H_6 adlayer at 0.3 V. Bias voltage: 100 mV; tunneling current: 30 nA.

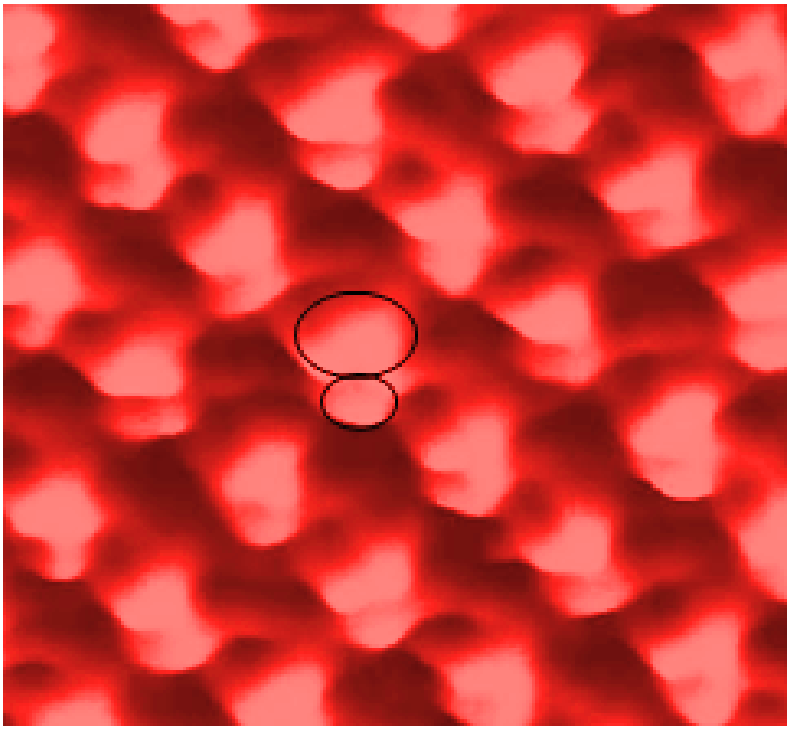

Figure 25. High-resolution EC-STM image of the Pd(111)-c(2√3 x 3)-*rect*-C_6H_6 adlattice at 0.55 V. Bias voltage: 120 mV; tunneling current: 30 nA.

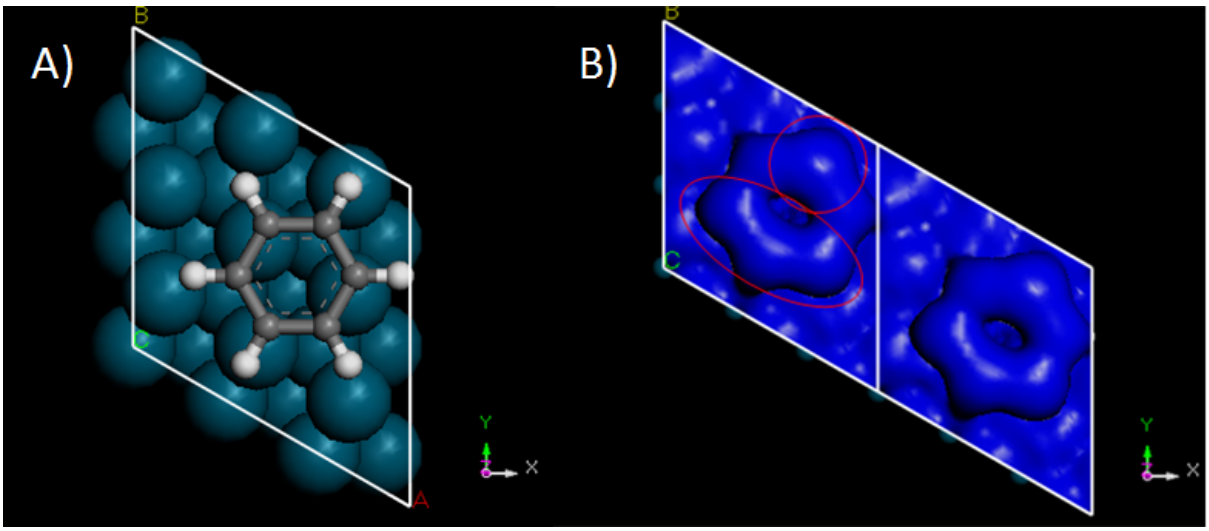

Figure 26. (A) Adsorption geometry and (B) simulated STM images of benzene chemisorbed on a site between a 3-fold hollow and a 2-fold bridge site on a Pd(111) surface.

Additional structural work, *via* EC-STM, was also undertaken and the results are displayed in Figures 28 and 29. Figure 28 shows a magnified height-shaded view of an unfiltered high-resolution EC-STM image of the BQS adlayer, designated as Pd(111)-(3×3)-BQS, with a coverage (Q) of 0.11 BQS molecules per Pd(111) surface atom. The flat orientation of the quinone group is evident and implies a surface chemical bond that involves the π-electron system of the quinone double bonds; a *completely* parallel orientation would, however, be hindered by the presence of the bulky sulfonate group as illustrated in the molecular model shown in Figure 30. The possibility then also exists that, in the chemisorbed state, the quinone ring may undergo slight distortions and the peripheral (C–S, C–S and C–O) bonds are no longer co-planar with the quinone moiety.

Two real-space geometries of the Pd(111)-(3×3)-BQS adlattice are possible, as shown in Figure 29. In both arrangements (A and B), the quinone ring is located on a high-symmetry two-fold bridge site. The only difference between the two configurations is in the location of the sulfonate O atoms. Unfortunately, it is not possible to determine from only EC-STM images which of the two possible sites is the correct one; from simple thermodynamic considerations, it had been surmised that model (A) is more favorable [43,44].

Based on the most stable adsorption configurations calculated for benzene on Pt(111) [47,48], the four most likely geometries of BQS adsorbed on Pd(111) that were chosen for this work are shown in Figure 31. BRI-0 designates the adsorbate-substrate structure in which the quinone is adsorbed on a two-fold bridge site with the peripheral

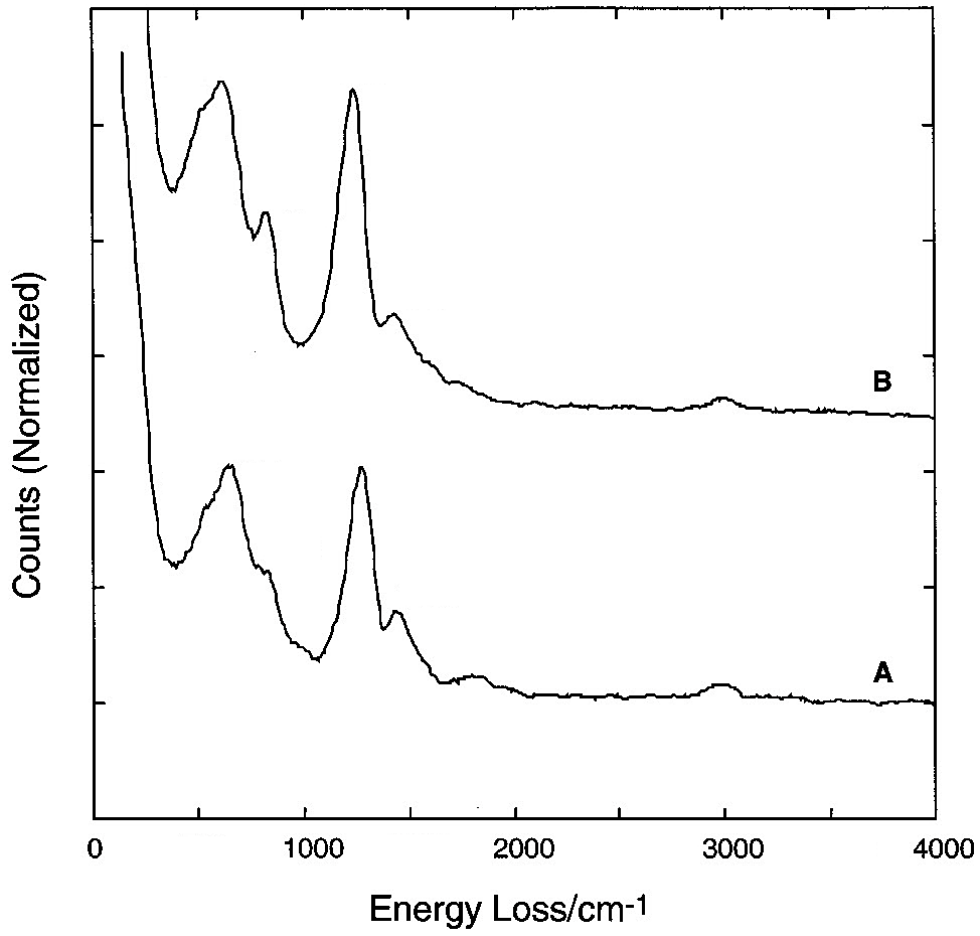

Figure 27. HREEL spectrum of a UHV-prepared Pd(111) surface. A: After emersion from an aqueous 0.1 mM H_2QS solution. B: After emersion from an aqueous 0.1 mM BQS solution. The crystal was rinsed with pure water solution prior to the HREELS measurements. Experimental conditions: incident beam energy = 4 eV. Incidence and detection angles = 62° from the surface normal. Beam current = 100 pA.

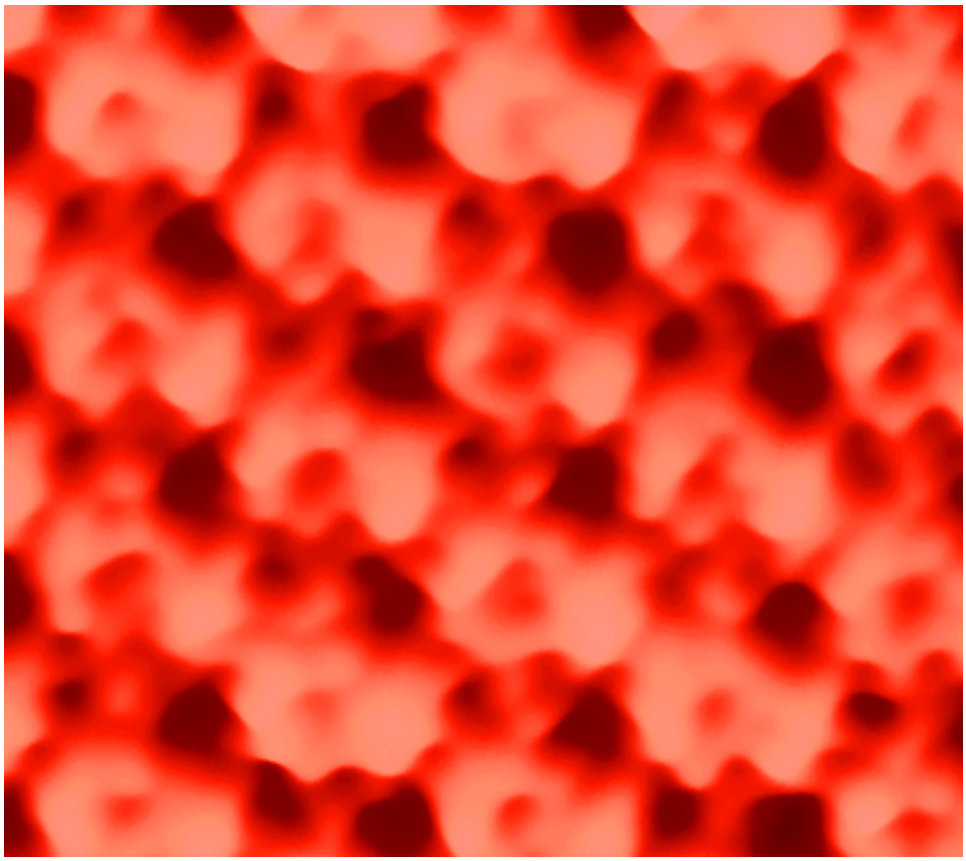

Figure 28. Magnified high-resolution EC-STM image of Pd(111)-(3×3)-BQS. Bias voltage: 100 mV; tunneling current: 30 nA.

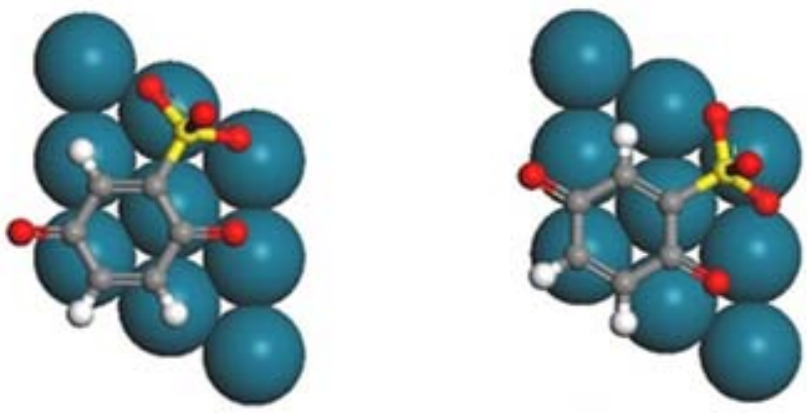

(A) (B)

Figure 29. Two possible real-space structures of the Pd(111)-(3×3)-BQS. The only difference between structures A and B are in the locations of the sulfonate O atoms.

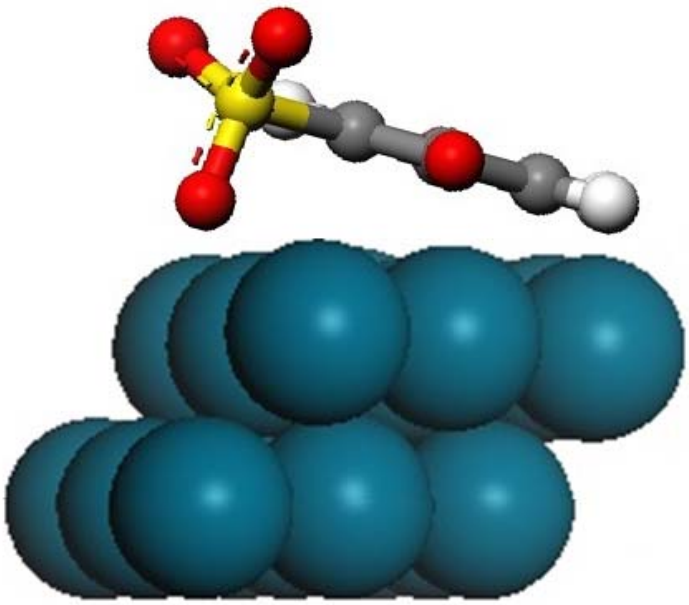

Figure 30. Molecular model of BQS chemisorbed in a tilted, flat orientation.

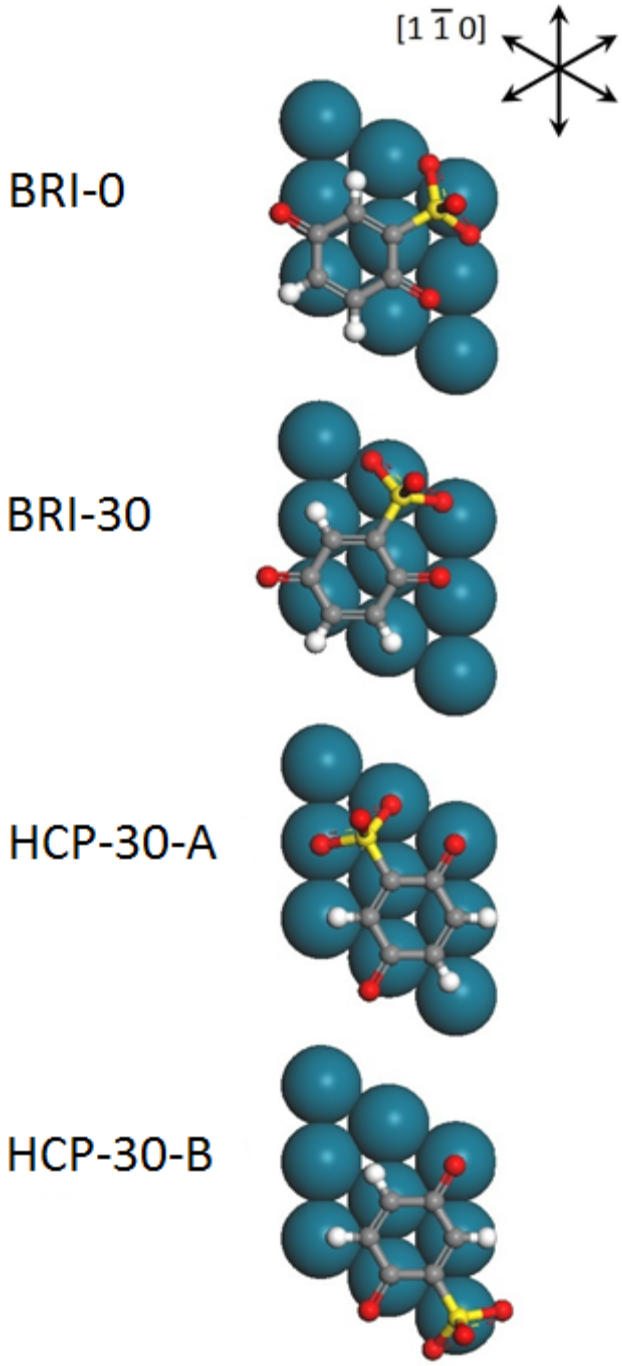

Figure 31. Four possible adsorption geometries of BQS on a Pd(111) surface (Only the uppermost Pd layer is shown).

bonds pointed in the [110] direction; BRI-30 is for when the molecule in which the bonds are rotated 30° from the [110] direction. HCP-30-A and HCP-30-B denote BQS on a three-fold hollow site with the peripheral bonds deviated 30^{o} from the [110] direction; the disparity lies on the location of the sulfonate functional group.

The calculated E_{ads} values for chemisorbed BQS as a function of optimized adsorption geometries are tabulated in Table 1. In agreement with the work cited above for benzene on Pt(111) [48], no evidence was found for significant lateral adsorbate-adsorbate interactions. However, the effect of counter cations was not explored in the present calculations although it will be addressed in a future study. The BRI-30 system has the most favorable adsorption energy; it is thus considered to be the most stable adsorbed-molecule configuration. It may be noted that such conformation is the same as that earlier conjectured from only EC-STM results [44].

By comparing the optimized structure of an isolated BQS molecule presented in Figure 32 with the BRI-30 Pd(111)-BQS interfacial system shown in Figure 33, it can be noted that when the molecule is chemisorbed flat on the metal surface, the C–H and C–S bonds are no longer co-planar with the quinone ring; they are slightly tilted (*ca.* 20^{o}) and directed away from the surface. This calculated puckered-ring structure of BQS may help explain two unexpected experimental observations [43,44]: (i) In the EC-STM image, there is an enhanced brightness of the 3,4-edge; this could arise from the fact that the two adjacent carbon atoms are located slightly above the rest of the quinone moiety. (ii) In what may appear as a violation of the metal-surface dipole selection rule, the C–H stretch mode is (weakly) HREELS-active; this may be due to a vibrational component

Table 1. Adsorption Energies (eV) of BQS at Various Adsorption Geometries on Pd(111)[a]

Adsorption geometry	Adsorption Energy (E_{ads})
BRI-0	–2.14
BRI-30	–2.41
HCP-30-A	–1.81
HCP-30-B	–1.02

[a]All calculations were performed using a 3 × 3 surface unit cell with a fixed cell volume equal to that of a bare Pd surface. The energy of the benzoquinone sulfonate molecule was calculated separately in a 12 x 12 x 12 $Å^3$ cell.

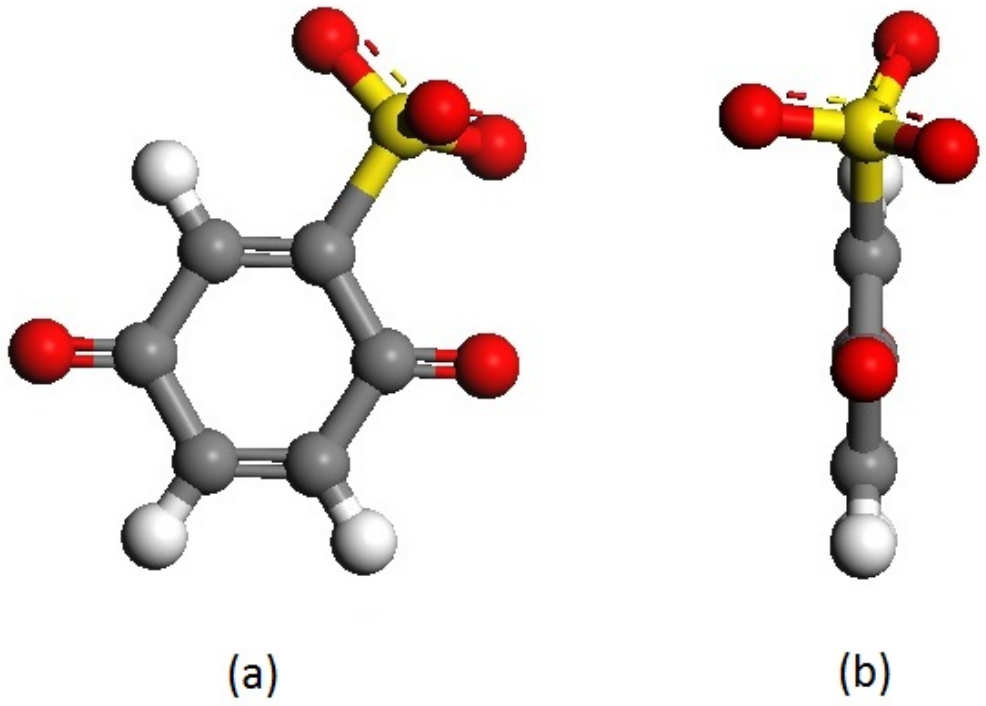

Figure 32. Optimized structure of an isolated BQS molecule: (A) top view and (B) side view.

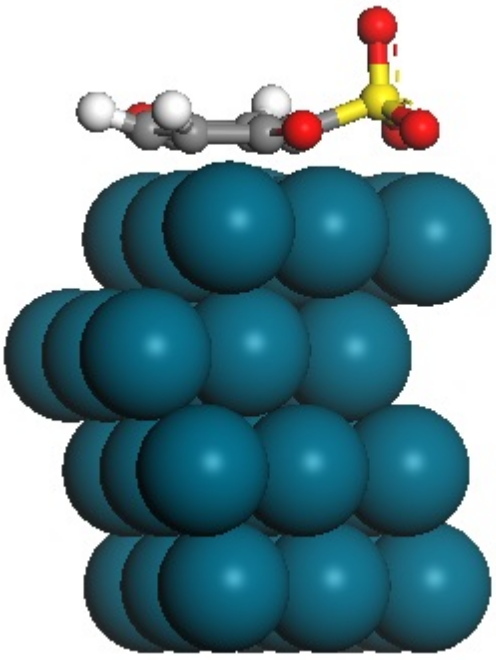

Figure 33. Side view of the optimized adsorption geometry of BRI-30.

perpendicular to the surface spawned by the non-coplanarity of the C–H bonds.

3.4 Hydroquinone and Benzoquinone on Pd(111)

Results from studies on the chemisorption of diphenols on Pd(*hkl*) surfaces based on EC, HREELS, and STM showed that when a well-defined Pd(111) electrode is immersed in a dilute aqueous solution (< 0.1 mM) of hydroquinone (H_2Q), an immediate chemisorption reaction occurs in which the surface-coordinated H_2Q molecule undergoes spontaneous oxidation to benzoquinone (Q) [23,51]. The latter adopts a Pd(111)-(3 x 3)-Q adlayer structure as shown in the EC-STM image in Figure 34. Detailed analysis of the EC-STM data indicated that, when Q is chemisorbed parallel to the Pd(111) surface: (i) it adopts an essentially flat orientation with a slight tilt, and (ii) the quinone ring is centered on a two-fold bridge site with two possible structures as illustrated in Figures 35A and 35B. It should be noted that the difference in the two structures lies in the location of the O atoms: In Figure 35A, the O atoms occupy atop sites; in Figure 35B, they are located on 2-fold sites. Unfortunately, it is not possible to determine from the EC-STM images alone which of the two possible geometries is the actual structure.

It was proposed from experimental results that the molecules are adsorbed parallel to the surface, albeit at a slight tilt, and with the C_2 axis rotated 30^o from the hexagonal close-packed [110] direction of the Pd(111) substrate. Again, from this, two real-space structures of the adlayer were proposed (Figures 35A and 35B).

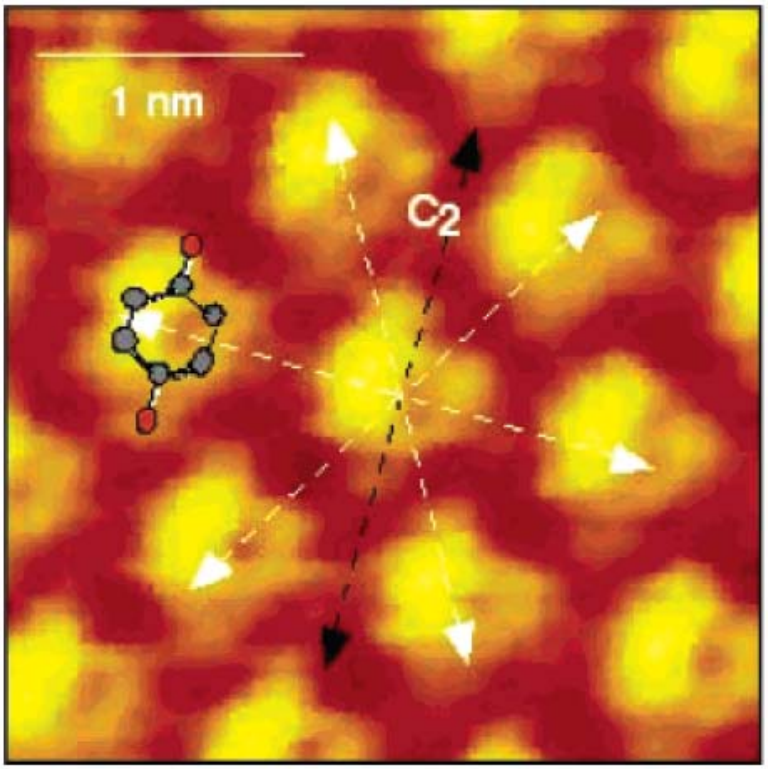

Figure 34. Unfiltered high-resolution EC-STM image of the (3 x 3)-Q adlayer of the Pd(111) electrode surface immersed in a 0.1 mM solution of Q in 0.05 M H_2SO_4 at 0.5 V. Bias voltage, 120 mV; tunneling current, 30 nA [52]. This figure is reproduced with permission from Y.-G. Kim, J.H. Baricuatro, M.P. Soriaga, Langmuir 22 (2006) 10762. Copyright American Chemical Society.

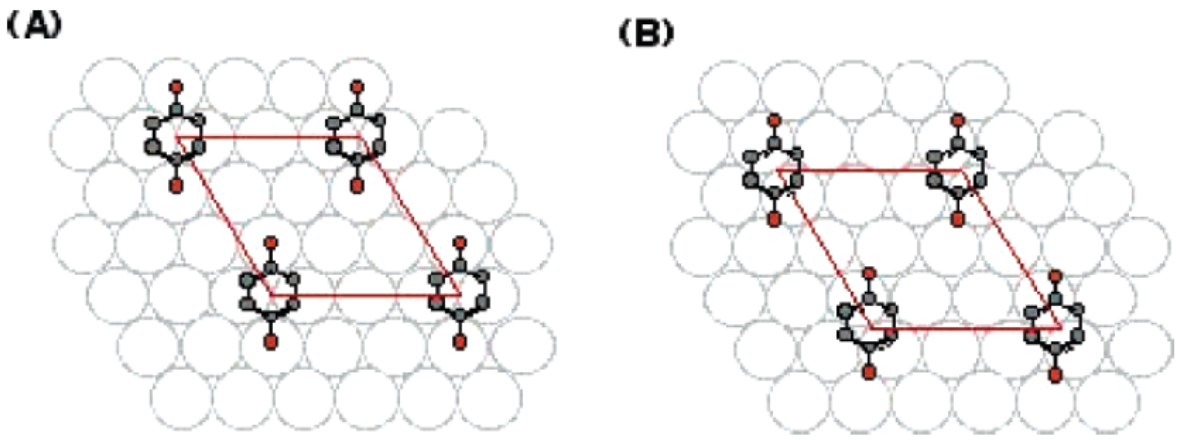

Figure 35. Possible real-space structures of Pd(111)-(3 x 3)-Q from EC-STM results. The oxygen atoms are located above atop sites in structure A but occupy bridge sites in B [52]. This figure is reproduced with permission from Y.-G. Kim, J.H. Baricuatro, M.P. Soriaga, Langmuir 22 (2006) 10762. Copyright American Chemical Society.

Unfortunately, differentiation between the two domains to identify the most likely structure could not be achieved from only the EC-STM images. Using a similar solution concentration, an HREEL spectrum was also obtained, Figure 36 [51]. It was proposed (Table 2) that peaks 1, 2, 3, and 4 correspond to aromatic out-of-plane bending (γ_{C-H}), aromatic in-plane bending (δ_{C-H}) or stretch ($\nu_{C=C}$), carbonyl stretch ($\nu_{C=O}$), and C–H stretch (ν_{C-H}) modes, respectively. The absence of a hydroxyl stretch (ν_{O-H}) peak at around 3600 cm^{-1} indicates the absence of a phenolic O–H functional group due to the oxidation of H_2Q to Q during chemisorption [51]. In addition, if the molecule adopts a rigidly flat (η^6) adsorbed-aromatic orientation, the metal-surface dipole selection rule would render peaks 2, 3, and 4 HREELS-inactive [84,85]; thus, the presence of peaks 2 to 4 suggests that chemisorbed Q is not entirely oriented flat on the surface, but is tilted slightly.

Figure 37 shows possible adsorbed-molecule structures of Q on Pd(111) based on the adsorption of a wide variety of aromatic compounds on Pt(111) and Pd(111) electrode surfaces [47,48]. Holl, Bri, and Atop represent adsorption centered on 3-fold hollow, 2-fold bridge, and atop sites, respectively; 0 and 30 correspond to the angles between the molecule's C_2 axis (or peripheral C–H and C=O bonds) and the [110] direction of the metal substrate. In some of the adsorption structures, two positions exist at which the carbonyl oxygen can be located; these are labeled A and B to differentiate. It is important to note that the structures in Figures 35A and 35B correspond to Bri-30-A and Bri-30-B, respectively.

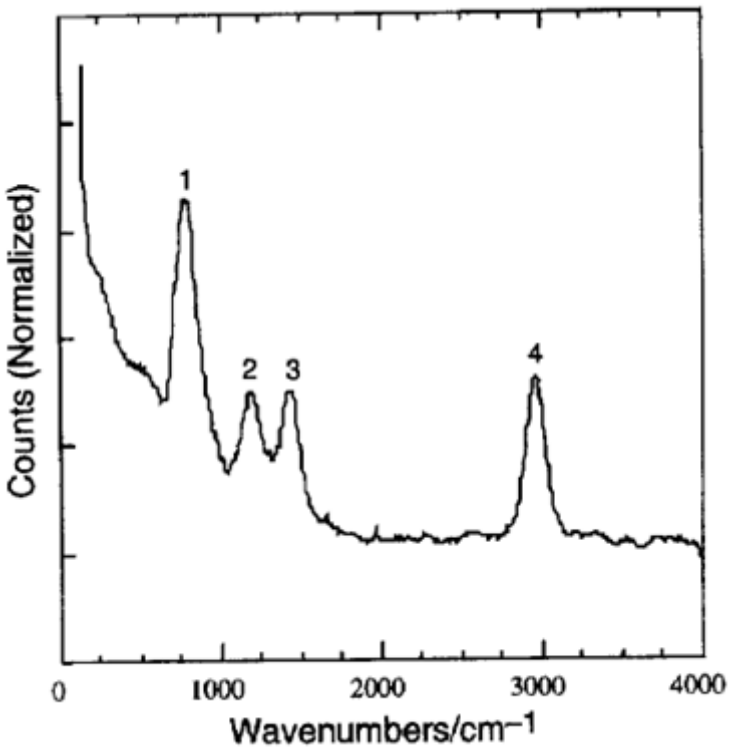

Figure 36. HREEL spectrum of a Pd(111) surface after emersion from a 0.1 mM aqueous solution of Q in 1 mM TFA. Peaks 1, 2, 3, and 4 correspond to aromatic $\gamma_{C\text{-}H}$, aromatic $\delta_{C\text{-}H}$, $\nu_{C=O}$, and $\nu_{C\text{-}H}$ modes, respectively [51]. This figure is reproduced with permission from J.E. Soto, Y.-G. Kim, M.P. Soriaga, Electrochem. Commun. 1 (1999) 135. Copyright Elsevier.

Table 2. Vibrational (HREELS) Frequencies of Adsorbed Benzoquinone on Pd(111) [51]

Peak	Description	Frequency (cm^{-1})
1	Out-of-plane C–H bend	810
2	C–H bend	1230
3	C=O stretch	1466
4	C–H stretch	3007

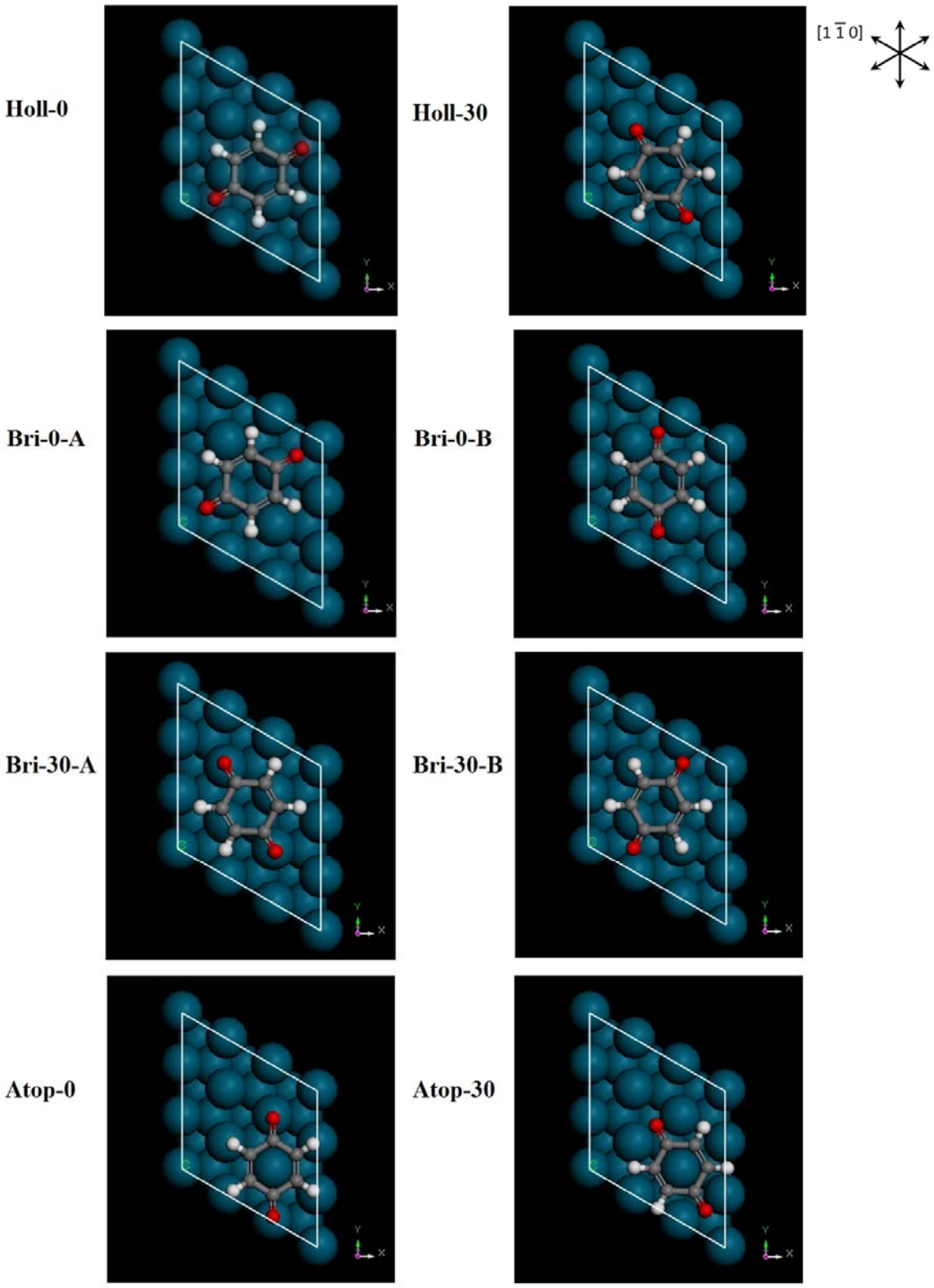

Figure 37. Possible adsorption structures of benzoquinone on a Pd(111) surface.

The adsorption energy of each structure is calculated and is presented in Table 3. E_{ads} values for Bri-0-B, Atop-0, and Atop-30 were not calculated since no stable geometries were obtained for these structures after geometry optimization. It shows that Bri-30-B, which is one of the structures proposed from EC-STM results, has the most negative adsorption energy (-1.09 eV) and may be interpreted as the most stable or probable structure. It is also important to mention that a significant difference in adsorption energy exists between the proposed Bri-30-A and Bri-30-B structures. Identification of the most likely structure based on a comparison of the adsorption energies at different adsorption sites has already been adopted in previous studies on benzene [47,48].

In an attempt to ascertain the actual structure, the frequencies of the different vibrational states in Bri-30-A and Bri-30-B, the two models proposed from EC-STM results, were calculated and are shown in Figure 38. It can be observed that the most significant difference is the frequency of the C=O stretch; 1564 cm^{-1} for Bri-30-A while 1464 cm^{-1} for Bri-30-B. Since the experimental ν(CO) is 1466 cm^{-1} from HREELS results (Table 2), this may indicate that Figure 35B or Bri-30-B may indeed most likely be the actual structure.

Figure 39 shows Bri-30-B after geometry optimization. Instead of a simple tilt of the ring as previously thought, the peripheral C–H bonds of the quinone ring are evidently tilted away from the surface at an angle of approximately 20°; this is clearly different from the planar Q molecule shown in Figure 40. Such deviation from planarity may explain why the in-plane C-H modes of the quinone ring are

Table 3. Adsorption Energy (eV) of Benzoquinone at Various Adsorption Sites on Pd(111)[a]

Adsorption structure	Adsorption Energy (E_{ads})
Holl-0	– 0.64
Holl-30	– 0.83
Bri-0-A	– 0.39
Bri-0-B	No stable structure
Bri-30-A	– 0.66
Bri-30-B	– 1.09
Atop-0	No stable structure
Atop-30	No stable structure

[a] All calculations were performed using a 3 × 3 surface unit cell with a fixed cell volume equal to that of a bare Pd surface. The energy of the benzoquinone molecule was calculated separately in a 12 x 12 x 12 $Å^3$ cell.

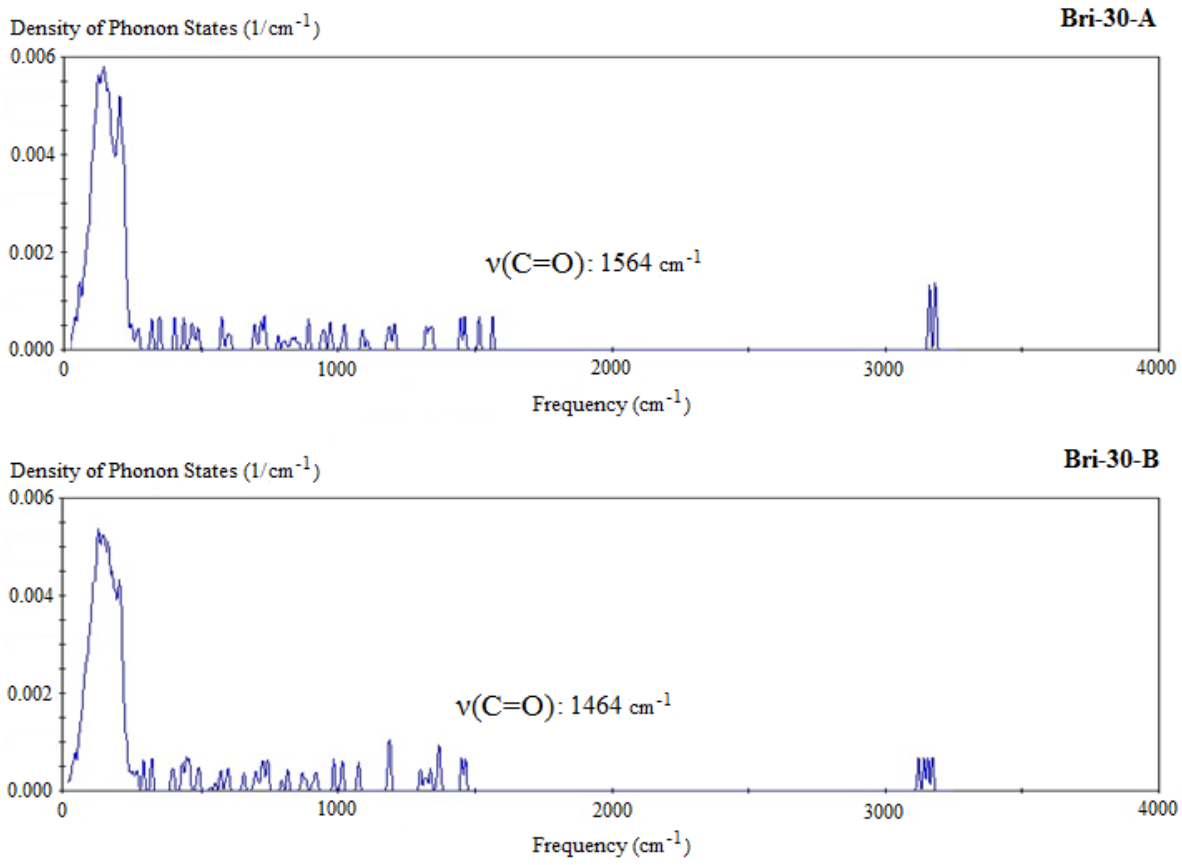

Figure 38. Calculated vibrational frequencies of various vibrational states in Bri-30-A and Bri-30-B.

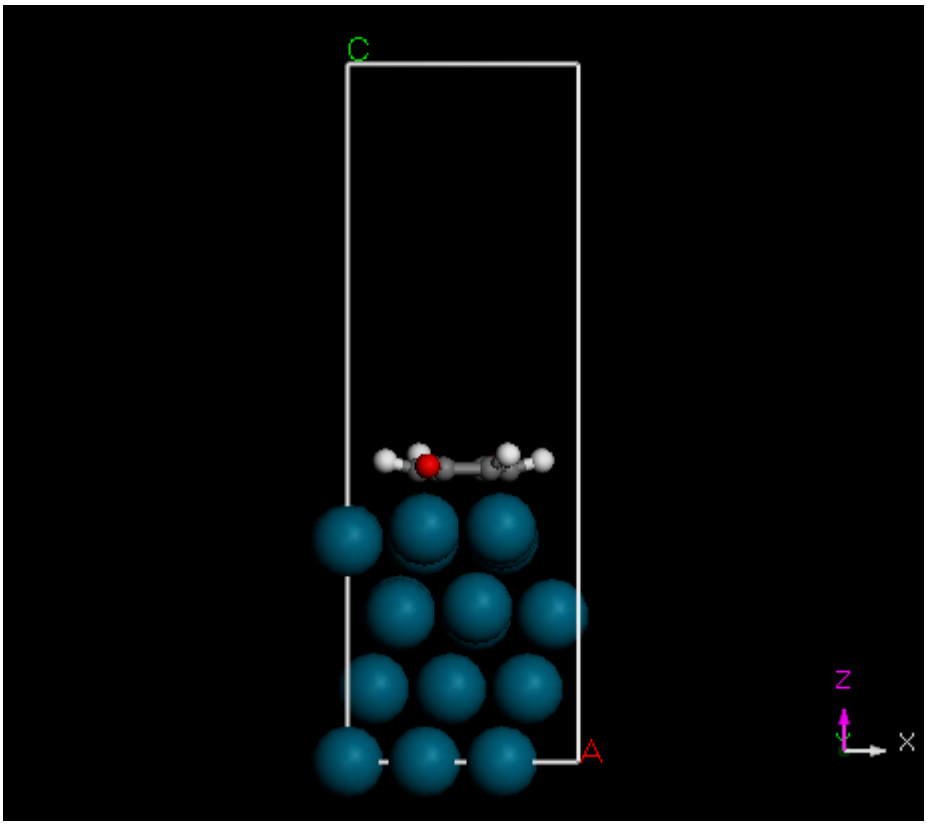

Figure 39. Side view of the optimized adsorption structure of Bri-30-B.

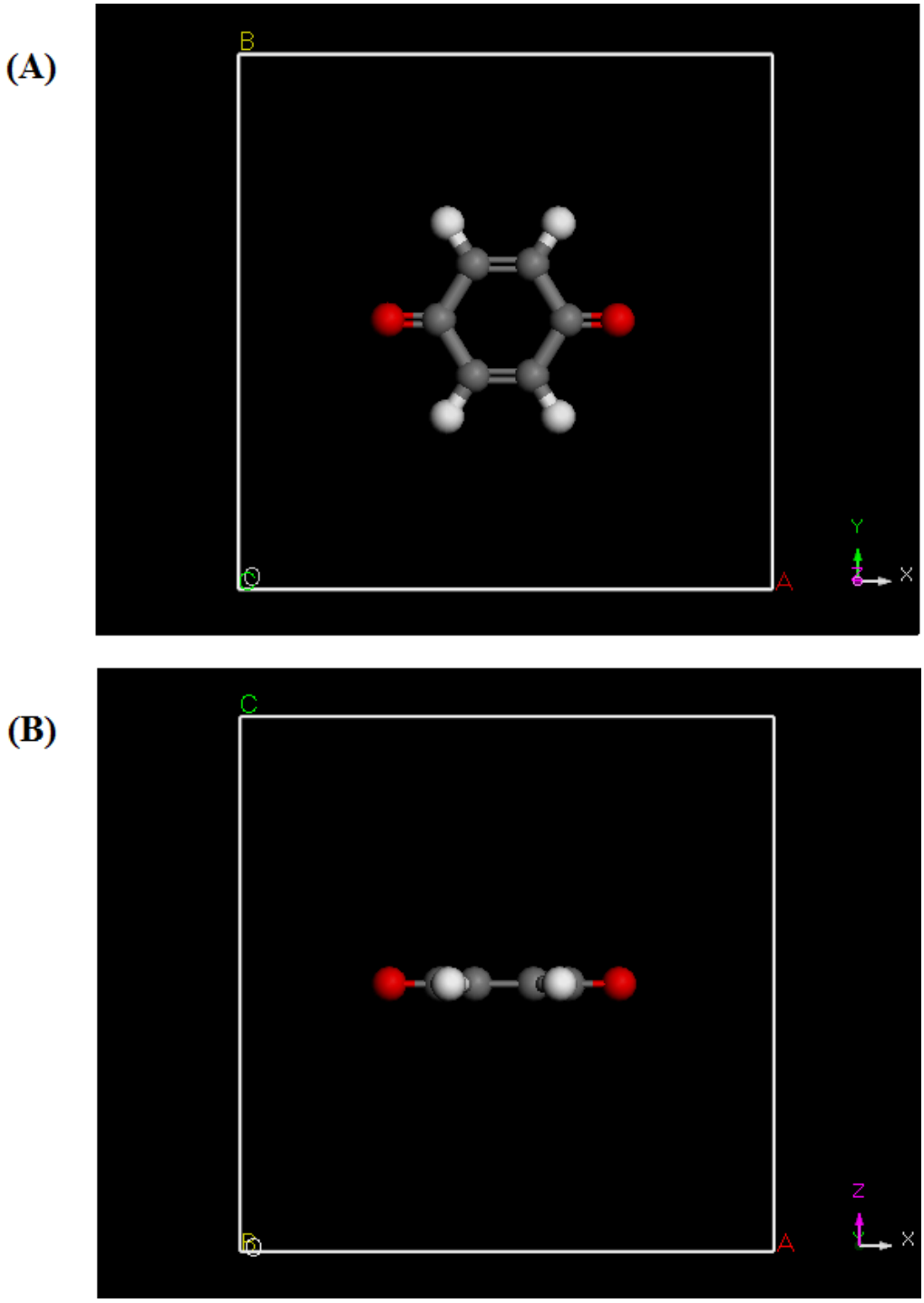

Figure 40. Optimized geometry of an isolated benzoquinone molecule: (A) top view and (B) side view.

HREELS-active in the specular direction. Similar behavior has been previously observed for benzene on Pt(111) [47,48].

It is important to mention that the method of identifying the most probable adsorption structure by comparing the theoretical and experimental vibrational spectra has previously been used on the study of the adsorption of benzene on Pt(111), Pd(111), and Rh(111) [48]. Furthermore, the computational method used in this work to obtain theoretical vibrational spectra has earlier been validated by comparing the spectra with those obtained experimentally and from well-known computational methods [104-108].

3.5 2,3-Dimethyhydroquinone and 2,3-Dimethylbenzoquinone on Pd(111)

Figure 41 shows the chemisorption isotherm of 2,3-dimethylhydroquinone on a polycrystalline Pd electrode [118]. The absolute surface concentration of the adsorbed molecule or surface coverage at low aqueous-solution concentrations (≤ 0.05 mM) was observed to be different from that at high concentrations (≥ 1 mM), which also has a higher value. This implies that the adsorbed-molecule surface concentration changes and suggests that the orientation of the adsorbed quinone also changes. At low concentrations, the surface coverage of the organic molecule is 0.18 nmol/cm^2, which corresponds to an experimental molecular cross section of 92.2 Å^2. This experimental value is larger than the calculated molecular cross section [9,23,109-112] of 68.7 Å^2 for the flat-adsorbed orientation and implies that the molecules are still parallel to the surface but are not closely packed. But, at high concentrations, the surface coverage is 0.51 nmol/cm^2, which corresponds to an experimental molecular cross section of

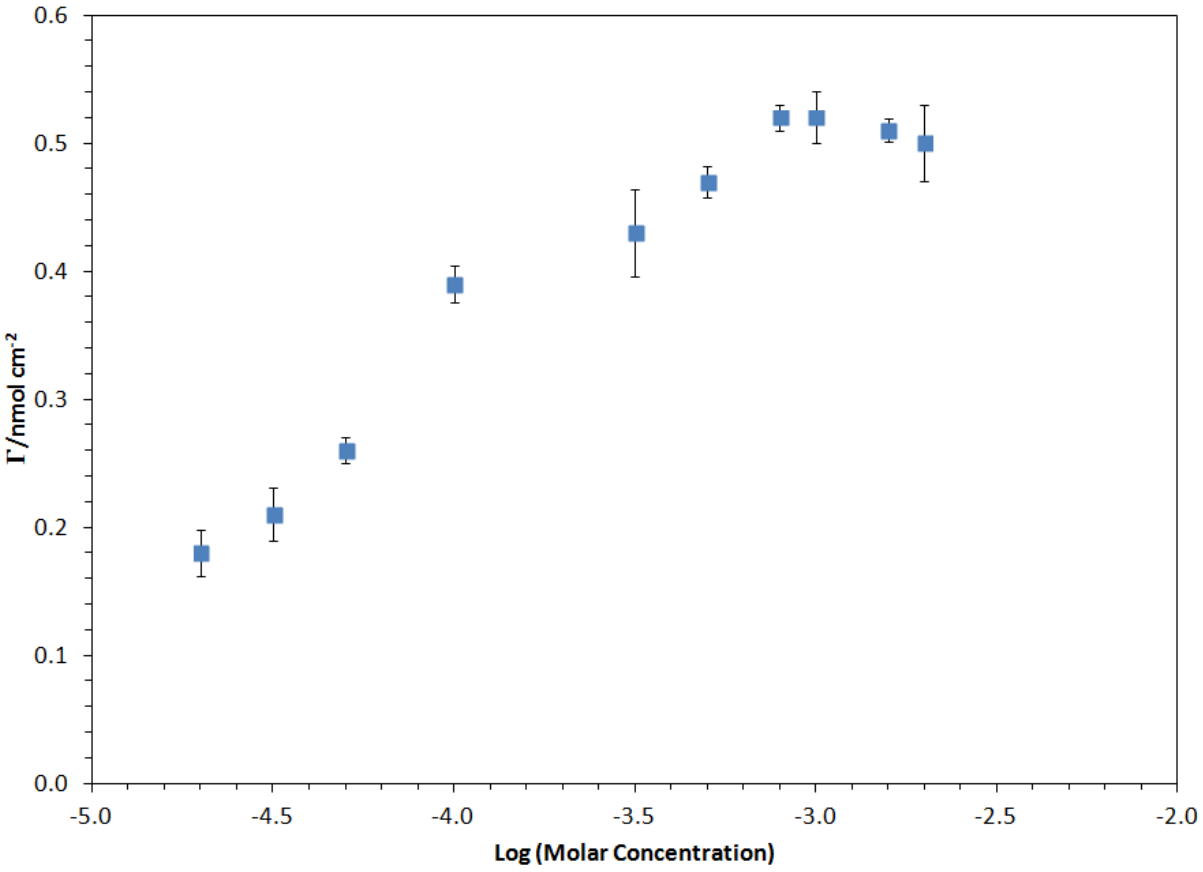

Figure 41. Chemisorption isotherm, Γ vs. log C plot, for 2,3-dimethylhydroquinone at a smooth polycrystalline Pd electrode.

32.5 $Å^2$ that is close to the computed cross section of 33.6 $Å^2$. This calculated cross section represents an orientation where the aromatic compound is chemisorbed edge-wise or perpendicular to the surface through C–H activation. This behavior is similar to that observed on hydroquinone and benzoquinone on polycrystalline Pd [23], various quinones on Pt(pc) [113,114], and 2,5-dihydroxybenzoic acid on Au(111) [115].

Figure 42 presents HREELS spectra of 0.05 mM, 0.5 mM and 5 mM 2,3-dimethylhydroquinone on Pd(111) surfaces [81]. Notable peaks common to all spectra are observed at 2969, 1429, 1223, and 611 cm^{-1}, which correspond to C–H stretching (ν_{C-H}), CO stretching (ν_{CO}), C–H bending (δ_{C-H}), and aromatic out-of-plane C–H bending (γ_{C-H}) vibrational modes.

Figure 43 presents the same TLE-based chemisorption isotherm in Figure 41 but instead of the actual surface coverages, the ratio relative to the lower coverage values is used. In addition, an HREELS-based chemisorption isotherm is made by plotting the aromatic out-of-plane C–H bending peak intensities at 611 cm^{-1} as a function of the concentration. Again, the ratio relative to the lowest peak intensity instead of the absolute intensity values are used [116]. It can be noted that there is a close resemblance between the two kinds of isotherms. This implies that both TLE and HREELS suggest that 2,3-dimethylhydroquinone undergoes reorientation on the Pd(111) surface; at low concentrations, the molecule is chemisorbed flat on the surface while at higher concentrations, the organic compound is adsorbed edgewise on the surface.

Earlier studies on hydroquinone chemisorbed on well-defined Pd(111) and Pd(100) surfaces based on EC, HREELS, and STM revealed that at low concentrations,

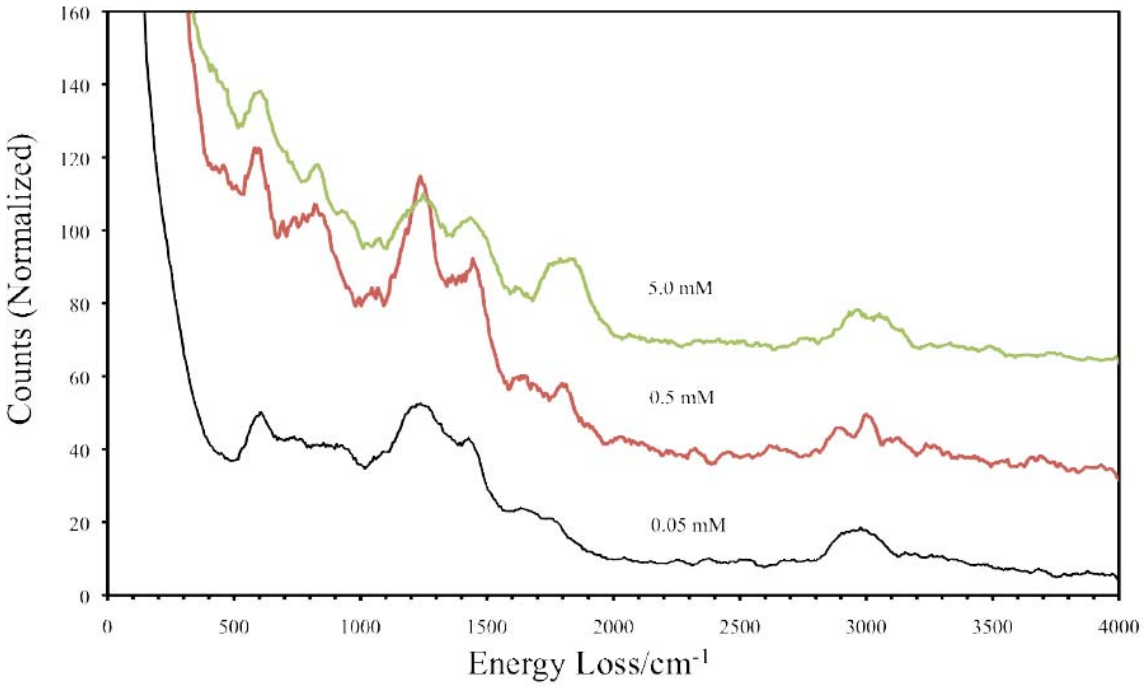

Figure 42. HREELS spectra of Pd(111) surfaces immersed from 0.05 mM, 0.5 mM, and 5.0 mM solutions of 2,3-dimethylhydroquinone.

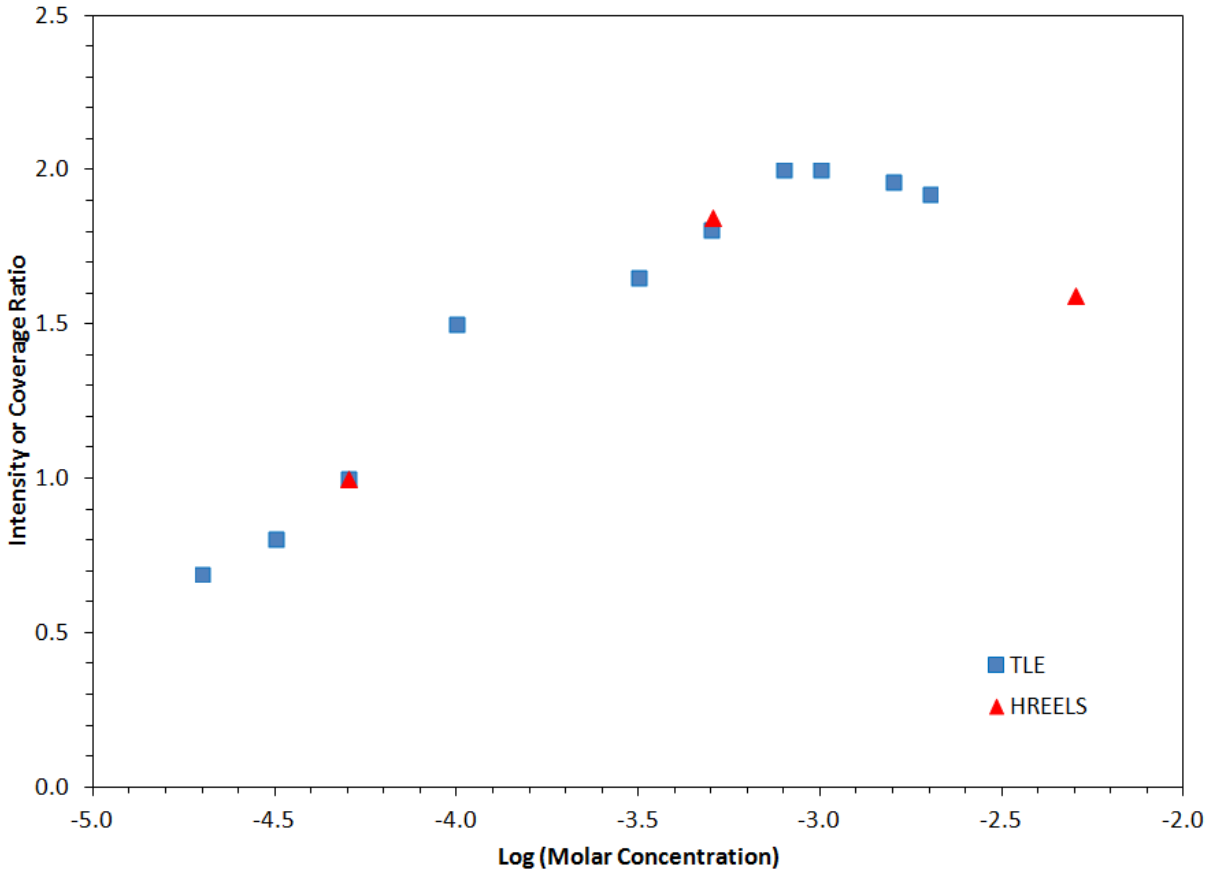

Figure 43. Comparison of 2,3-dimethylhydroquinone chemisorption isotherms, expressed as ratios of TLE surface packing density (Γ/Γ_{Lower}) and HREELS integrated intensity (A/A_{Lower}).

whether the solution initially contained the diphenol or its oxidized quinone form (benzoquinone), the species on the surface was the quinone [51]; identical HREELS spectra were obtained for both species. This means that when hydroquinone is chemisorbed flat on the surface, it undergoes oxidative chemisorption producing benzoquinone. A similar behavior is observed on 2,5-dihydroxybenzenesulfonate (hydroquinone sulfonate) [43,44]. Hence, it can also be inferred that 2,3-dimethylhydroquinone is oxidatively chemisorbed forming 2,3-dimethylbenzoquinone when chemisorbed parallel to the surface.

To determine the flat-adsorbed structure and adsorption site, several possible adsorption structures of 2,3-dimethylbenzoquinone are modeled and geometrically optimized by DFT as shown in Figure 44 based from the different adsorption structures found for benzoquinone. Holl, Bri, and Atop represent adsorption where the quinone ring is chemisorbed or centered on three-fold hollow, two-fold bridge, and atop sites, respectively; 0 and 30 correspond to the angle of the compound's peripheral C–H, C=O, or C–CH_3 bonds relative to the [110] direction of the metal substrate. In some of the structures, there are two possible locations the carbonyl oxygen can be positioned; these are labeled with A and B to differentiate the two geometries.

The calculated adsorption energies of the structures in Figure 44 are presented in Table 4. It can be noted that Bri-30-B has the most negative adsorption energy value of -0.70 eV thus corresponds to the most stable adsorption structure. According to previous DFT studies on benzene, hydroquinone, and hydroquinone sulfonate, the above structure must be the actual or the most probable structure [47].

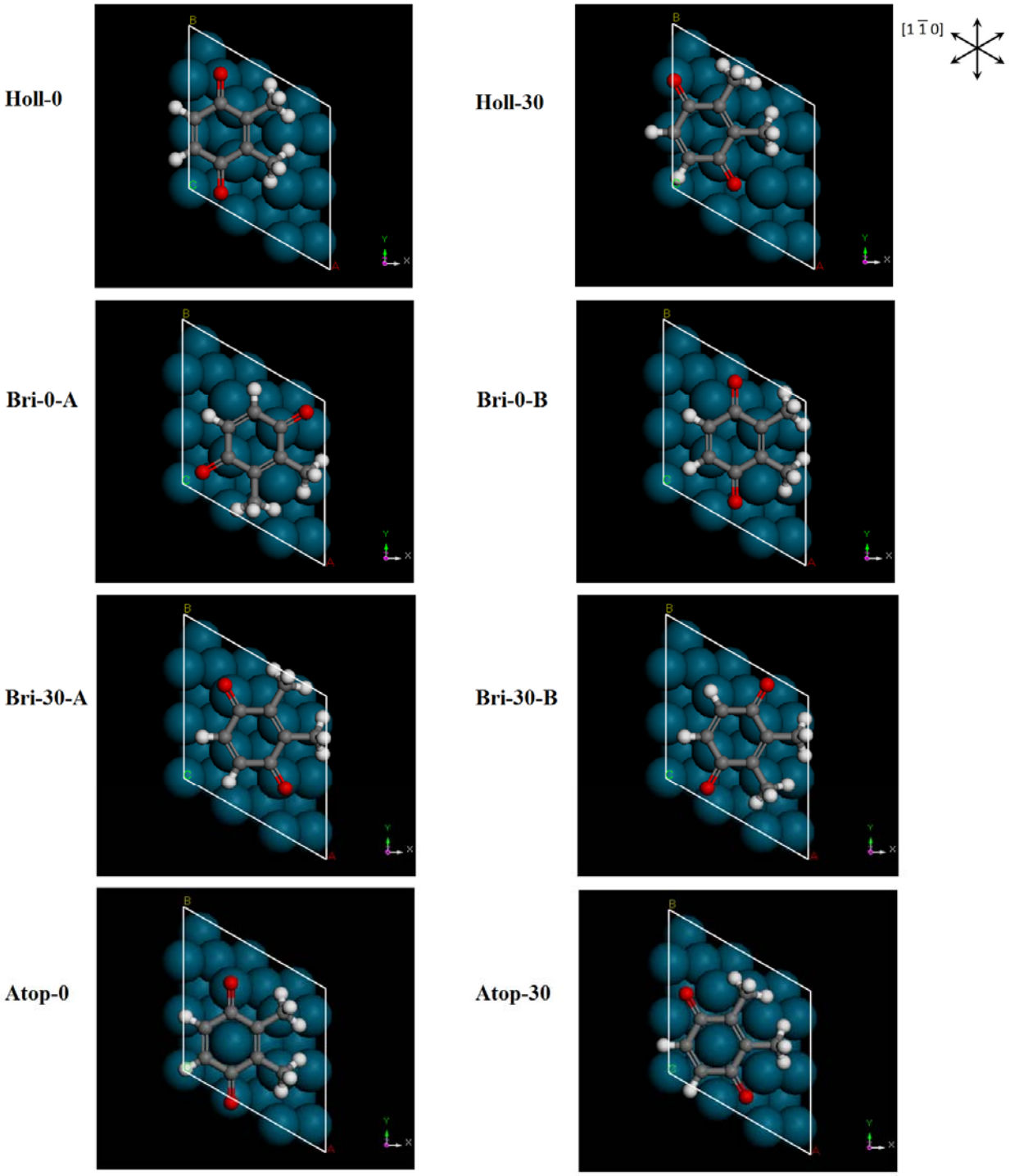

Figure 44. Possible adsorption structures of 2,3-dimethylbenzoquinone on Pd(111) surfaces.

Table 4. Adsorption Energy (eV) of 2,3-Dimethylbenzoquinone at Various Adsorption Sites on Pd(111)[a]

Adsorption structure	Adsorption Energy (E_{ads})
Holl-0	– 0.28
Holl-30	No stable structure
Bri-0-A	– 0.11
Bri-0-B	No stable structure
Bri-30-A	– 0.38
Bri-30-B	– 0.70
Atop-0	No stable structure
Atop-30	No stable structure

[a]All calculations were performed using a 3 × 3 surface unit cell with a fixed cell volume equal to that of a bare Pd surface. The energy of the 2,3-dimethylbenzoquinone molecule was calculated separately in a 12 x 12 x 12 $Å^3$ cell.

Figure 45 shows the optimized structure of Bri-30-B or the structure of 2,3-dimethylbenzoquinone chemisorbed parallel to the surface. It can be observed that similar to those found for benzene, benzoquinone, and benzoquinone sulfonate, the peripheral bonds of the quinone ring are tilted away from the surface [47].

The previous study on hydroquinone on Pd surfaces [23] also indicated that at high concentrations, oxidative chemisorption occurs through C–H activation yielding edge-oriented diphenolic species instead of the oxidized benzoquinone form as confirmed by infrared (IR) spectra [117]. Figure 46 shows the optimized structure of the edge-oriented diphenolic specie on the Pd(111) surface as suggested by IR, TLE, and HREELS. Only one possible adsorption structure for this orientation was obtained and the molecule is chemisorbed on a bridge site.

To ascertain that the compound assumes different orientations at different concentrations, theoretical vibrational spectra were calculated. Figure 47 presents the calculated vibrational spectra for the flat-adsorbed specie (Figure 45) while Figure 48 shows the theoretical spectra for the edge-oriented molecule (Figure 46). The most notable difference is the frequency of the CO stretch; 1458 cm^{-1} for the former and 1635 cm^{-1} for the latter. It can also be observed on the experimental HREELS spectra in Figure 42 that at 5.0 mM, the vibrational peak at around 1700 cm^{-1} is greatly enhanced while this peak is almost non-existent at 0.05 mM. This implies that indeed at a low concentration (0.05 mM), 2,3-dimethylhydroquinone is chemisorbed as 2,3-dimethylbenzoquinone oriented parallel to the surface whereas at a higher concentration

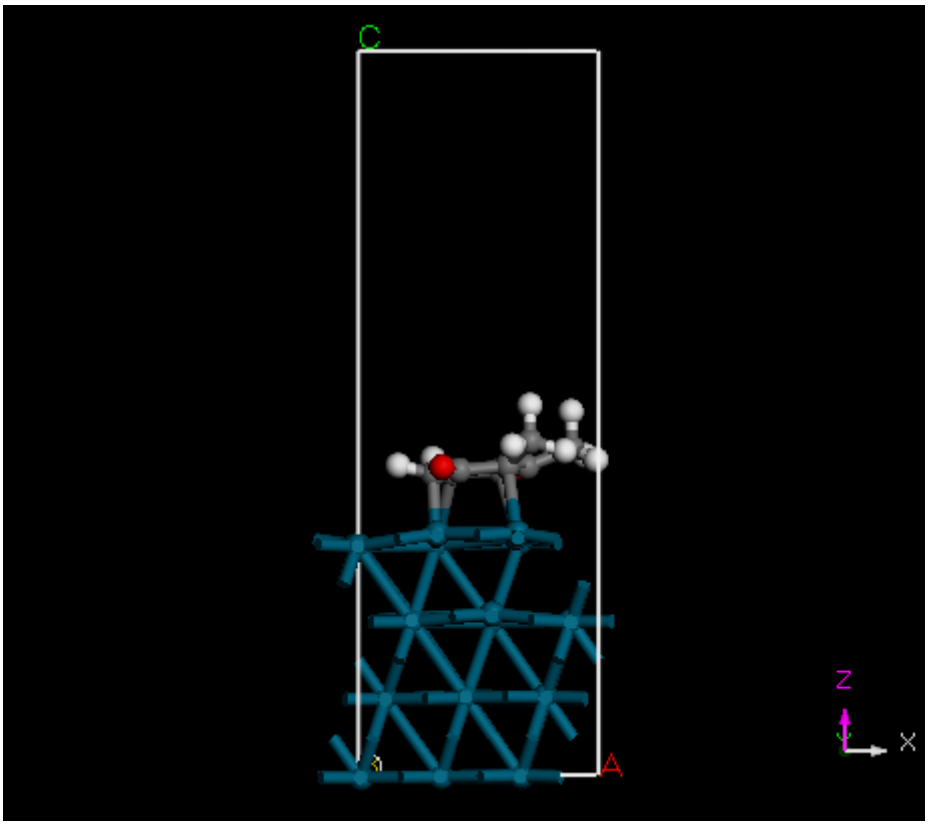

Figure 45. Optimized adsorption structure of the flat-adsorbed 2,3-dimethylbenzoquinone (Bri-30-B) on the Pd(111) surface.

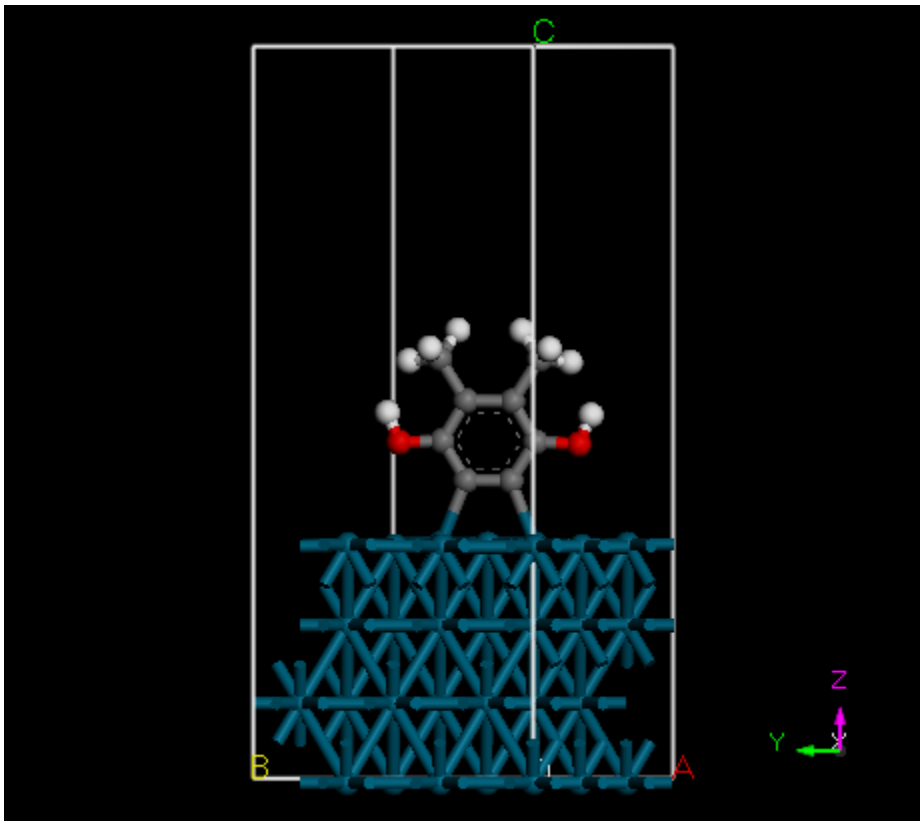

Figure 46. Optimized adsorption structure of the edge-oriented 2,3-dimethylhydroquinone molecule.

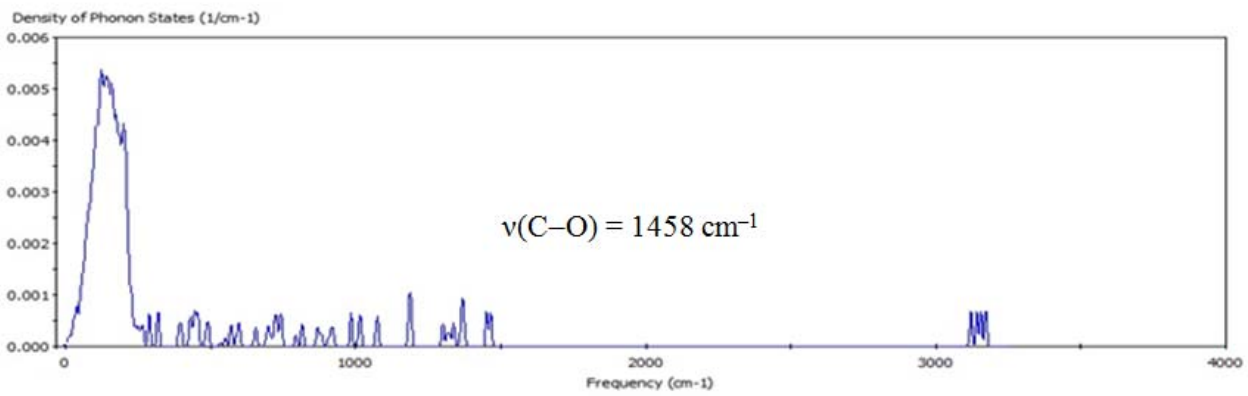

Figure 47. Computed vibrational spectrum of the flat-adsorbed 2,3-dimethylbenzoquinone.

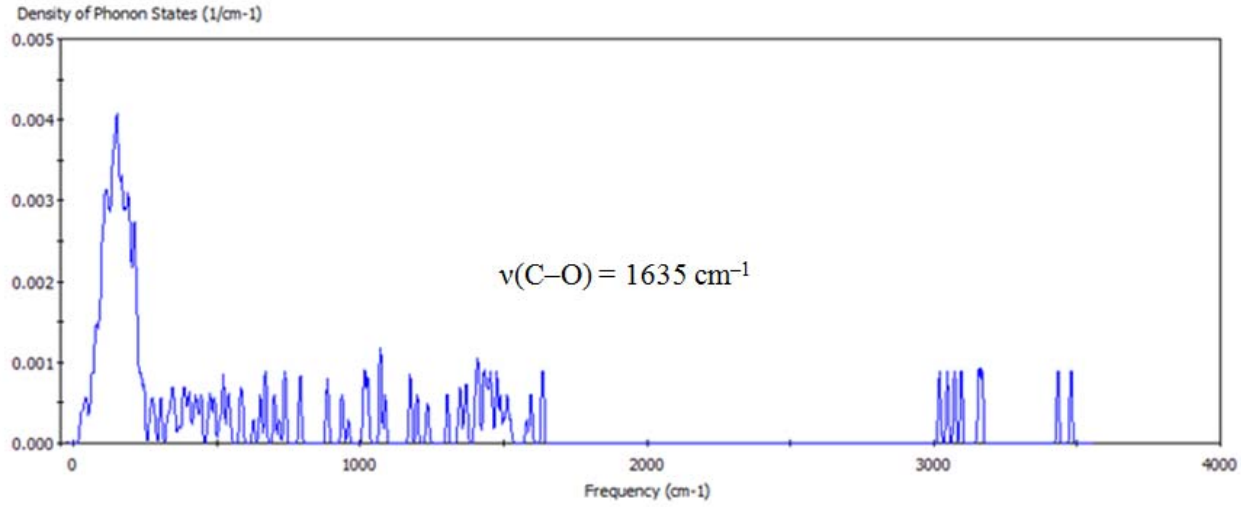

Figure 48. Computed vibrational spectrum of the edge-oriented 2,3-dimethylhydroquinone.

5.0 mM) the molecule remains as a diphenolic specie but is oriented edgewise on the Pd(111) surface.

3.6 Hydrogen on Ultrathin Pd Films Deposited on Pt(111)

Figure 49 shows the top view of various absorption and adsorption sites the hydrogen atom can occupy on the Pd(111) surface or subsurface located above a Pt layer. T, B, H_{fcc}, and H_{hcp} represent adsorption on atop, 2-fold bridge, 3-fold fcc hollow, and 3-fold hcp hollow sites respectively, on the Pd surface. On the other hand, sub H_{fcc} and sub H_{hcp} correspond to absorption in subsurface holes below the fcc hollow and hcp hollow sites, respectively, in the Pd surface. It is also important to mention that an octahedral hole lies beneath an fcc hollow site while a tetrahedral hole resides below the hcp hollow site as presented in Figure 50.

Table 5 shows the absorption and adsorption energies of hydrogen atom on various sites in the Pd surface or subsurface after geometry optimization as the number of Pd layers (surface coverage) above the Pt(111) layer is increased. Computational results show that there are no stable adsorption structures on the bridge and atop sites.

Figure 51 presents the absorption and adsorption energies at various sites as a function of Pd surface coverage. At 1-2 ML of Pd, adsorption on the 3-fold hollow site (H_{fcc} or H_{hcp}) on the Pd surface is the most stable structure. However, at 3 ML of Pd or more, the absorption in the Pd subsurface, particularly in the fcc hole below the hollow site, becomes as favorable as the adsorption on the 3-fold site.

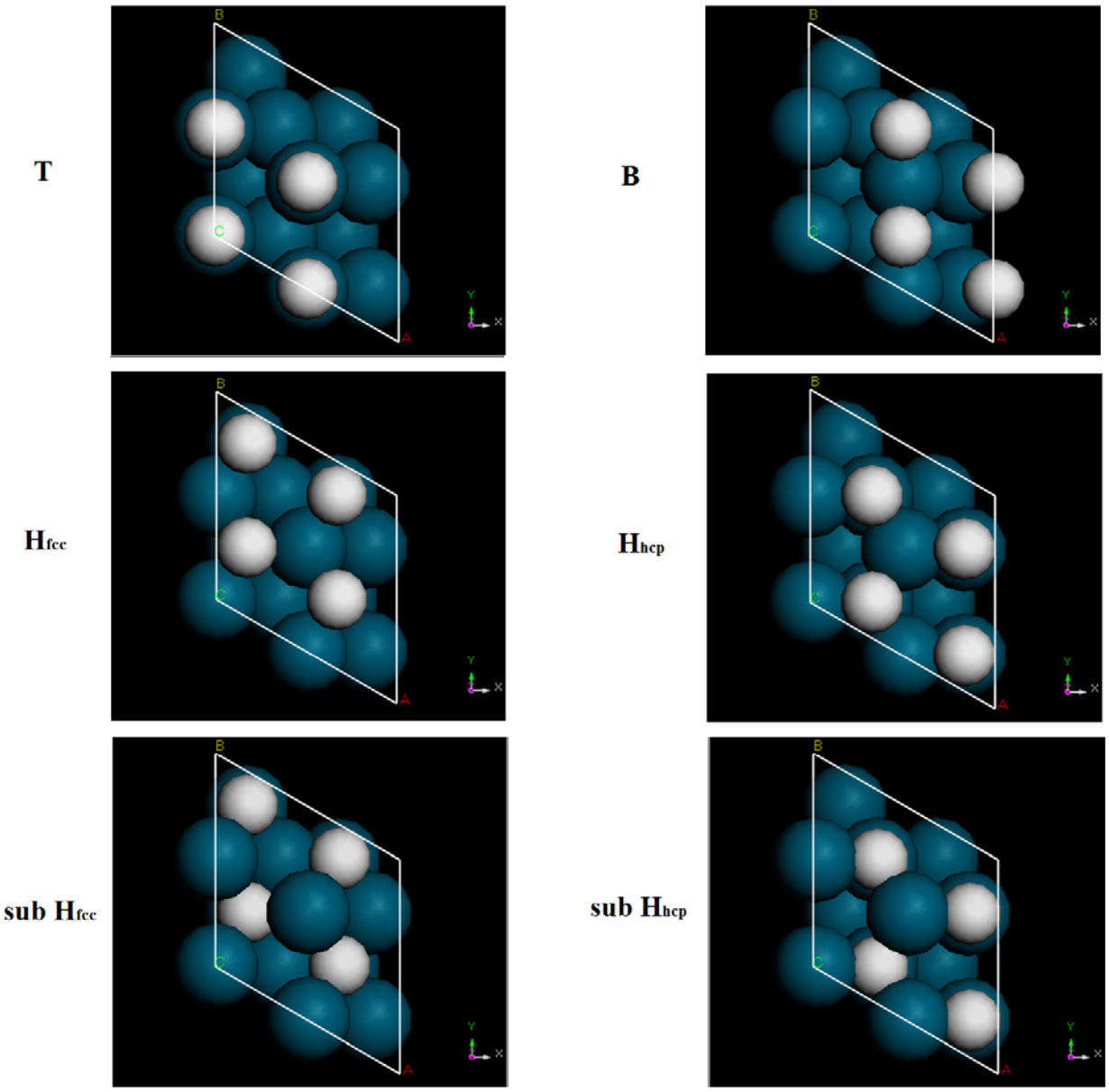

Figure 49. Possible adsorption and absorption sites of atomic hydrogen on a Pd(111) surface deposited on a Pt(111) substrate.

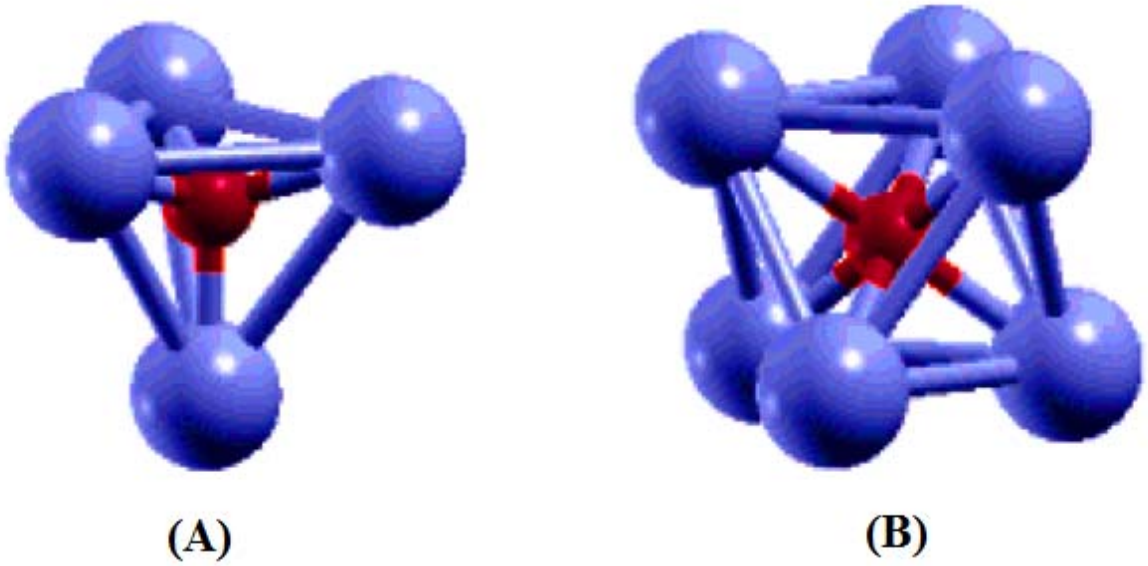

Figure 50. (A) Tetrahedral hole (red) below a 3-fold hollow hcp site of a (111) surface (sub H_{hcp}). (B) Octahedral hole (red) beneath a 3-fold hollow fcc site of a (111) surface (sub H_{fcc}).

Table 5. Adsorption and Absorption Energy (eV) of Atomic Hydrogen at Various Adsorption Sites on Pd Deposited on Pt(111)[a]

ML Pd on Pt(111)	**Adsorption Energy**				**Absorption Energy**	
	H_{fcc}	H_{hcp}	T	B	sub H_{fcc}	sub H_{hcp}
1	– 2.20	– 2.21	Not stable	Not stable	– 1.93	– 1.93
2	– 2.14	– 2.19	Not stable	Not stable	– 1.99	– 1.91
3	– 2.34	– 2.38	Not stable	Not stable	– 2.33	– 2.18
4	– 2.26	– 2.39	Not stable	Not stable	– 2.33	– 2.06
5	– 2.36	– 2.39	Not stable	Not stable	– 2.28	– 2.08
6	– 2.28	– 2.34	Not stable	Not stable	– 2.31	– 2.09

[a]All calculations were performed using a 1 × 1 surface unit cell with a fixed cell volume equal to that of a bare Pd surface. The energy of the hydrogen atom was calculated separately in a 12 x 12 x 12 $Å^3$ cell.

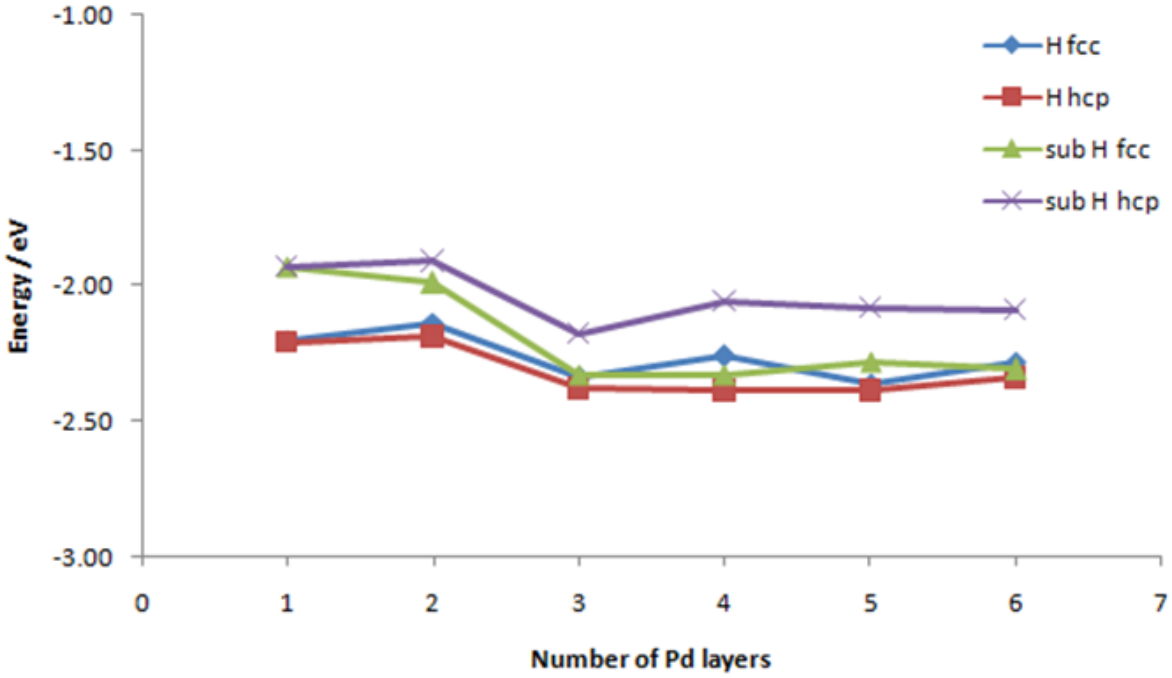

Figure 51. Adsorption and absorption energies of atomic hydrogen on the surface or subsurface, respectively, of 1-6 ML of Pd deposited on a Pt(111) substrate.

These results imply that at 1-2 ML of Pd, hydrogen atoms are only adsorbed on the surface, while at 3 ML of Pd or more, hydrogen is either adsorbed or absorbed on the surface. Moreover, 1-2 ML of Pd behaves as a thin film whereas 3 or more ML of Pd acts like bulk Pd. Indeed, these computational results ascertain that Pd electrodeposited on Pt(111) started to exhibit bulk-like properties at 3 ML as found experimentally by electrochemistry [54].

3.7 Iron Hydrogenase Model Complex on Au

Figures 52 and 53 show the voltammograms of complexes **I** and **II**, respectively, in supporting electrolyte using a Au bead electrode. For both voltammograms, two reduction peaks are observed at –1.8 V to –1.9 V and –2.3 V to –2.6 V, which correspond to the two reduction processes ($Fe^{I}Fe^{I} \rightarrow Fe^{I}Fe^{0}$ and $Fe^{I}Fe^{0} \rightarrow Fe^{0}Fe^{0}$) during the negative potential scans [61-64,66].

Figure 54 shows the voltammograms of the supporting electrolyte as acetic acid (HOAc) was added unto the solution using a Au bead electrode while Figure 55 presents those of complex **I** as increments of the acid were added. Although an increase in current was observed for complex **I**, the electrocatalysis of H_2 was not that pronounced. However, when complex **II** was used such that the complex was chemisorbed and immobilized unto the Au surface through the thiol functional group, an enhancement of the electrocatalysis process was observed as indicated in Figure 56. Large cathodic currents were found implying an increased rate of H_2 production.

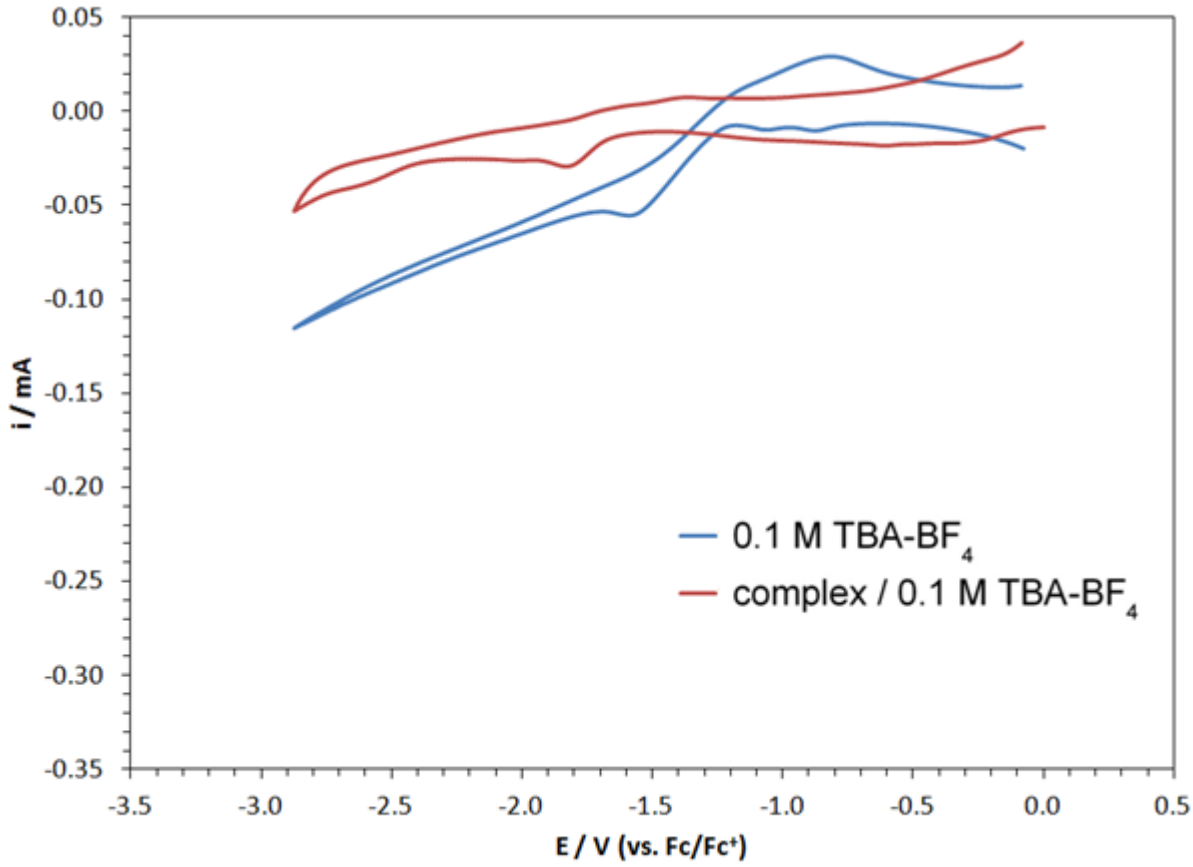

Figure 52. Cyclic voltammograms of the Au electrode in the presence (red trace) and absence (blue trace) of complex **I** in supporting electrolyte. Solution: 0.5 mM complex **I** / 0.1 M TBA-BF_4, s.r. = 200 mV/s, T = 25.0°C, V_{total} = 10.0 mL.

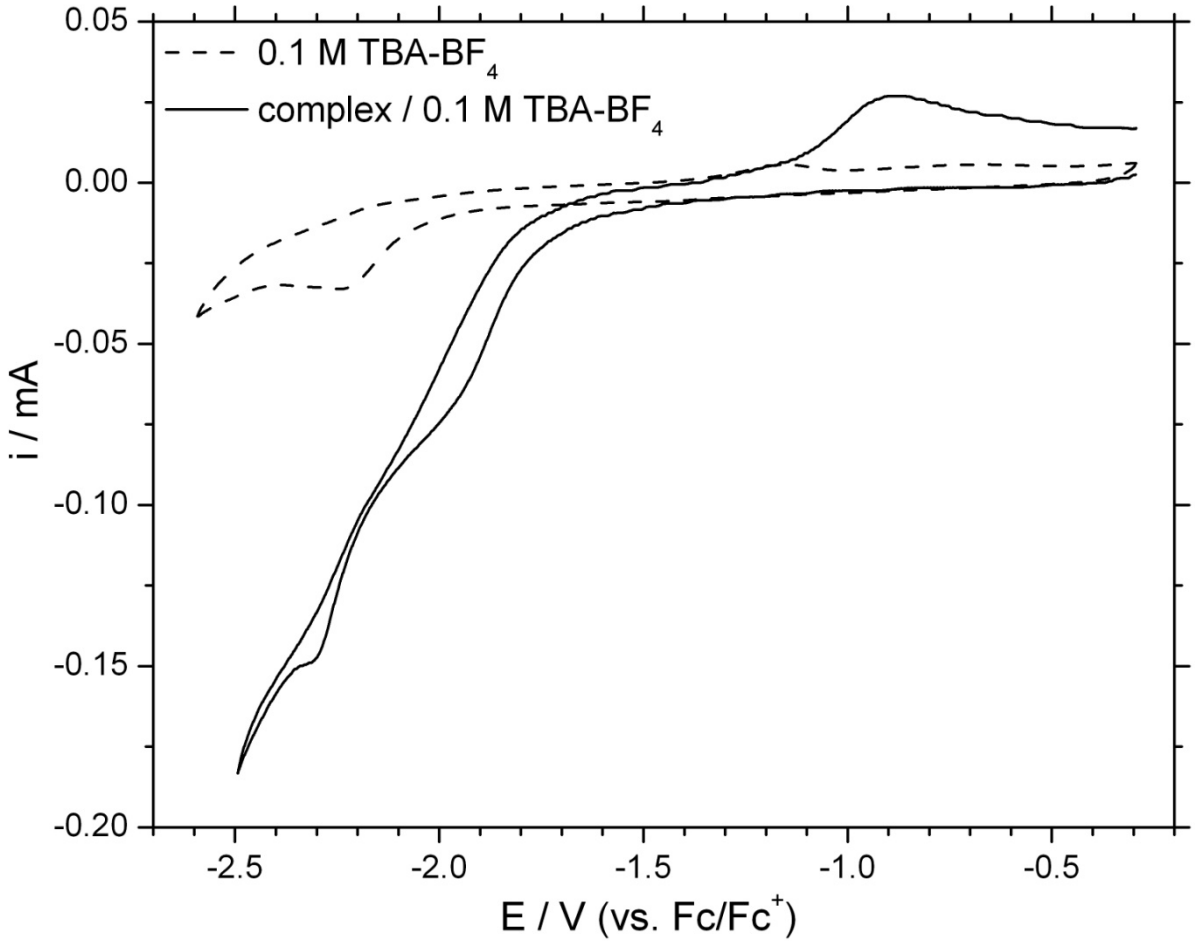

Figure 53. Cyclic voltammograms of the surface-modified Au electrode in the presence (solid curve) and absence (broken curve) of complex **II** in supporting electrolyte. Solution: 0.5 mM complex **II** / 0.1 M TBA-BF_4, s.r. = 200 mV/s, T = 25.0^{o}C, V_{total} = 10.0 mL.

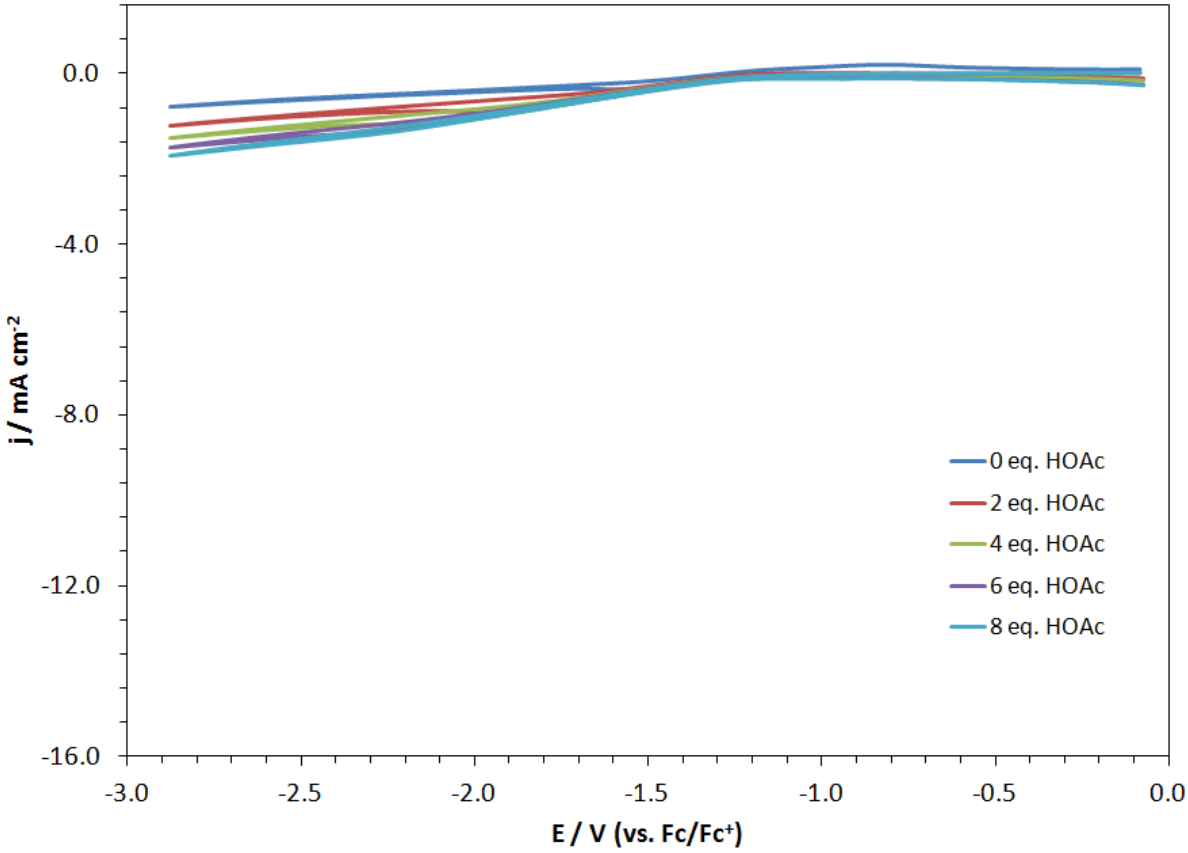

Figure 54. Cyclic voltammograms of the Au electrode in supporting electrolyte after adding consecutive aliquots of HOAc. Solution: 0.1 M TBA-BF_4, s.r. = 200 mV/s, T = 25.0°C, V_{total} = 10.0 mL, 2 eq. HOAc = 1.75 x 10^{-4} HOAc.

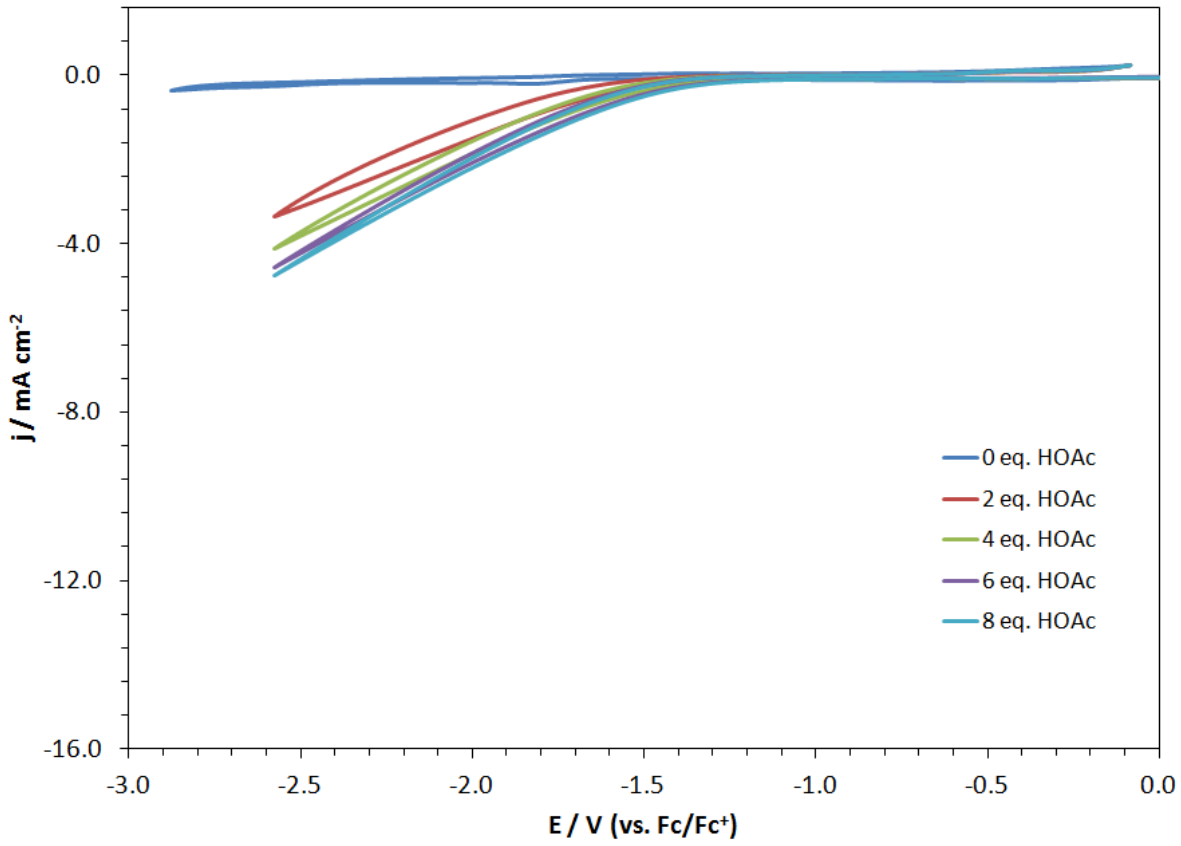

Figure 55. Cyclic voltammograms of the Au electrode in the presence of complex **I** in supporting electrolyte after adding aliquots of HOAc. Experimental conditions as in Figure 52, 2 eq. HOAc = 1.75 x 10^{-4} HOAc.

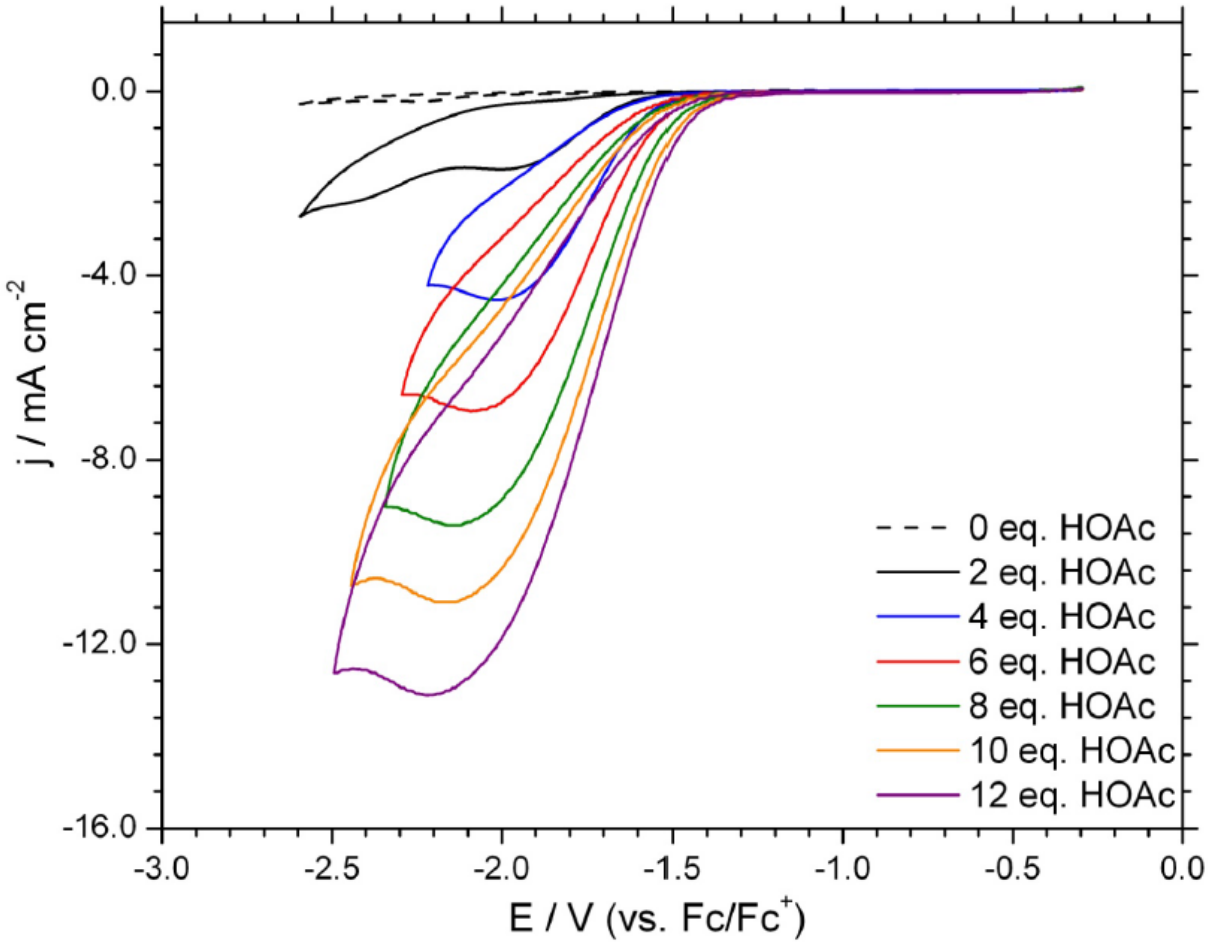

Figure 56. Cyclic voltammograms of the surface-modified Au electrode in contact with the bulk solution of complex **II** after the addition of consecutive aliquots of HOAc. Experimental conditions as in Figure 53, 2 eq. HOAc = 1.75 x 10^{-4} HOAc.

4. CONCLUSIONS

The adsorption of (i) sulfuric acid on Pd(111), (ii) benzene on Pd(111), (iii) hydroquinone and benzoquinone on Pd(111), (iv) hydroquinone sulfonate and benzoquinone sulfonate on Pd(111), (v) 2,3-dimethylhydroquinone and 2,3-dimethylbenzoquinone on Pd(111) and Pd(pc), (vi) hydrogen on 1-6 monolayers (ML) of Pd deposited on a Pt(111) substrate, and (vii) a thiolated iron hydrogenase model complex on polycrystalline Au were investigated by experimental electrochemical methods (cyclic voltammetry, CV), ultrahigh vacuum spectroscopies (Auger electron spectroscopy, AES; low energy electron diffraction, LEED; high-resolution electron energy loss spectroscopy, HREELS), and electrochemical scanning tunneling microscopy, EC-STM, as well as by computational techniques based on density functional theory, DFT.

To resolve compositional and structural issues pertaining to the EC-STM measurements on a well-defined Pd(111) electrode surface in aqueous sulfuric acid solution, DFT computations were utilized. The geometry-optimization and total-energy calculation results indicated that two non-co-planar layers of water molecules and hydronium ions are formed between the rows of surface-coordinated sulfate anions. Hydronium counter cations compose the slightly elevated layer. As a future work, the effect of the presence of unadsorbed solvent molecules and electrolyte ions on the interfacial structure will be computationally studied.

The STM images of benzene chemisorbed on a Pd(111) electrode were simulated in order to confirm the adsorption site of the aromatic compound on the Pd surface held at a particular applied potential. The simulation results indicated that, when the potential of the Pd electrode is held at 0.3 V, benzene is chemisorbed on a 3-fold hollow site; while at 0.55 V, the molecule is adsorbed on a position between a 3-fold and a 2-fold bridge site. A huge limitation in this method is the fact that the potential cannot be applied to the surface computationally prior to any geometry optimization calculations. Hence, the comparison between actual and simulated STM images was the only viable option to determine the adsorption site. If a computational method that allows studying the effect of the applied potential to the energetics of adsorption can be devised, pursuing such investigation would indeed be worthwhile.

The chemisorption of hydroquinone sulfonate (H_2QS) from aqueous solutions unto a well-defined Pd(111) electrode surface had previously been investigated by HREELS, AES, and EC-STM. The experimental results in addition with the DFT calculations implied that (i) at low concentrations, H_2QS undergoes oxidative chemisorption forming benzoquinone sulfonate (BQS) on the surface, (ii) at this concentration, BQS adopts a flat orientation in which the quinone ring is centered over a 2-fold bridge site, and (iii) optimization of the adsorbed-molecule structure yields a BQS conformation in which the C–H and C–S bonds are no longer co-planar with the quinone ring but are slightly tilted, directed away from the surface. It is important to mention that the effect of counter cations was not explored in this work and will thus be the subject for future studies.

The chemisorption of hydroquinone (H_2Q) on well-defined Pd(111) surfaces based on EC, HREELS, and *in situ* STM measurements revealed that at low concentrations (< 0.1 mM), H_2Q undergoes oxidative chemisorption to generate an adlayer of benzoquinone (Q) oriented flat, albeit with a slight tilt. Computational methods were then employed to calculate the total adsorption energies of the possible adsorption configurations and to simulate their respective vibrational spectra. The results suggested that (i) the flat-adsorbed quinone ring is centered on a bridge site in which the C_2 axis that points along the *para*-oxygen atoms is rotated 30^o from the [110] direction of the Pd(111) substrate, (ii) the *p*-oxygen atoms are located above two-fold sites, and (iii) the quinonoid ring is slightly puckered with the C–H bonds tilted away from the surface, at an angle of *ca.* 20^o. It is also recommended to determine the effect of the presence of solvent molecules and ions on the structure, energy or stability in a potential study.

Experimental and computational investigations on the chemisorption of 2,3-dimethylhydroquinone (2,3-dimethylH_2Q) on the Pd surface indicated that (i) at low concentrations, 2,3-dimethylH_2Q is oxidatively chemisorbed producing 2,3-dimethyl-1,4-benzoquinone (2,3-dimethylBQ) oriented flat on the surface; (ii) the flat-adsorbed quinone rings are centered above bridge sites wherein the C=O bonds are pointing 30^o from the [110] direction of the substrate, the para-oxygen atoms are located above 2-fold sites and the quinone C–H and C–CH_3 bonds are tilted away from the surface at *ca.* 20^o; and (iii) at higher concentrations, 2,3-dimethylH_2Q species oriented edgewise are formed. As a future direction, different number and types of functional groups aside

from methyl substituents may also be used in the calculations to evaluate how these groups affect the adsorption of the quinone moiety.

Density functional periodic calculations were used to evaluate the adsorption and absorption energies and determine the most energetically favorable site for atomic hydrogen chemisorbed on the surface and subsurface of 1-6 monolayers (ML) of Pd deposited on a Pt(111) substrate. Computational results implied that at 1-2 ML Pd on Pt(111), the hydrogen atom is only adsorbed on a 3-fold hollow site while at 3 ML of Pd or more, atomic hydrogen may be chemisorbed on the 3-fold site or absorbed in the octahedral hole underneath the hollow site. This confirms the experimental results based from EC and electron spectroscopy obtained earlier that the Pd electrodeposit started to exhibit bulk-like properties at 3 ML. To substantiate this result, different types of adsorbates, films, or substrates should also be investigated in potential research projects. These kinds of results have profound technological implications especially to those that require modifying electrode surfaces, tweaking surface properties, or utilizing minute amounts of film materials.

In the study regarding the electrocatalysis of H_2 production by iron hydrogenase analogue complexes on Au electrodes, the model complex (μ-pdt)[$Fe(CO)_3$][$Fe(CO)_2L$] (pdt = $–SCH_2CH_2CH_2S–$; L = $P(Ph)_3$) was found to slightly catalyze the H_2 evolution process. However, when the complex was immobilized unto the Au electrode via chemisorption through the thiol functional group using (μ-pdt)[$Fe(CO)_3$][$Fe(CO)_2L$] (pdt = $–SCH_2CH_2CH_2S–$; L = $P(Ph)_2CH_2CH_2SH$), the electrocatalytic activity was greatly enhanced. It would also be beneficial if other model complexes or electrodes are

explored in succeeding works to ascertain this behavior on other analogues. These kinds of results would provide a huge impact on technological applications such as in fuel cells that by functionalizing electrode surfaces, the catalytic properties are improved.

The method of integrating computational and experimental methods was indeed found to be useful in studying structures at various surfaces. This is truly significant for this method may then be used in eventually aiding the elucidation of mechanisms of various surface processes or the identification of structure-composition-function relationships occurring at different interfaces.

REFERENCES

[1] J. Evans, Platinum Metals Rev. 46 (2002) 165.

[2] G.A. Somorjai, Y. Li, Introduction to Surface Chemistry and Catalysis, Wiley, New York, New York, 2010.

[3] J. Lipkowski, P.N. Ross, Electrocatalysis, Wiley-VCH, New York, New York, 1998.

[4] F.A. Lewis, The Palladium Hydrogen System, Academic Press, London, England, 1967.

[5] P.J. Durrant, B. Durrant, Introduction to Advanced Inorganic Chemistry, John Wiley & Sons, Inc., New York, New York, 1970.

[6] M.P. Soriaga, Y.-G. Kim, J.E. Soto, in: A. Wieckowski (Ed.), Interfacial Electrochemistry, Marcel Dekker, New York, New York, 1999.

[7] D.R. Lide, Handbook of Chemistry and Physics, CRC Press, Boca Raton, Florida, 1998.

[8] P. Quaino, N.B. Luque, R. Nazmutdinov, E. Santos, W. Schmickler, Angew. Chem. Int. Ed. 51 (2012) 12997.

[9] M.P. Soriaga, R.J. Barriga, in: A.T. Hubbard (Ed.), Surface Imaging and Visualization, CRC Press, Boca Raton, Florida, 1995.

[10] M.P. Soriaga, J.L. Stickney, A.T. Hubbard, J. Mol. Catal. 21 (1983) 211.

[11] R. Winard, Electrochim. Acta 39 (1994) 1091.

[12] E. Rach J. Heitbaum, Electrochim. Acta 32 (1987) 1173.

[13] J. Stickney, in: R. Alkire, D.M. Kolb (Eds.), Advances in Electrochemical Science and Engineering, Vol. 7, Wiley-VCH Verlag GmbH, Weinheim, Germany, 2002.

[14] M. Paunovic, M. Schlesinger, Fundamentals of Electrochemical Deposition, John Wiley & Sons, Inc., New York, New York, 1998.

[15] J. Kua, W. Goddard III, J. American Chem. Soc. 121 (1999) 10928.

[16] N.M. Markovic, P.N. Ross CATTECH 4 (2001, Volume Date 2000) 110.

[17] C. Rice, S. Ha, R.I. Masel, A. Wieckowski, J. Power Sources 115 (2003) 229.

[18] G. Palumbo, J.L. McCrea, U. Erb, in: H.S. Nalwa, Encyclopedia of Nanoscience and Nanotechnology 1, American Scientific Publishers, Valencia, California, 2004.

[19] J.M.D. Coey, Europhysics News 34 (2003) 246.

[20] T. Imokawa, G. Denuault, Chem. Sensors 20 (Suppl. A) (2004) 106.

[21] K.A. Friedrich, K.P. Geyzers, A.J. Dickinson, U. Stimming, J. Electroanal. Chem. 524-525 (2002) 261.

[22] A.J. Arvia, R.C. Salvarezza, W.E. Triaca, J. New Mater. for Electrochem. Sys. 72 (2004) 133.

[23] X. Chen, J. Sanabria-Chinchilla, M.P. Soriaga, Electroanalysis 17 (2005) 2121.

[24] Y.-G. Kim, J. Soriaga, G. Vigh, M.P. Soriaga, J. Colloid Interface Sci. 227 (2000) 505.

[25] O.M. Magnusen, J. Hagebock, J. Hotlos, R.J. Behm, Faraday Discuss. Chem. Soc. 94 (1992) 329.

[26] K. Sato, S. Yoshimoto, J. Inukai, K. Itaya, Electrochem. Commun. 8 (2006) 725.

[27] A.M. Funtikov, U. Linke, U. Stimming, A. Vogel, Surf. Sci. 324 (1995) L343.

[28] A.M. Funtikov, U. Stimming, A. Vogel, J. Electroanal. Chem. 428 (1997) 147.

[29] L.-J. Wan, S. L. Yau, K. Itaya, J. Phys. Chem. 99 (1995) 9507.

[30] M. Wilms, P. Broekmann, M. Kruft, Z. Park, C. Stuhlmann, K. Wandelt, Surf. Sci. 83 (1998) 402.

[31] W.-H. Li, R. J. Nichols, J. Electroanal. Chem. 456 (1998) 153.

[32] M. Wilms, P. Broekmann, C. Stuhlmann, K. Wandelt, Surf. Sci. 416 (1998) 121.

[33] M. Arenz, P. Broekmann, M. Lennartz, E. Vogler, K. Wandelt, Phys. Stat. Sol. (a) 187 (2001) 63.

[34] L.-J. Wan, M. Hara, J. Inukai, K. Itaya, J. Phys. Chem. B 103 (1999) 6978.

[35] T. Senna, N. Ikemiya, M. Ito, J. Electroanal. Chem. 511 (2001) 115.

[36] G. E. Edens, X. Gao, M. J. Weaver, J. Electroanal. Chem. 375 (1994) 357.

[37] P. Sautet, M.-L. Bocquet, Phys. Rev. B 53 (1996) 4910.

[38] P.S. Weiss, D.M. Eigler, Phys. Rev. Lett. 71 (1993) 3139.

[39] P. Sautet, M.-L. Bocquet, Surf. Sci. 304 (1994) L445.

[40] P. Sautet, Chem. Rev. 97 (1997) 1097.

[41] D.N. Futaba, S. Chiang, Jpn. J. Appl. Phys. 38 (1999) 3809.

[42] Y.-G. Kim, J.E. Soto, X. Chen, Y.S. Park, M.P. Soriaga, J. Electroanal. Chem. 554-555 (2003) 167.

[43] Y.-G. Kim, M.P. Soriaga, Phys. Chem. Chem. Phys. 3 (2001) 3303.

[44] J. Soto, Y.-G. Kim, X. Chen, Y.-S. Park, M.P. Soriaga, J. Electroanal. Chem. 500 (2001) 374.

[45] Y.H. Lu, H.J. Zhang, Y.F. Xu, B. Song, H.Y. Li, S.N. Bao, P. He, Appl. Surf. Sci. 253 (2006) 2025.

[46] H.Q. Qian, H.Y. Mao, F. Song, S.Q. Shi, H.J. Zhang, H.Y. Li, P.M. He, S.N. Bao, Appl. Surf. Sci. 256 (2010) 2686.

[47] C. Morin, D. Simon, P. Sautet, J. Phys. Chem. B 107 (2003) 2995.

[48] C. Morin, D. Simon, P. Sautet, J. Phys. Chem. B 108 (2004) 5653.

[49] A.T. Hubbard, Chem. Rev. 88 (1988) 633.

[50] M.P. Soriaga, Prog. Surf. Sci. 39 (1992) 325.

[51] J.E. Soto, Y.-G. Kim, M.P. Soriaga, Electrochem. Commun. 1 (1999) 135.

[52] Y.-G. Kim, J.H. Baricuatro, M.P. Soriaga, Langmuir 22 (2006) 10762.

[53] J.E. Soto, D. Li, J. Sanabria-Chinchilla, X. Chen, M.P. Soriaga, J. Mol. Struc. 890 (2008) 298.

[54] Y.S. Park, J.H. Baricuatro, M.A. Hossain, M.P. Soriaga, ECS Trans. 3 (2007) 65.

[55] F. Ample, A. Clotet, J.M. Ricart, Surf. Sci. 558 (2004) 111.

[56] Z. Gu, P.B. Balbuena, J. Phys. Chem. C 111 (2007) 9877.

[57] Z. Gu, P.B. Balbuena, J. Phys. Chem. C 111 (2007) 17388.

[58] P.J. Feibelman, B. Hammer, J.K. Norskov, F. Wagner, M. Scheffler, R. Stumpf, R. Watwe, J. Dumesic, J. Phys. Chem. B 105 (2001) 4018.

[59] D. Loffreda, D. Simon, P. Sautet. Surf. Sci. 425 (1999) 68.

[60] B. Hammer, Y. Morikawa, J.K. Norskov, Phys. Rev. Lett. 76 (1996) 2141.

[61] F. Gloaguen, J.D. Lawrence, T.B. Rauchfuss, J. Am. Chem. Soc. 123 (2001) 9476.

[62] F. Gloaguen, J.D. Lawrence, T.B. Rauchfuss, M. Benard, M.-M. Rohmer, Inorg. Chem. 41 (2002) 6573.

[63] D. Chong, I.P. Georgakaki, R. Mejia-Rodriguez, J. Sanabria-Chinchilla, M.P. Soriaga, M.Y. Darensbourg, J. Chem. Soc., Dalton Trans. (2003) 4158.

[64] R. Mejia-Rodriguez, D. Chong, J.H. Reibenspies, M.P. Soriaga, M.Y. Darensbourg, J. Am. Chem. Soc. 126 (2004) 12004.

[65] C. Vericat, M.E. Vela, G.A. Benitez, J.A. Martin Gago, X. Torrelles, R.C. Salvarezza, J. Phys.: Condens. Matter 18 (2006) R867.

[66] A.M. Kluwer, R. Kapre, F. Hartl, M. Lutz, A.L. Spek, A.M. Brouwer, P.W.N.M. van Leeuwen, J.N.H. Reek, PNAS 106 (2009) 10460.

[67] I. Levine, Quantum Chemistry, Pearson Prentice Hall, Upper Saddle River, New Jersey, 2009.

[68] R.G. Parr, W. Yang, Density-Functional Theory of Atoms and Molecules, Oxford University Press, New York, New York, 1989.

[69] P. Hohenberg, W. Kohn, Phys. Rev. B 136 (1964) 864.

[70] M. Levy, Proc. Natl. Acad. Sci. U.S.A. 76 (1979) 6062.

[71] W. Kohn, L.J. Sham, Phys. Rev. A 140 (1965) 1133.

[72] S.J. Clark, M.D. Segall, C.J. Pickard, P.J. Hasnip, M.J. Probert, K. Refson, M.C. Payne, Z. Kristallogr. 220 (2005) 567.

[73] J.P. Perdew, K. Burke, M. Ernzehof, Phys. Rev. Lett. 77 (1996) 3865.

[74] J.P. Perdew, Y. Wang, Phys. Rev. B 45 (1992) 13244.

[75] R.A. Evarestov, Th. Bredow, K. Jug, Phys. Solid State 43 (2001) 1774.

[76] J.Z. Sexton, A.C. Kummel, J. Vac. Sci. Technol. B 21 (2003) 1908.

[77] E.B. Wilson, J.C. Decius, P.C. Cross, Molecular Vibrations, Dover, New York, New York, 1955.

[78] J. Tersoff, D.R. Hamann, Phys. Rev. B 31 (1985) 805.

[79] G. Ertl, J. Kuppers, Low Energy Electrons and Surface Chemistry, VCH, Boca Raton, Florida, 1985.

[80] P.N. Ross, F.T. Wagner, in: H. Gerischer, C.W. Tobias, Adv. Electrochem. Electrochem. Eng. Volume 13, John Wiley & Sons, New York, New York, 1984.

[81] D. Li, Ph. D. Dissertation, Texas A&M University, 2010.

[82] M.P. Soriaga, X. Chen, D. Li, J.L. Stickney, in: R.A. Scott, C.M. Lukehart (Eds.), Applications of Physical Methods to Inorganic and Bioinorganic Chemistry, John Wiley & Sons, New York, New York, 2007.

[83] D.P. Woodruff, T.A. Delchar, Modern Techniques of Surface Science, Cambridge University Press, New York, New York, 1986.

[84] H. Ibach, D.A. Mills, Electron Energy Loss Spectroscopy, Academic Press, New York, New York, 1982.

[85] N.R. Avery, in: J.T. Yates, Jr, T.E. Madey (Eds.), Vibrational Spectroscopy of Molecules on Surfaces, Plenum Press, New York, New York, 1987.

[86] F.M. Hoffman, Surf. Sci. Rep. 3 (1983) 2.

[87] H.A. Pearce, N. Sheppard, Surf. Sci. 59 (1976) 205.

[88] A. Bewick, B.S. Pons, in: R.J.H. Hester, R.E. Clark (Eds.), Advances in Infrared and Raman Spectroscopy, Wiley-Hayden, London, England, 1985.

[89] H.G. Tompkins, in: A. Czanderna (Ed.), Methods of Surface Analysis, Elsevier, New York, New York, 1975.

[90] D. Lin-Vein, N.B. Colthup, W.G. Fately, J.G. Grasselli, The Handbook of Infrared and Raman Characteristic Frequencies of Organic Molecules, Academic Press, San Diego, California, 1991.

[91] E. Maslowski, Vibrational Spectra of Organometallic Compounds, Wiley, New York, New York, 1977.

[92] J. Jungwirthova, L.L. Kesmodel, J. Phys. Chem. B 105 (2001) 674.

[93] X. Chen, Ph. D. Dissertation, Texas A&M University, 2004.

[94] D.A. Bonnell (Ed.), Scanning Tunneling Microscopy and Spectroscopy; Theory, Techniques, and Applications, VCH Publishers, New York, New York, 1993.

[95] J. Clavilier, R. Faure, G. Guinet, R. Durand, J. Electroanal. Chem. 107 (1980) 205.

[96] J. Clavilier, J. Electroanal. Chem. 107 (1980) 211.

[97] Y.-G. Kim, M.P. Soriaga, J. Phys. Chem. B 102 (1998) 6188.

[98] P. Li, M. Wang, C.J. He, G.H. Li, X.Y. Liu, C.N. Chen, B. Akermark, L.C. Sun, Eur. J. Inorg. Chem. 2005 (2005) 2506.

[99] A.C. Javier, Y.-G. Kim, J.B. Soriaga, P.B. Balbuena, M.P. Soriaga, Phil. Sci. Letters 4 (2011) 18.

[100] A. Javier, D. Li, P.B. Balbuena, M.P. Soriaga, Reports in Electrochemistry 3 (2013) 1.

[101] A. Javier, D. Li, P.B. Balbuena, M.P. Soriaga, Electrocatal. 1 (2010) 159.

[102] A. Javier, Y.-G. Kim, J.H. Baricuatro, P.B. Balbuena, M.P. Soriaga, Electrocatal. 3 (2012) 353.

[103] S.-L. Yau, Y.-G. Kim, K. Itaya, J. Am. Chem. Soc. 118 (1996) 7795.

[104] V. Milman, K. Refson, S.J. Clark, C.J. Pickard, J.R. Yates, S.-P. Gao, P.J. Hasnip, M.I.J. Probert, A. Perlov, M.D. Segall, J. Mol. Struct. (Theochem) 954 (2010) 22.

[105] T. Lin, X. Liu, C. He, J. Phys. Chem. B 116 (2012) 1524.

[106] P. Hermet, M. Goffinet, J. Kreisel, Ph. Ghosez, Phys. Rev. B 75 (2007) 220102.

[107] E. Balan, A.M. Saitta, F. Mauri, G. Calas, Am. Mineral. 86 (2001) 1321.

[108] S.F. Parker, K. Refson, K.P.J. Williams, D.A. Braden, B.S. Hudson, K. Yvon, Inorg. Chem. 45 (2006) 10951.

[109] M.P. Soriaga, A.T. Hubbard, J. Electroanal. Chem. 167 (1984) 79.

[110] a) A.L. McClellan, H.F. Harnsberger, J. Coll. Interf. Sci. 23 (1967) 577; b) T.L. Hill, J. Chem. Phys. 16 (1948) 181.

[111] L. Pauling, The Nature of the Chemical Bond, Cornell University Press, New York, New York, 1960.

[112] N. K. Adam, The Physics and Chemistry of Surfaces, Oxford University Press, London, England, 1941.

[113] M.P. Soriaga, A.T. Hubbard, J. Am. Chem. Soc. 104 (1982) 2735.

[114] M.P. Soriaga, P.H. Wilson, A.T. Hubbard, C.S. Benton, J. Electroanal. Chem. 142 (1982) 317.

[115] P.-X. Dai, T. Chen, D. Wang, L.-J. Wan, J. Phys. Chem. C 116 (2012) 6208.

[116] J. Sanabria-Chinchilla, X. Chen, D. Li, M.P. Soriaga, Electrocatal. (2013) DOI 10.1007/s12678-013-0125-6.

[117] a) M.P. Soriaga, V.K.F. Chia, J.L. Stickney, S.D. Rosasco, G.N. Salaita, A.T. Hubbard, J.B. Benziger, K.W.P. Pang, J. Electroanal. Chem. 163 (1984) 407; b) J.B. Benziger, F.A. Pascale, S.L. Bernasek, M.P. Soriaga, A.T. Hubbard, J. Electroanal. Chem. 198 (1986) 65.

[118] J. Cruz, Ph. D. Dissertation, Texas A&M University, 2012.

APPENDIX A

Density Functional Study of Benzoquinone Sulfonate Adsorbed on a Pd(111) Surface

Alnald Javier[1], Ding Li[1], Perla B. Balbuena[2] and Manuel P. Soriaga[1*]

[1]Department of Chemistry

[2]Department of Chemical Engineering

Texas A&M University

College Station, TX 77843

Published: Electrocatalysis, Springer, September 8, 2010

A. Javier, D. Li, P.B. Balbuena, M.P. Soriaga, Electrocatal. 1 (2010) 159.

The final publication is available at **link.springer.com**

[*]Corresponding author

Phone: (979) 845-1846. Fax: (979) 845- 3523. E-mail: m-soriaga@tamu.edu

ABSTRACT

The chemisorption of benzoquinone sulfonate (BQS) from aqueous solutions onto a well-defined Pd(111) electrode surface had been previously investigated by high-resolution electron energy loss spectroscopy (HREELS), Auger electron spectroscopy (AES) and electrochemical scanning tunneling microscopy (EC-STM). Important structural (adsorbed-molecule orientation) and compositional (surface coverage) information were obtained, but certain details such as the spatial configuration of the adsorbed quinone and the most favorable adsorption site could not be unambiguously ascertained. These issues have been addressed through the use of first-principles density functional periodic calculations. The results: (i) The adsorption geometry with the most favorable adsorption energy suggests that BQS adopts a flat orientation in which the quinone ring is centered over a two-fold bridge site. (ii) Optimization of the adsorbed-molecule structure yields a BQS conformation in which the C–H and C–S bonds are no longer co-planar with the quinone ring but are slightly tilted, directed away from the surface.

Keywords:

DFT calculations

Benzoquinone sulfonate adsorption

Pd(111) electrode surface

Total-energy calculations

Adsorbed-molecule geometry

INTRODUCTION

We earlier published results from studies based upon the combination of electrochemistry (EC), high-resolution electron-energy loss spectroscopy (HREELS), Auger electron spectroscopy (AES) and scanning tunneling microscopy (STM), of the chemisorption of substituted *p*-diphenols from aqueous solutions onto well-defined Pd(111) and Pd(100) electrode surfaces [A1,A2]. The EC and HREELS measurements indicated that, whether the solution initially contained the diphenol or its oxidized (quinone) form, the species present on the surface was invariably the quinone. For example, when 1,4-dihydroxybenzene is chemisorbed on the platinum metals, it undergoes oxidation to benzoquinone; identical HREELS spectra were found for both species. 2,5-Dihydroxybenzenesulfonate [hydroquinone sulfonate (H_2QS)] was later investigated; consistent with earlier work on the unsubstituted diphenols, it was likewise determined from HREEL spectra (Figure A-1) that H_2QS underwent oxidative chemisorption to benzoquinone sulfonate (BQS).

Additional structural work, *via* EC-STM, was also undertaken for BQS. The results are displayed in Figures A-2 and A-3. Figure A-2 shows a magnified height-shaded view of an unfiltered high-resolution EC-STM image of the BQS adlayer, designated as Pd(111)-(3×3)-BQS, with a coverage (Q) of 0.11 BQS molecules per Pd(111) surface atom. The flat orientation of the quinone group is evident and implies a surface chemical bond that involves the π-electron system of the quinone double bonds; a *completely* parallel orientation would, however, be hindered by the presence of the bulky sulfonate group as illustrated in the molecular model shown in Fig. A-4. The

possibility then also exists that, in the chemisorbed state, the quinone ring may undergo slight distortions and the peripheral (C–S, C–S and C–O) bonds are no longer co-planar with the quinone moiety.

Two real-space geometries of the Pd(111)-(3×3)-BQS adlattice are possible, as shown in Figure A-3. In both arrangements (A and B), the quinone ring is located on a high-symmetry two-fold bridge site. The only difference between the two configurations is in the location of the sulfonate O atoms. Unfortunately, it is not possible to determine from only EC-STM images which of the two possible sites is the correct one; from simple thermodynamic considerations, it had been surmised that model (A) is more favorable [A1,A2].

To help resolve the two issues as to (i) whether or not the quinone ring suffers distortions from a planar geometry, and (ii) which of the two possible arrangements in Figure A-3 is more stable, insights from theoretical studies would obviously be of substantial advantage. It is in this regard that the present computational work, based on density functional theory (DFT), was undertaken.

Density functional calculations have been used to investigate the adsorption geometries of aromatic compounds on various metal surfaces [A3-A6]. In some of the work, theoretical computations were employed in order to validate assertions or resolve conflicted ideas that arise from various experimental results. The chemisorption of benzene on Pt(111), Pd(111) and Rh(111) surfaces has thus been studied by first-principles density functional theory; the results from the energy calculations were then correlated with measurements from a host of surface-characterization techniques such as

infrared absorption-reflection spectroscopy (IRAS), HREELS, low-energy electron diffraction (LEED) and STM [A5,A6]. In the present research, density functional periodic calculations were similarly employed not only to optimize the adsorbed-molecule structure of BQS on Pd(111) but also to ascertain which of the likely adsorption sites would be the most favored.

COMPUTATIONAL DETAILS

The Cambridge Sequential Total Energy Package (CASTEP), a first-principles density functional theory (DFT) code integrated in the Material Studio application of Accelrys Inc., was employed for the calculations [A7]. This simulation module solves the Kohn-Sham DFT equations based on the Vanderbilt-type ultrasoft pseudopotentials to permit computations to be carried out at lower cutoff energies for a plane-wave basis set. In this model, the generalized gradient approximation (GGA) [A8] and the Perdew-Wang exchange-correlation functional (PW91) [A9] were adopted.

A 3 × 3 supercell was selected since it corresponds to the Pd(111)-BQS unit mesh observed by EC-STM. In this model, the surface was depicted as a metal slab consisting of four layers of Pd atoms; the upper two layers allowed to relax, and the cell was separated from periodic images with a vertical vacuum space of approximately 15 Å [A4]. It will be mentioned that lateral interactions between an aromatic molecule and its periodic images have been shown to be trivial in this particular cell size (< 0.05 eV per molecule) [A6].

Geometry-optimization, undertaken with a cutoff energy of 300 eV, employed the Broyden-Fletcher-Goldfarb-Shanno (BFGS) method and utilized a 3 × 3 × 1 Monkhorst-Pack grid with Fermi smearing of 0.1 eV. The convergence tolerances in terms of energy, force, and displacement were 2.0 x 10^{-5} eV/atom, 0.05 eV/Å, and 0.002 Å, respectively. These values were noted to be sufficient to achieve reasonable convergence for the total and adsorption energies [A4,A5].

The relative stabilities of the adsorption configurations selected for study were evaluated from the calculated adsorption energy, E_{ads}, defined as:

$$E_{ads} = E_{Pd\text{-}BQS} - E_{BQS} - E_{Pd} \quad (1)$$

In Equation (1), $E_{Pd\text{-}BQS}$, E_{BQS} and E_{Pd} correspond to the total energies of the Pd-BQS interfacial system, the unadsorbed BQS molecule, and the clean Pd(111) surface, respectively. It can be seen that the lower (more negative) the adsorption energy, the stronger the adsorption.

RESULTS AND DISCUSSION

Based on the most stable adsorption configurations calculated for benzene on Pt(111) [A5,A6], the four most likely geometries of BQS adsorbed on Pd(111) that were chosen for this work are shown in Figure A-5. BRI-0 designates the adsorbate-substrate structure in which the quinone is adsorbed on a two-fold bridge site with the peripheral bonds pointed in the [110] direction; BRI-30 is for when the molecule in which the bonds are rotated 30° from the [110] direction. HCP-30-A and HCP-30-B denote BQS

on a three-fold hollow site with the peripheral bonds deviated 30^{o} from the [110] direction; the disparity lies on the location of the sulfonate functional group.

The calculated E_{ads} values for chemisorbed BQS as a function of optimized adsorption geometries are tabulated in Table A-1. In agreement with the work cited above for benzene on Pt(111) [A6], no evidence was found for significant lateral adsorbate-adsorbate interactions. However, the effect of counter cations was not explored in the present calculations although it will be addressed in a future study. The BRI-30 system has the most favorable adsorption energy; it is thus considered to be the most stable adsorbed-molecule configuration. It may be noted that such conformation is the same as that earlier conjectured from only EC-STM results [A2].

By comparing the optimized structure of an isolated BQS molecule presented in Figure A-6 with the BRI-30 Pd(111)-BQS interfacial system shown in Figure A-7, it can be noted that when the molecule is chemisorbed flat on the metal surface, the C–H and C–S bonds are no longer co-planar with the quinone ring; they are slightly tilted (*ca.* 20^{o}) and directed away from the surface. This calculated puckered-ring structure of BQS may help explain two unexpected experimental observations [A1,A2]: (i) In the EC-STM image, there is an enhanced brightness of the 3,4-edge; this could arise from the fact that the two adjacent carbon atoms are located slightly above the rest of the quinone moiety. (ii) In what may appear as a violation of the metal-surface dipole selection rule, the C–H stretch mode is (weakly) HREELS-active; this may be due to a vibrational component perpendicular to the surface spawned by the non-coplanarity of the C–H bonds.

CONCLUSIONS

The chemisorption of benzoquinone sulfonate (BQS) from aqueous solutions onto a well-defined Pd(111) electrode surface had been previously investigated by high-resolution electron energy loss spectroscopy (HREELS), Auger electron spectroscopy (AES) and electrochemical scanning tunneling microscopy (EC-STM). Important structural (adsorbed-molecule orientation) and compositional (surface coverage) information were obtained, but certain details such as the spatial configuration of the adsorbed quinone and the most favorable adsorption site could not be unambiguously ascertained. These issues have been addressed through the use of first-principles density functional periodic calculations. The results: (i) The adsorption geometry with the most favorable adsorption energy suggests that BQS adopts a flat orientation in which the quinone ring is centered over a two-fold bridge site. (ii) Optimization of the adsorbed-molecule structure yields a BQS conformation in which the C–H and C–S bonds are no longer co-planar with the quinone ring but are slightly tilted, directed away from the surface.

ACKNOWLEDGMENTS

Acknowledgment is made to The Welch Foundation (A-1064) for financial support of this work, and to the Laboratory for Molecular Simulation at Texas A&M University for the computational software.

REFERENCES

[A1] Y.-G. Kim, M.P. Soriaga, Phys. Chem. Chem. Phys. 3 (2001) 3303.

[A2] J. Soto, Y.-G. Kim, X. Chen, Y.-S. Park, M.P. Soriaga, J. Electroanal. Chem. 500 (2001) 374.

[A3] Y.H. Lu, H.J. Zhang, Y.F. Xu, B. Song, H.Y. Li, S.N. Bao, P. He, Appl. Surf. Sci. 253 (2006) 2025.

[A4] H.Q. Qian, H.Y. Mao, F. Song, S.Q. Shi, H.J. Zhang, H.Y. Li, P.M. He, S.N. Bao, Appl. Surf. Sci. 256 (2010) 2686.

[A5] C. Morin, D. Simon, P. Sautet, J. Phys. Chem. B 107 (2003) 2995.

[A6] C. Morin, D. Simon, P. Sautet, J. Phys. Chem. B 108 (2004) 5653.

[A7] S.J. Clark, M.D. Segall, C.J. Pickard, P.J. Hasnip, M.J. Probert, K. Refson, M.C. Payne, Z. Kristallogr. 220 (2005) 567.

[A8] J.P. Perdew, K. Burke, M. Ernzehof, Phys. Rev. Lett. 77 (1996) 3865.

[A9] J.P. Perdew, Y. Wang, Phys. Rev. B 45 (1992) 13244.

Table A-1. Adsorption Energies (eV) of BQS at Various Adsorption Geometries on Pd(111)[a]

Adsorption geometry	Adsorption Energy (E_{ads})
BRI-0	–2.14
BRI-30	–2.41
HCP-30-A	–1.81
HCP-30-B	–1.02

[a]All calculations were performed using a 3 × 3 surface unit cell with a fixed cell volume equal to that of a bare Pd surface. The energy of the benzoquinone sulfonate molecule was calculated separately in a 12 x 12 x 12 $Å^3$ cell.

FIGURES AND CAPTIONS

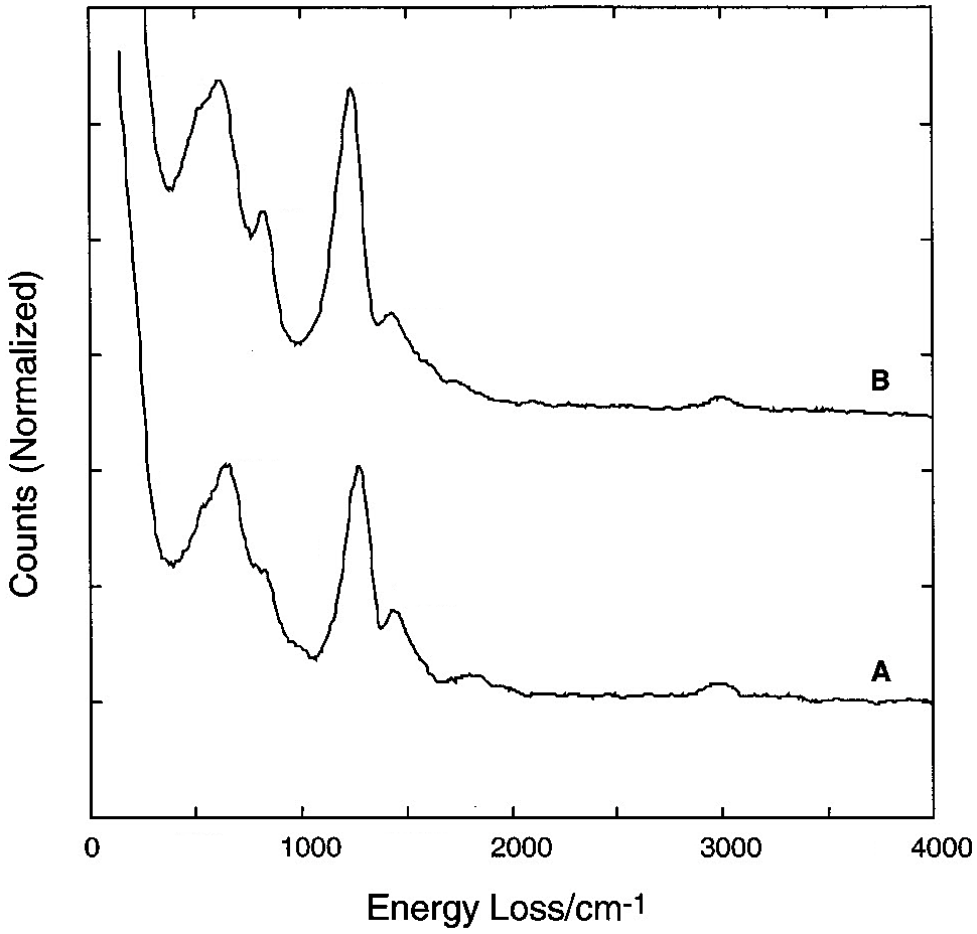

Figure A-1. HREEL spectrum of a UHV-prepared Pd(111) surface. A: After emersion from an aqueous 0.1 m*M* H_2QS solution. B: After emersion from an aqueous 0.1 m*M* BQS solution. The crystal was rinsed with pure water solution prior to the HREELS measurements. Experimental conditions: incident beam energy = 4 eV. Incidence and detection angles = 62° from the surface normal. Beam current = 100 pA.

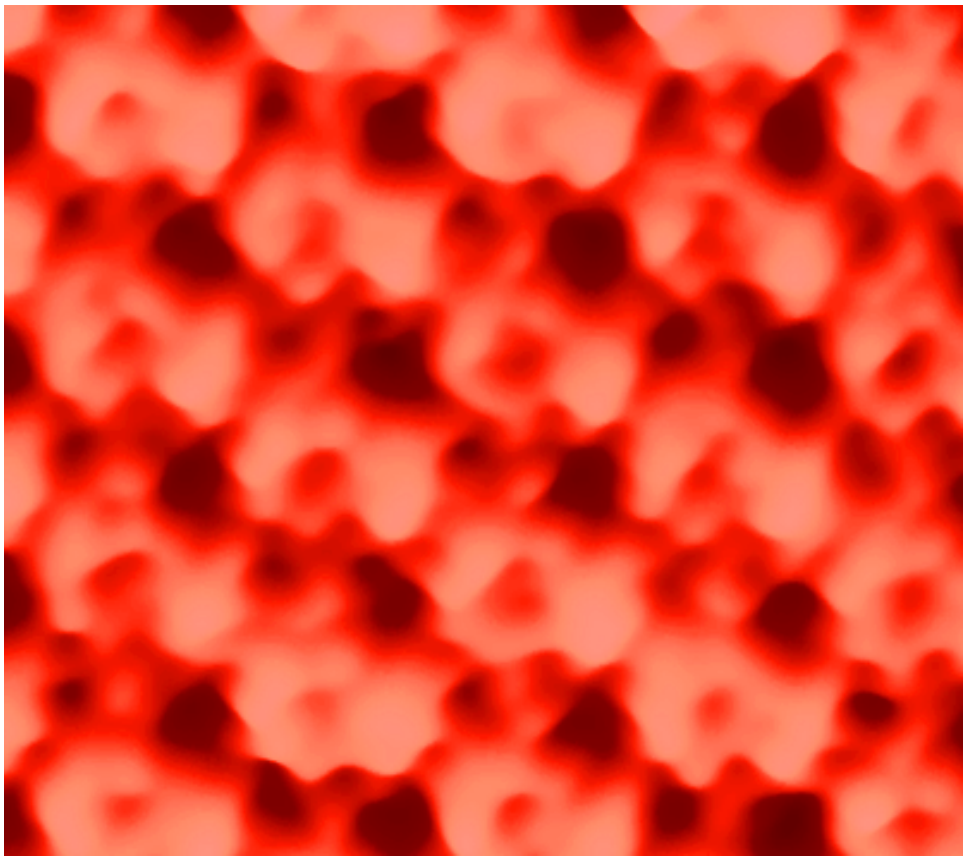

Figure A-2. Magnified high-resolution EC-STM image of Pd(111)-(3×3)-BQS. Bias voltage: 100 mV; tunneling current: 30 nA.

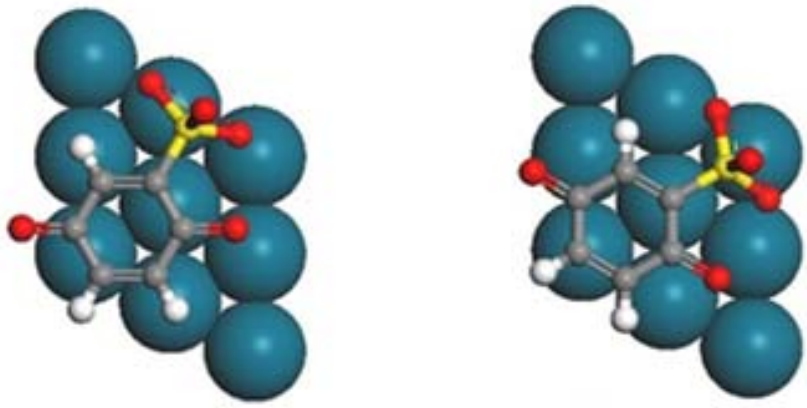

Figure A-3. Two possible real-space structures of the Pd(111)-(3×3)-BQS. The only difference between structures A and B are in the locations of the sulfonate O atoms.

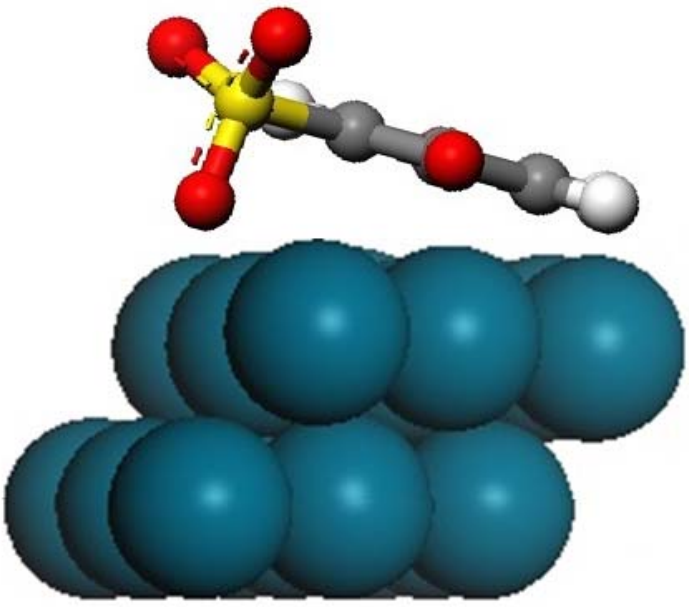

Figure A-4. Molecular model of BQS chemisorbed in a tilted, flat orientation.

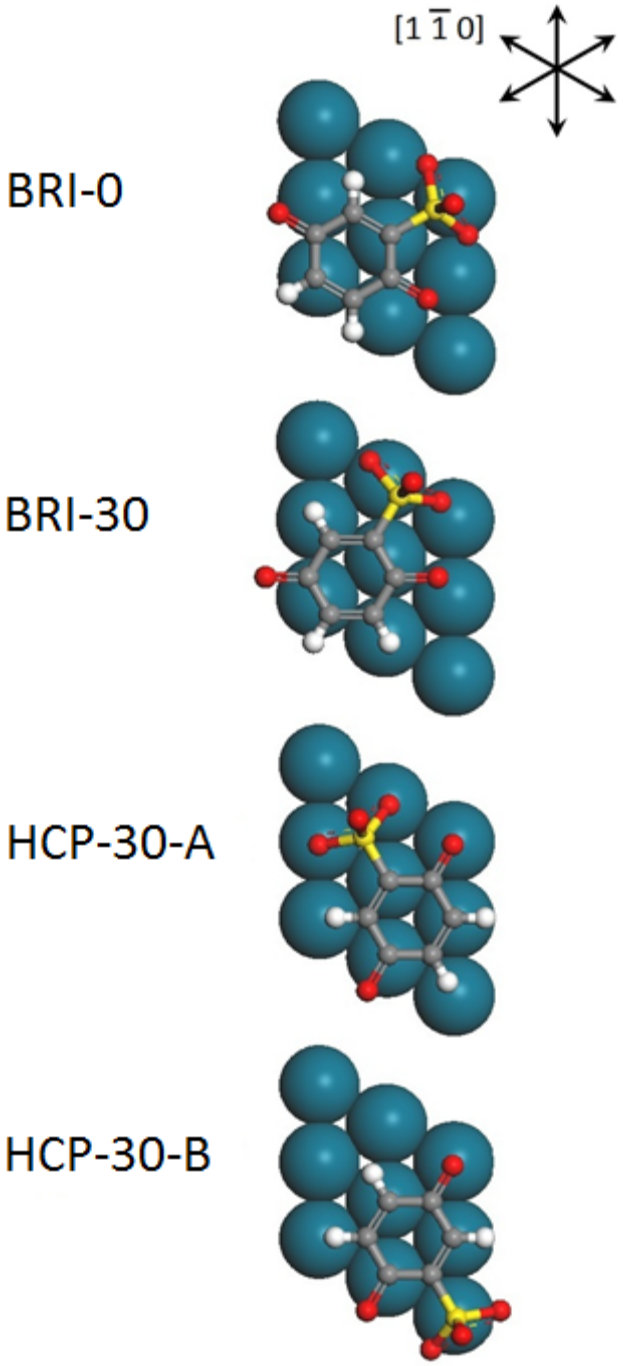

Figure A-5. Four possible adsorption geometries of BQS on a Pd(111) surface (Only the uppermost Pd layer is shown).

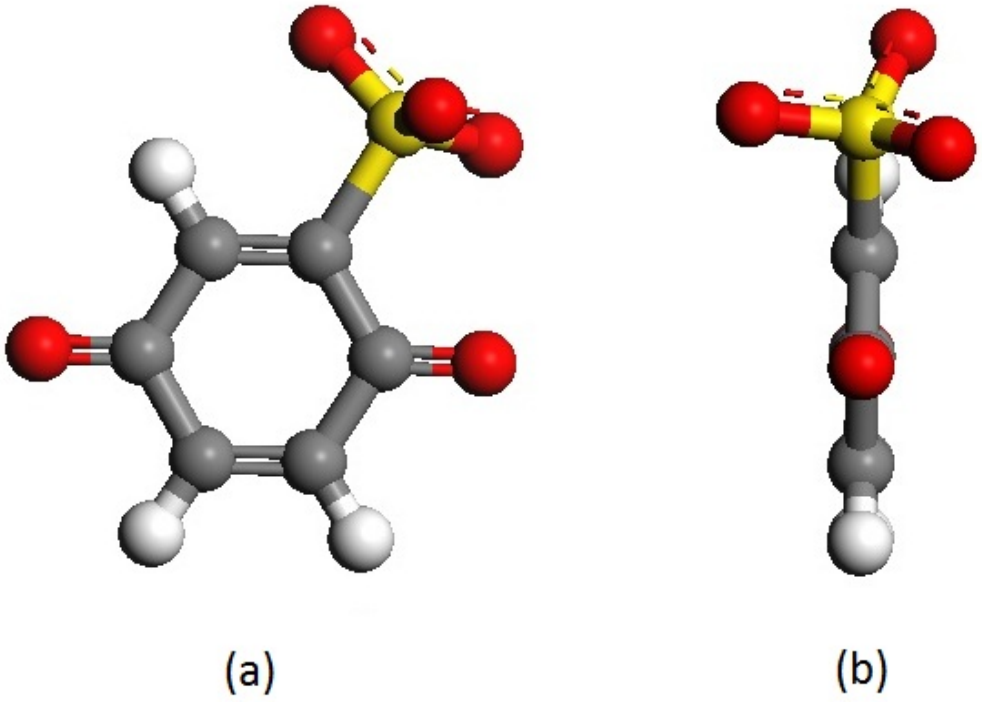

Figure A-6. Optimized structure of an isolated BQS molecule: **(a)** top view and **(b)** side view.

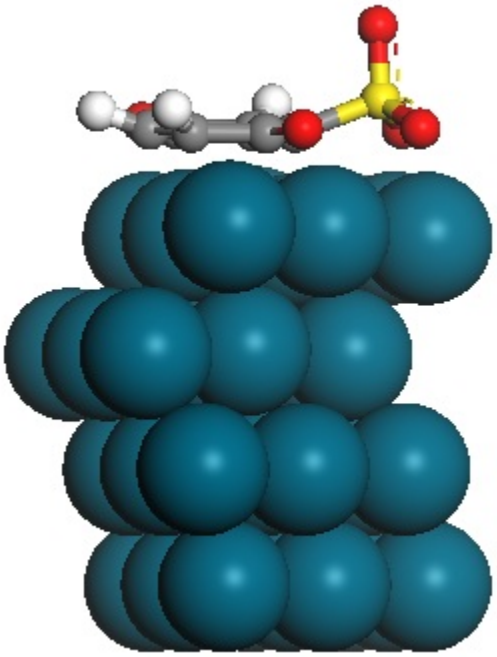

Figure A-7. Side view of the optimized adsorption geometry of BRI-30.

APPENDIX B

STM and DFT Studies of Anion Adsorption at Well-Defined Surfaces:

Pd(111) in Sulfuric Acid Solution

Alnald C. Javier[1], Youn-Geun Kim[1], Joseph B. Soriaga[1],

Perla B. Balbuena[2] and Manuel P. Soriaga[1*]

[1]Department of Chemistry

[2]Department of Chemical Engineering

Texas A&M University

College Station, TX 77843

Published: Philippine Science Letters, January 2011

A.C. Javier, Y.-G. Kim, J.B. Soriaga, P.B. Balbuena, M.P. Soriaga, Phil. Sci. Letters 4 (2011) 18.

The final publication is available at **www.philsciletters.org**

[*]Corresponding author

Phone: (979) 845-1846. Fax: (979) 845- 3523. E-mail: m-soriaga@tamu.edu

ABSTRACT

Density functional theory (DFT) has been employed to resolve compositional and structural issues related to the *in situ* (electrochemical) scanning tunneling microscopy (EC-STM) of a well-defined Pd(111) electrode surface in aqueous sulfuric acid solution. Fundamental concepts in inorganic chemistry had earlier been invoked to postulate that SO_4^{2-} anions, H_3O^+ counter-cations and H_2O were the most likely constituents in the compact layer. However, while the STM images distinctly revealed ordered rows of anions interspersed with hydronium ions and water molecules, details such as the orientations, spatial configurations and adsorption-site locations of the interfacial species could not be unambiguously ascertained. The present DFT-based geometry-optimization and total-energy calculations indicate that two layers of water molecules and hydronium ions are assembled, non-co-planar with one another, between the rows of surface-coordinated anions; the layer that is slightly elevated is comprised of counter cations.

Keywords:

Density functional theory

Electrochemical scanning tunneling microscopy

Anion adsorption at well-defined electrode surfaces

The electrode–electrolyte interface

Computational surface electrochemistry

INTRODUCTION

The role of supporting-electrolyte anions in reactions that proceed at the electrode-solution interface is of fundamental importance in electrochemical surface science. The observation that the morphology of the current-potential curve of Pt(111) in perchloric-acid electrolyte is dramatically different than that in sulfuric acid is a well-known example [B1].

The prevalent use of sulfuric acid as an "inert" supporting electrolyte has led to extensive studies on its interaction with the noble-metal electrodes [B1-B13]. A variety of experimental techniques that included electrochemical scanning tunneling microscopy (EC-STM), cyclic voltammetry, chronocoulometry, radiotracer measurements and optical spectroscopy has been employed; computational methods were also exploited. While results from various laboratories on interfacial coverages, structures and reactivities are in reasonable agreement with one another, the nature or identity of the adsorbed anion has not been unambiguously established. In an earlier investigation,[1] we invoked fundamental concepts from inorganic chemistry to argue that only sulfate ions would be present on the electrode surface: If HSO_4^- were surface-coordinated via the oxygen lone-pairs, the inductive effect brought about by the pull of electron density away from the sulfur atom towards the more electronegative coordinated-oxygen atoms weakens the O-H bond since the decreased negative-charge density on sulfur would extract electron density from the O-H group. Consequently, when HSO_4^- binds to a transition-metal center, whether in homogeneous or heterogeneous complexes, the

enhanced acidity of the O-H group will most likely yield SO_4^{2-} di-anions in the coordination sphere (compact layer).

We earlier reported results from EC-STM investigations on the interfacial structure of a Pd(111) electrode surface in 0.05 M H_2SO_4 [B1]. That study showed that, when a Pd(111) electrode is immersed in a dilute sulfuric acid solution, a well-ordered ($\sqrt{3} \times \sqrt{7}$) adlattice is formed on the Pd surface as shown in Figure B-1. This structure is similar to those obtained from EC-STM studies on Au(111) [B2,B3], Pt(111) [B4,B5], Rh(111) [B6], Cu(111) [B7-B10], and Ir(111) [B11,B12] in dilute sulfuric acid solutions. The rows of bright spots are believed to represent the adsorbed anions, whereas the dim rows arise from the hydrogen-bonded chains of water molecules [B3,B6,B10,B11] and hydronium cations [B1,B4,B5,B12,B13].

Further examination of the three-dimensional and the zoomed-in images of the ($\sqrt{3} \times \sqrt{7}$) adlattice (Figures B-2a and B-2b) reveal important structural details: (i) the adsorbed sulfate is trigonally coordinated on the Pd(111) surface such that the ion is directly above a 3-fold hollow site, and (ii) two layers of water molecules and hydronium cations are formed between the anionic rows; the layers, however, are not co-planar with one another with the slightly elevated layer constituted by hydronium counter-cations. Two real-space structures, depicted in Figure B-3, were proposed; the major differences in the two structures lie in the spatial orientations and the adsorption-site locations of the molecular and cationic species. EC-STM was not able to ascertain the actual structure. It is in this context that the EC-STM results have been revisited and computationally scrutinized.

The two issues targeted in the present study are: (i) the nature of the two co-adsorbed but non-co-planar layers of water molecules and hydronium cations, and (ii) the most favorable structure of the interfacial ensemble. The computational work was based on density functional theory (DFT). The dissection of structural nuances was accomplished by geometry-optimization calculations. The identification of the most favorable real-space structure was achieved by total-energy calculations in combination with STM-image simulations.

COMPUTATIONAL METHOD

The experimental details of the EC-STM measurements have already been published elsewhere [B1] and will not be reproduced here; only the DFT-based computational algorithms will be described.

DFT states that all ground-state properties of a system are functionals of the charge density, ρ. Hence, the ground-state total energy, E_t, may be written as:

$$E_t[\rho] = T[\rho] + U[\rho] + E_{XC}[\rho] \quad (1)$$

where $T[\rho]$ is the kinetic energy arising from non-interacting particles, $U[\rho]$ is the electrostatic energy attributable to Coulombic interactions, and $E_{XC}[\rho]$ is the exchange and correlation energy from many-body contributions [B14,B15]. The total energy is calculated by solving the Kohn-Sham equations, adopting the variational approach, and using a Self-Consistent Field (SCF) procedure. In this study, the Cambridge Sequential Total Energy Package (CASTEP), a first-principles DFT code integrated in Material Studio 5.0 of Accelrys Inc., was employed to perform the calculations [B16].

Vanderbilt-type ultrasoft pseudopotentials were used to allow computations to be done at lower cutoff energies and the generalized gradient approximation (GGA) [B17] and the Perdew-Wang exchange-correlation functional, PW91, [B18] were utilized to treat exchange and correlation effects. The plane-wave basis set was employed in this method since a periodic system was used.

The ability of various computational methods to evaluate the derivative of the total energy, E_t, with respect to variations in geometry is a valuable tool since it permits the determination of the structure with the lowest energy and thus, allows the prediction of the true chemical structure during structural optimization calculations. In this work, geometry optimization was performed with a cutoff energy of 300 eV and the Broyden-Fletcher-Goldfarb-Shanno (BFGS) method was employed as the energy minimization algorithm. A 3 × 3 × 1 k-point set was chosen for the Monkhorst-Pack grid and the Fermi smearing was set to 0.1 eV. As a criterion for convergence, the tolerance in energy, force, and displacement were 2.0 x 10^{-5} eV/atom, 0.05 eV/Å, and 0.002 Å, respectively. All of these variables were sufficient in achieving a reasonable convergence in determining the optimized structure and the total energy of all the systems studied [B19,B20].

In an attempt to model the interface, a 5 × 5 supercell was used in order to accurately represent the Pd(111)-($\sqrt{3} \times \sqrt{7}$)-SO_4^{2-}-H_3O^+-H_2O adlattice structures in Figure B-3. The (111) metal surface was formed by using a metal slab consisting of two layers of Pd atoms; only the upper Pd layer was allowed to relax. A vertical vacuum space of *ca.* 15 Å separated the metal surface from its periodic images [B19] and the

adlattice consisting of sulfate anions, hydronium cations, and water molecules is placed in this vacuum space.

An actual STM image shows the surface local density of states (LDOS) or the electron density surface produced by electronic states with a certain energy difference relative to the Fermi energy level. The energy difference from the Fermi level is determined by the applied bias on the STM tip. Simulated STM images in this work are obtained in a similar manner. Density functional periodic calculations determine the electronic energy levels of the interfacial system. By specifying a hypothetical tip potential, CASTEP can display a two-dimensional plot of the surface LDOS from electronic states at a specific energy relative to the Fermi level using the Tersoff-Hamann method [B21] and hence, simulate an STM image. A theoretical tip voltage of 0.200 V was used in this method to model the conditions used in obtaining the EC-STM images done in the previous experiment [B1].

In this study, the two structural models [structure (a) and structure (b) in Figure B-3] proposed for the ($\sqrt{3} \times \sqrt{7}$) adlattice are structurally optimized. The resulting geometries are evaluated as to whether or not (i) the two layers of water molecules and hydronium cations are present between rows of sulfate ions, and (ii) hydronium ions compose the upper layer. The more stable or favorable adsorption structure is determined by comparing the total energies, identifying the structure with the lesser total energy, and comparing the simulated STM images of the optimized structures with the experimental EC-STM images.

RESULTS AND DISCUSSION

The top and the side views of the optimized geometry of Structure (a) (Figure B-3) are shown in Figures B-4a and B-4b, respectively. It can be observed that the original model in Figure B-3 closely resembles the optimized structure except that the O–H bonds of water are pointing towards the metal surface for the latter.

Figures B-5a and B-5b display the top and the side views, respectively, of the optimized geometry of Structure (b) (Figure B-3). The optimized structure differs from the model in Figure B-3 mainly on the spatial orientation of the water molecules and the hydronium ions.

It is surprising to note that, on both structures, two layers of adsorbed species are formed between the sulfate rows wherein water molecules constitute the lower layer while the hydronium cations compose the upper layer. This substantiates the results acquired earlier from the EC-STM study [B1].

Structures of various chemical systems have been identified based on total energy calculations [B19,B20,B22,B23]. Likewise, in an attempt to determine the more favorable interfacial structure, the total energies of the two proposed structural models in Figure B-3 were calculated. Structure (b) is found to be more stable than Structure (a) by 0.073 eV per sulfate anion. Due to this small difference, the more favorable structure cannot be identified with absolute certainty based on total energy calculations alone. However, comparison of the EC-STM images with the optimized structures can provide useful insights. Since the hydronium ions are situated above the water molecules, the regions in the STM image (Figure B-2b) where these ions are located should show

enhanced brightness. By comparing Figures B-2b and B-4b, it can be observed that regions where the hydronium ions are positioned in Figure 4b correspond to empty areas in Figure B-2b. This indicates that Structure (a) is not likely to be the correct structure. On the contrary, the location of the hydronium ions in Figure B-5b appears to be bright in Figure B-2b, implying that Structure (b) is most certainly to be the true real-space structure.

To prove the argument cited above, simulated STM images of Structures (a) and (b) were obtained and are shown in Figures B-6a and B-6b, respectively. It is evident that Figure B-2b closely resembles Figure B-6b more than B-6a since the bright spots between the sulfate rows in the actual EC-STM image (Figure B-2b) coincide with the (rounded) protrusions in the simulated STM image in Figure B-6b. This signifies that Structure (b) is most likely to be the prevalent structure.

CONCLUSION

Density functional theory was employed to resolve compositional and structural issues related to the electrochemical scanning tunneling microscopy of a well-defined Pd(111) electrode surface in aqueous sulfuric acid solution. Fundamental concepts in inorganic chemistry had earlier been invoked to postulate that SO_4^{2-} anions, H_3O^+ counter-cations and H_2O were the most likely constituents in the compact layer. The STM images clearly revealed ordered rows of anions interspersed with the hydronium ions and the water molecules; but other aspects such as the orientations, spatial configurations and adsorption-site locations of the interfacial species could not be

unambiguously ascertained. The present DFT-based geometry-optimization and total-energy calculations indicate that two layers of water molecules and hydronium ions are assembled, non-co-planar with one another, between the rows of surface-coordinated anions; the layer that is slightly elevated is comprised of counter cations.

ACKNOWLEDGMENTS

Acknowledgment is made to the Welch Foundation (A-1064) for financial support and to the Laboratory for Molecular Simulation (Dr. L. M. Pérez) at Texas A&M University for the computational software and computer time. J.B.S. thanks the California Institute of Technology for a Summer Undergraduate Research Fellowship.

REFERENCES

[B1] Y.-G. Kim, J. Soriaga, G. Vigh, M.P. Soriaga, J. Colloid Interface Sci. 227 (2000) 505.

[B2] O.M. Magnusen, J. Hagebock, J. Hotlos, R.J. Behm, Faraday Discuss. Chem. Soc. 94 (1992) 329.

[B3] K. Sato, S. Yoshimoto, J. Inukai, K. Itaya, Electrochem. Commun. 8 (2006) 725.

[B4] A.M. Funtikov, U. Linke, U. Stimming, A. Vogel, Surf. Sci. 324 (1995) L343.

[B5] A.M. Funtikov, U. Stimming, A. Vogel, J. Electroanal. Chem. 428 (1997) 147.

[B6] L.-J. Wan, S. L. Yau, K. Itaya, J. Phys. Chem. 99 (1995) 9507.

[B7] M. Wilms, P. Broekmann, M. Kruft, Z. Park, C. Stuhlmann, K. Wandelt, Surf. Sci. 83 (1998) 402.

[B8] W.-H. Li, R. J. Nichols, J. Electroanal. Chem. 456 (1998) 153.

[B9] M. Wilms, P. Broekmann, C. Stuhlmann, K. Wandelt, Surf. Sci. 416 (1998) 121.

[B10] M. Arenz, P. Broekmann, M. Lennartz, E. Vogler, K. Wandelt, Phys. Stat. Sol. (a) 187 (2001) 63.

[B11] L.-J. Wan, M. Hara, J. Inukai, K. Itaya, J. Phys. Chem. B 103 (1999) 6978.

[B12] T. Senna, N. Ikemiya, M. Ito, J. Electroanal. Chem. 511 (2001) 115.

[B13] G. E. Edens, X. Gao, M. J. Weaver, J. Electroanal. Chem. 375 (1994) 357.

[B14] P. Hohenberg, W. Kohn, Phys. Rev. B 136 (1964) 864.

[B15] M. Levy, Proc. Natl. Acad. Sci. U.S.A. 76 (1979) 6062.

[B16] S.J. Clark, M.D. Segall, C.J. Pickard, P.J. Hasnip, M.J. Probert, K. Refson, M.C. Payne, Z. Kristallogr. 220 (2005) 567.

[B17] J.P. Perdew, K. Burke, M. Ernzehof, Phys. Rev. Lett. 77 (1996) 3865.

[B18] J.P. Perdew, Y. Wang, Phys. Rev. B 45 (1992) 13244.

[B19] H.Q. Qian, H.Y. Mao, F. Song, S.Q. Shi, H.J. Zhang, H.Y. Li, P.M. He, S.N. Bao, Appl. Surf. Sci. 256 (2010) 2686.

[B20] C. Morin, D. Simon, P. Sautet, J. Phys. Chem. B 107 (2003) 2995.

[B21] J. Tersoff, D.R. Hamann, Phys. Rev. B 31 (1985) 805.

[B22] C. Morin, D. Simon, P. Sautet, J. Phys. Chem. B 108 (2004) 5653.

[B23] Y.H. Lu, H.J. Zhang, Y.F. Xu, B. Song, H.Y. Li, S.N. Bao, P. He, Appl. Surf. Sci. 253 (2006) 2025.

FIGURES AND CAPTIONS

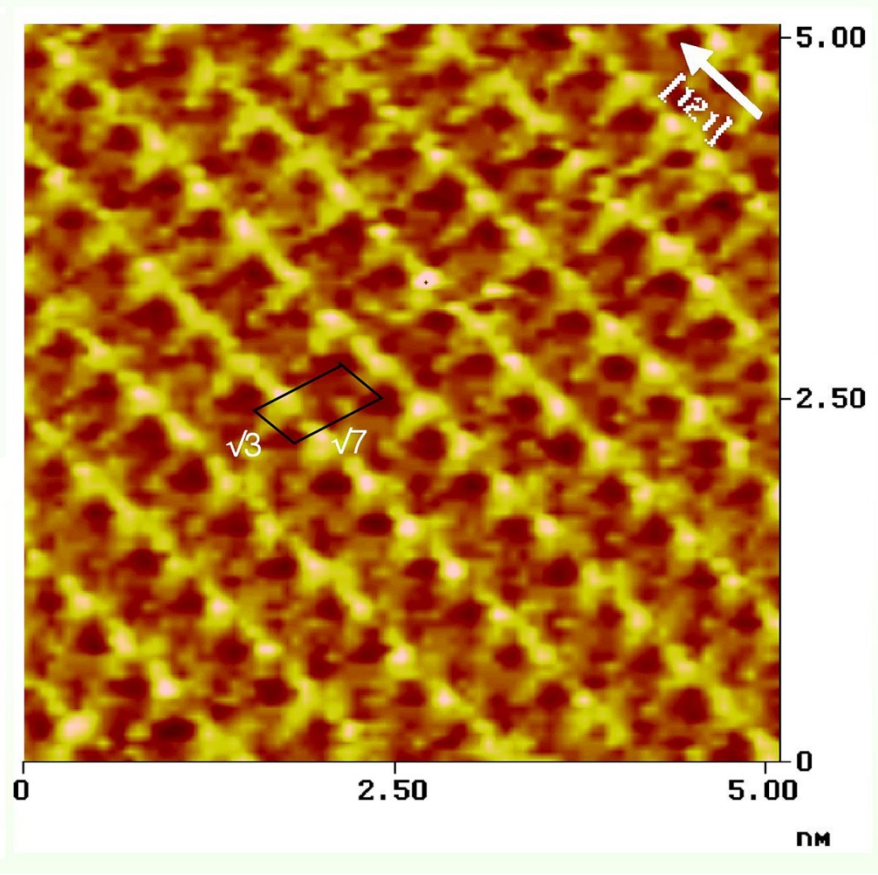

Figure B-1. EC-STM image of a Pd(111) electrode surface in 0.05 M H_2SO_4 at 0.4 V that shows a ($\sqrt{3} \times \sqrt{7}$) adlattice structure. Tunneling current = 20 nA [B1]. This figure is reproduced with permission from Y.-G. Kim, J. Soriaga, G. Vigh, M.P. Soriaga, J. Colloid Interface Sci. 227 (2000) 505. Copyright Elsevier.

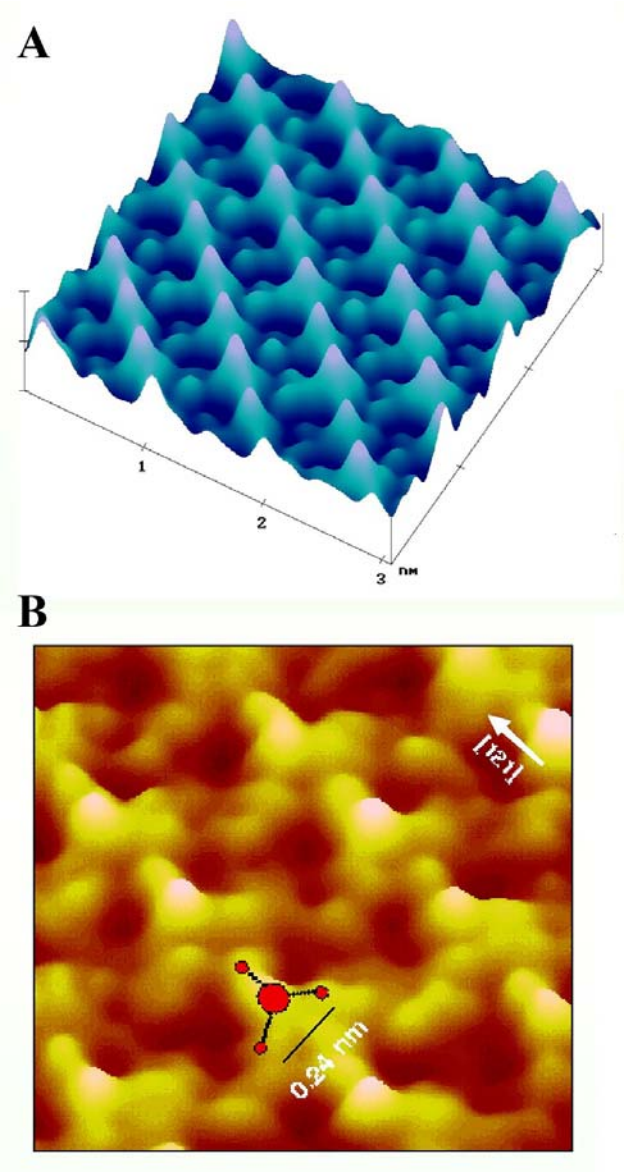

Figure B-2. A: Three-dimensional plot of the ($\sqrt{3} \times \sqrt{7}$) adlattice on the Pd(111) surface in 0.05 *M* H_2SO_4 at 0.4 V. B: Zoomed-in high-quality EC-STM image of the same adlayer [B1]. This figure is reproduced with permission from Y.-G. Kim, J. Soriaga, G. Vigh, M.P. Soriaga, J. Colloid Interface Sci. 227 (2000) 505. Copyright Elsevier.

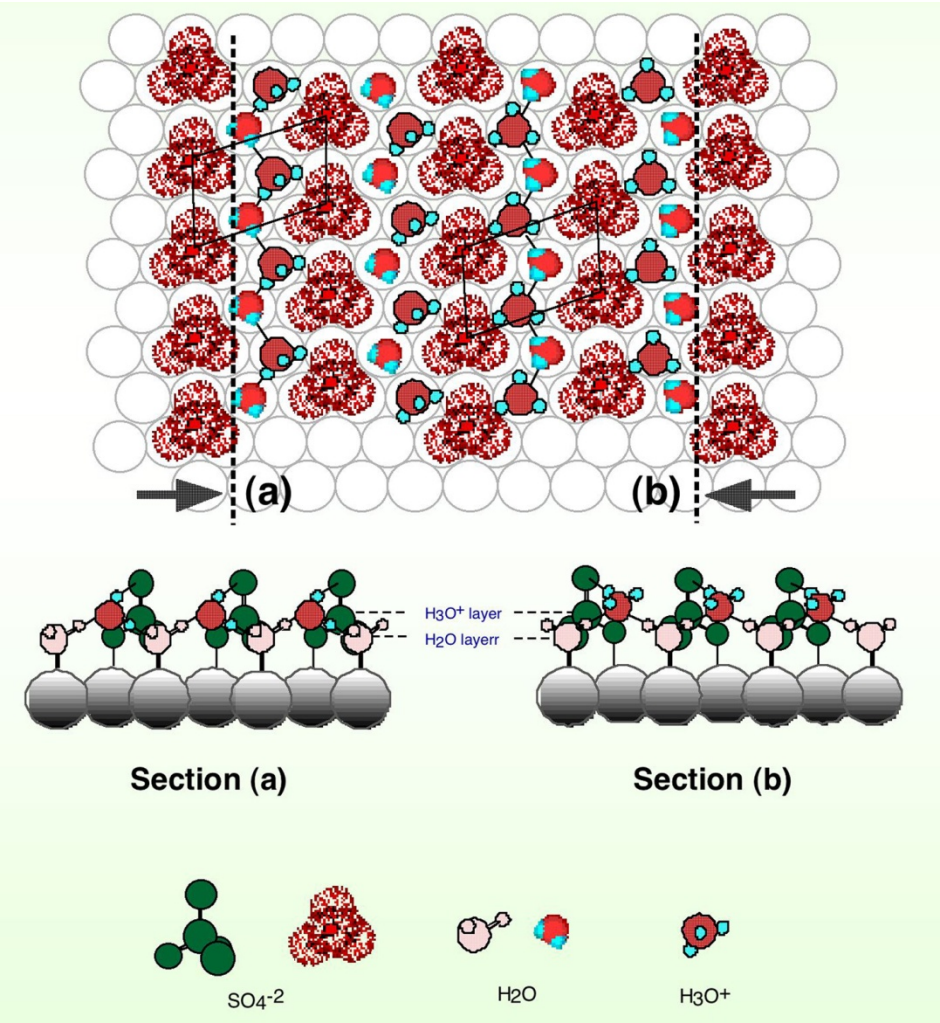

Figure B-3. Two possible real-space structures of the Pd(111)-($\sqrt{3} \times \sqrt{7}$)-SO_4^{2-}-H_3O^+-H_2O adlattice [B1]. This figure is reproduced with permission from Y.-G. Kim, J. Soriaga, G. Vigh, M.P. Soriaga, J. Colloid Interface Sci. 227 (2000) 505. Copyright Elsevier.

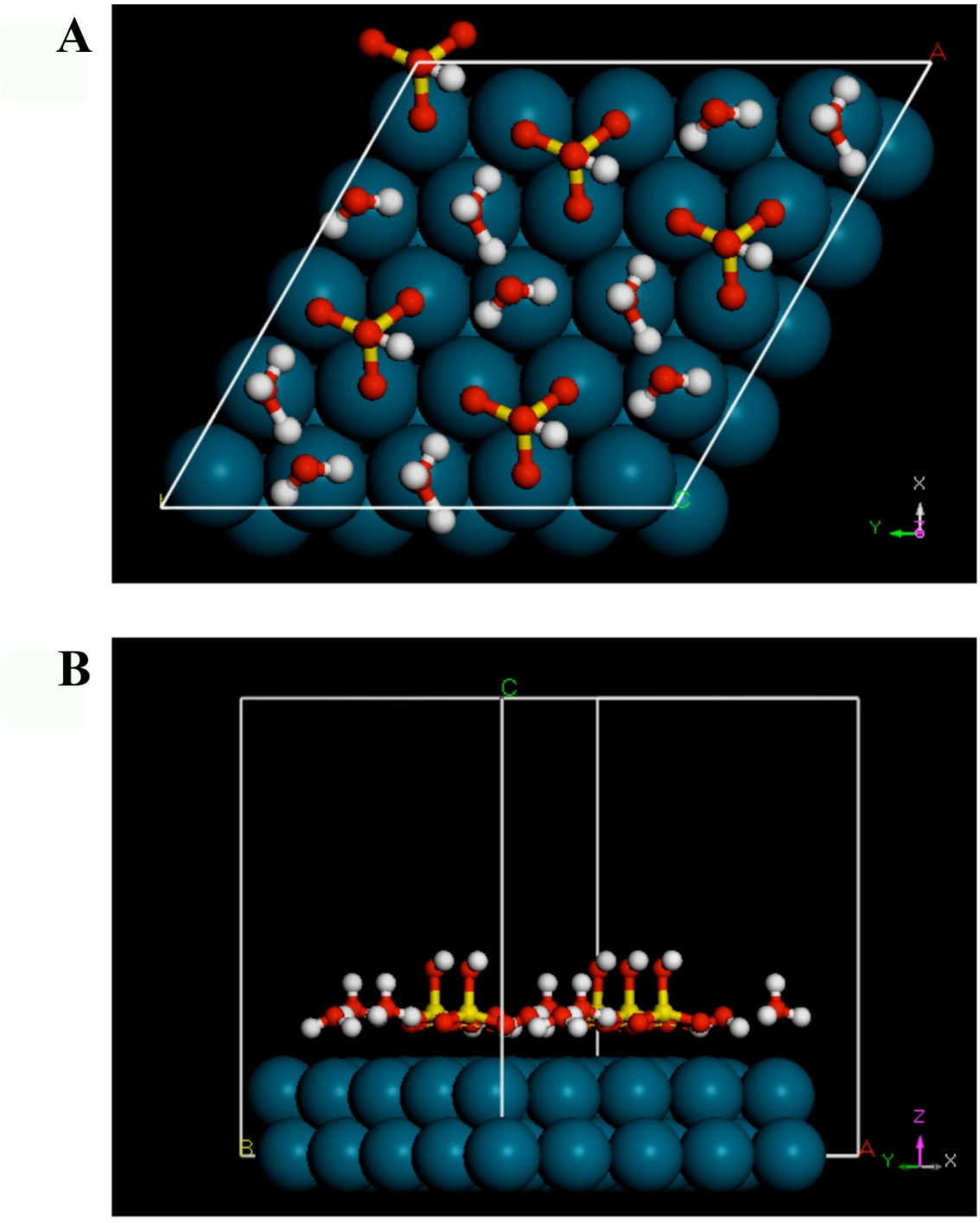

Figure B-4. Top view (A) and side view (B) of the optimized geometry of structure (a).

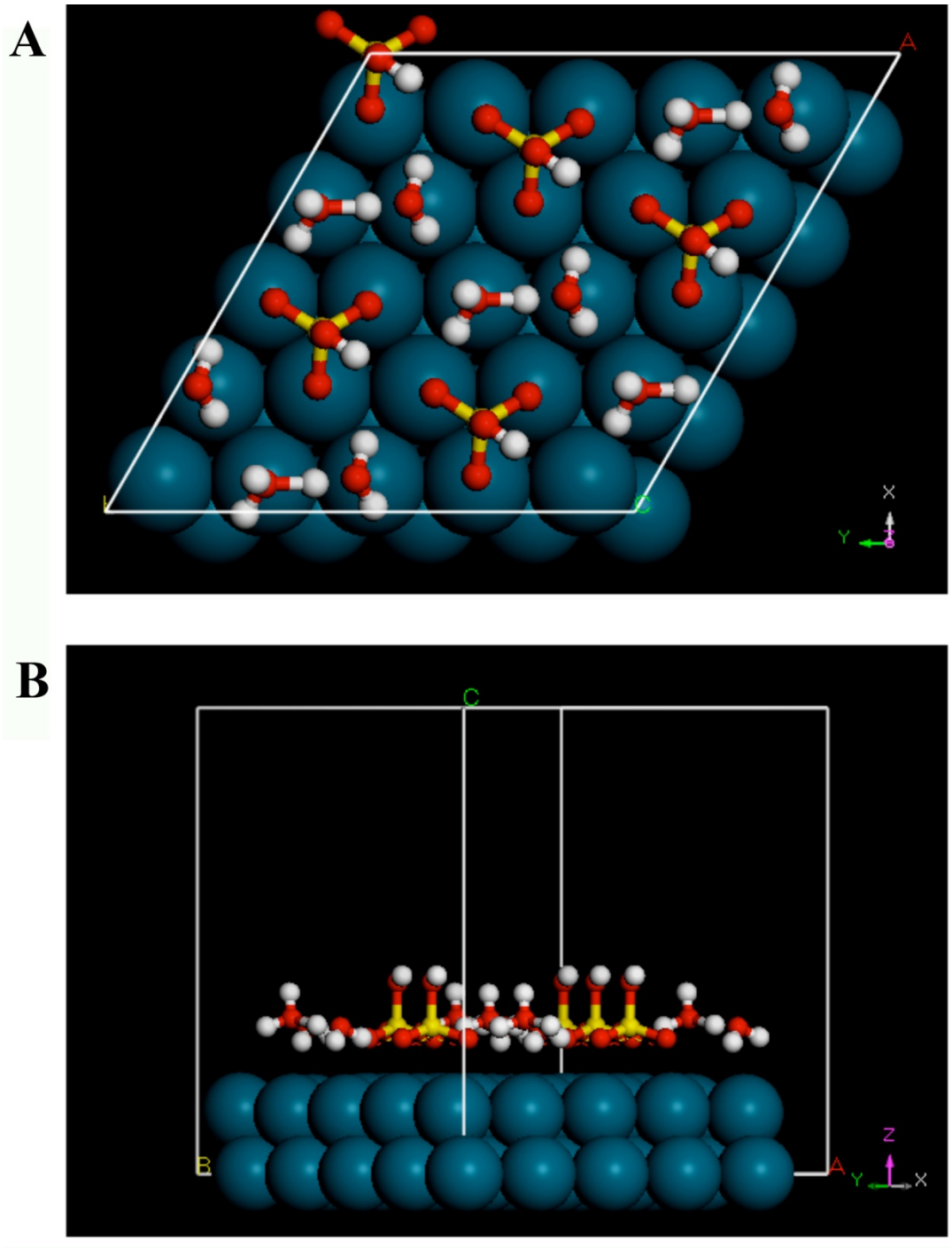

Figure B-5. Top view (A) and side view (B) of the optimized geometry of structure (b).

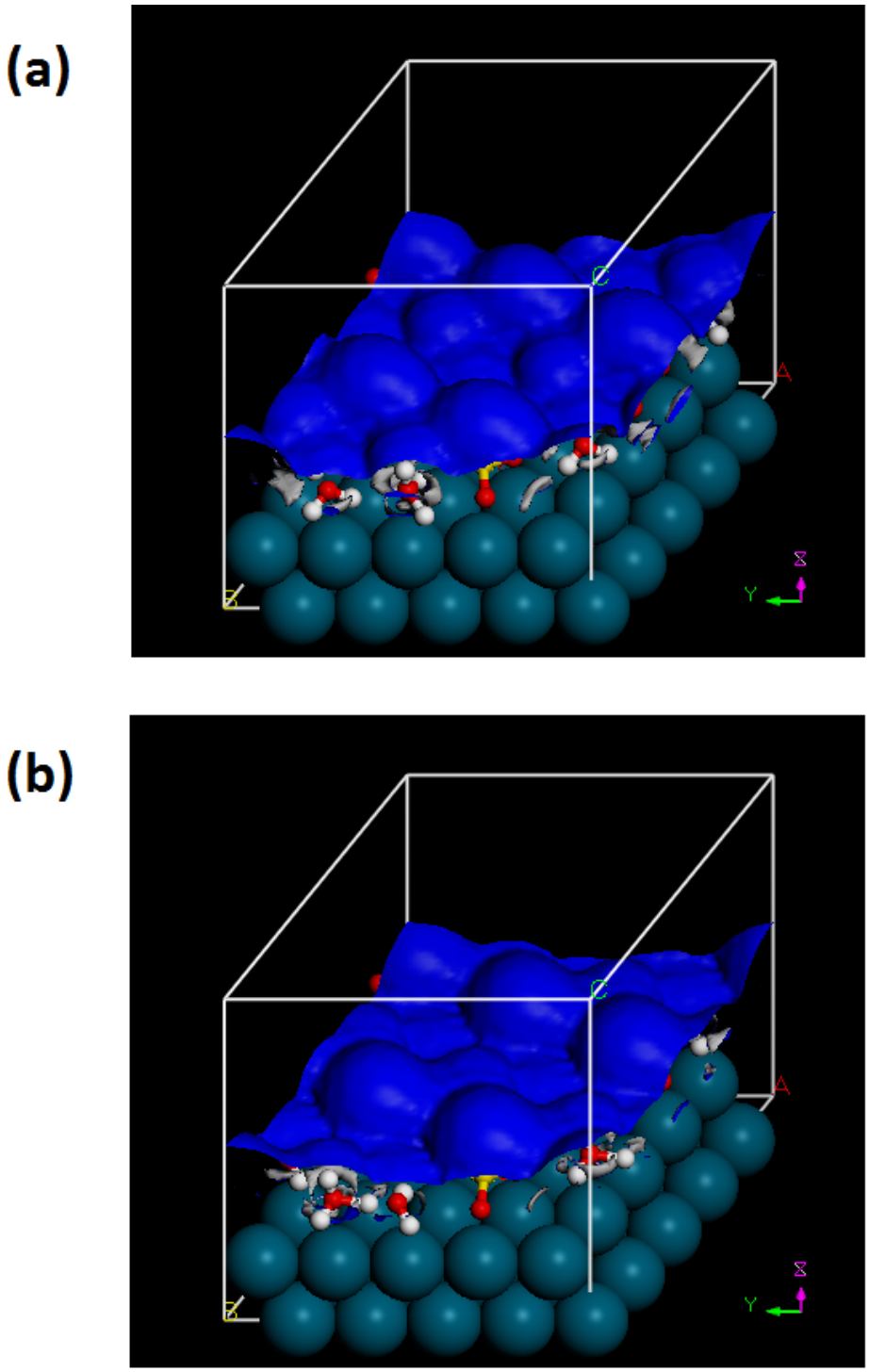

Figure B-6. Simulated STM image of the optimized geometry of structures (a) and (b).

APPENDIX C

The Structure of Benzoquinone Chemisorbed on Pd(111): Simulation of EC-STM Images and HREELS Spectra by Density Functional Theory

Alnald Javier[1], Youn-Geun Kim[1], Jack Hess Baricuatro[1], Perla B. Balbuena[2], and Manuel P. Soriaga[1,*]

[1]Department of Chemistry

[2]Department of Chemical Engineering

Texas A&M University

College Station, TX 77843

Published: Electrocatalysis, Springer, September 5, 2012

A. Javier, Y.-G. Kim, J.H. Baricuatro, P.B. Balbuena, M.P. Soriaga, Electrocatal. 3 (2012) 353.

The final publication is available at **link.springer.com**

[*]Corresponding author

Phone: (979) 845-1846. Fax: (979) 845- 3523. E-mail: m-soriaga@tamu.edu

ABSTRACT

Earlier studies on the chemisorption of hydroquinone (H_2Q) on well-defined Pd(111) surfaces based on electrochemistry, high-resolution electron energy loss spectroscopy, and *in situ* scanning tunneling microscopy revealed that H_2Q undergoes oxidative chemisorption to generate an adlayer of benzoquinone (Q) oriented flat, albeit with a slight tilt. Certain structural details, however, such as the actual adsorbate structure and the surface-coordination site could not be unambiguously confirmed solely from the experimental measurements. Density functional theory was thus employed not only to calculate the total adsorption energies of the likely configurations but also to simulate their respective vibrational spectra. The results suggest that: (i) the flat-adsorbed quinone ring is centered on a bridge site in which the C_2 axis that points along the *para*-oxygen atoms is rotated 30^o from the [110] direction of the Pd(111) substrate; (ii) the *p*-oxygen atoms are located above two-fold sites; and (iii) quinonoid ring is slightly puckered with the C–H bonds tilted away from the surface, at an angle of approximately 20^o.

Keywords:

Oxidative hydroquinone chemisorption on Pd(111) electrode

Benzoquinone chemisorption on Pd(111) electrode

Density functional theory

Electrochemical scanning tunneling microscopy

High-resolution electron energy loss spectroscopy

INTRODUCTION

It is well known that, in electrocatalytic processes, direct interaction between the electrode surface and the reagent molecule is a pre-requisite. Hence, if substantial advances are to be gained in fuel-cell and related technologies that rely on electrochemical catalysis, the nature and aftermath of such interactions must be documented and understood [C1-C3]. It is towards this objective that we are compelled to examine the structure, composition and reactivity of a wide variety of organic molecules at well-defined noble-metal electrode surfaces [C4-C10]. We earlier described results from studies on the chemisorption of diphenols on Pd(*hkl*) surfaces based on electrochemistry (EC), high-resolution electron energy loss spectroscopy (HREELS), and scanning tunneling microscopy (STM) [C4-C10]. We noted that, when a well-defined Pd(111) electrode is immersed in a dilute aqueous solution of hydroquinone (H_2Q), an immediate chemisorption reaction occurs in which the surface-coordinated H_2Q molecule undergoes spontaneous oxidation to benzoquinone (Q) [C4,C8]. The latter adopts a Pd(111)-(3 x 3)-Q adlayer structure as shown in the EC-STM image in Figure C-1. Detailed analysis of the EC-STM data indicated that, when Q is chemisorbed parallel to the Pd(111) surface: (i) it adopts an essentially flat orientation with a slight tilt, and (ii) the quinone ring is centered on a two-fold bridge site with two possible structures as illustrated in Figures C-2A and C-2B. It should be noted that the difference in the two structures lies in the location of the O atoms: In Figure C-2A, the O atoms occupy atop sites; in Figure C-2B, they are located on 2-fold sites. Unfortunately, it is

not possible to determine from the EC-STM images alone which of the two possible geometries is the actual structure.

We recently published computational results based on density functional theory (DFT) that, along with experimental HREELS and EC-STM data, made possible a more precise depiction of the adsorbed-molecule structure of benzoquinone sulfonate on the Pd(111) surface [C11]. In a similar vein, we employed DFT total-energy calculations to identify the most plausible interfacial structure of Pd(111)-(3 × 3)-Q overlayer. As an added feature, DFT simulation was also carried out to obtain surface-vibrational frequencies of the chemisorbed Q; comparison of the calculated results with the experimental HREELS data helps to (i) ascertain the geometry of the chemisorbed molecule, and (ii) determine which of the two structures in Figure C-2 is more likely.

COMPUTATIONAL METHOD

The details of the HREELS and EC-STM experiments have been described elsewhere [C4,C9] and will not be repeated here. Only the computational method based on density functional theory (DFT) will be discussed.

DFT is based on the Hohenberg-Kohn theorem which states that all ground-state properties of a system can be expressed in terms of the charge-density distribution, ρ. In this formalism, the ground-state total energy, E_t, may be expressed as:

$$E_t[\rho] = T[\rho] + U[\rho] + E_{XC}[\rho] \quad (1)$$

where $T[\rho]$ is the kinetic energy, $U[\rho]$ is the electrostatic energy, and $E_{XC}[\rho]$ is the exchange and correlation energy arising from non-interacting particles, Coulombic

interactions, and many-body contributions, respectively [C14,C15]. $E_{XC}[\rho]$ is calculated by solving the Kohn-Sham equations self-consistently for single-particle wavefunctions [C16].

In the present work, the Cambridge Sequential Total Energy Package (CASTEP), a first-principles DFT code in the Material Studio 5.0 simulation software (Accelrys Inc.), was used for the computations [C17]. To solve exchange and correlation contributions, the generalized gradient approximation (GGA) [C18] and the Perdew-Wang exchange-correlation functional, PW91, [C19] were adopted. The plane-wave basis set and norm-conserving pseudopotentials were utilized to describe the periodic system and to allow calculations to be performed at lower cutoff energies.

Knowledge of the derivative of the total energy, E_t, with respect to variations in geometry is rather advantageous because it allows the determination of the lowest-energy structure during geometry optimization; that is, it permits the identification of the most plausible chemical structure. Geometry optimization in this study was undertaken with a cutoff energy of 450 eV based on the Broyden-Fletcher-Goldfarb-Shanno (BFGS) energy-minimization algorithm. The Monkhorst-Pack grid (k-point set) and Fermi smearing were set to $3 \times 3 \times 1$ and 0.1 eV, respectively. The tolerance in energy, force, and displacement were set to 1.0×10^{-5} eV/atom, 0.03 eV/Å, and 0.001 Å, respectively, as the criteria for convergence. All these parameters were more than sufficient to attain a reasonable convergence in the determination of the optimized structure and total energy [C11,C12,C20].

In order to model the Pd(111)-(3 × 3)-Q structures in Figure C-2, 3 × 3 supercells were used in the calculations. A metal slab that consisted of four layers of Pd atoms, where only the upper two Pd layers were allowed to relax, represented the Pd(111) surface. A vertical vacuum space of approximately 15 Å isolated the metal surface from its periodic images [C20] and the quinone molecule is placed in this vacuum space. A slab model was used since it overcomes many of the difficulties faced in cluster models.

To determine the relative stabilities of the adsorption structures, the adsorption energy, E_{ads}, was calculated. E_{ads} is defined as:

$$E_{ads} = E_{Pd\text{-}Q} - E_{Q} - E_{Pd} \qquad (2)$$

where $E_{Pd\text{-}Q}$, E_{Q} and E_{Pd} represent the total energies of the Pd-Q interfacial system, the unadsorbed Q molecule, and the clean Pd(111) surface, respectively. It would follow that the more negative the adsorption energy, the stronger the adsorption.

Vibrational frequencies may be calculated from the matrix of Cartesian second derivatives (the Hessian matrix) of a periodic or molecular system [C21]. In this computational study, the finite-displacement method was used to calculate the different vibrational frequencies and assign the various vibrational states in the system.

All possible flat-adsorbed structures of Q on Pd(111) were geometrically optimized. Selection of the most stable form was based not only on the criterion of lowest (most negative) adsorption energy but also on closest agreement of the simulated and experimental (HREELS) vibrational spectra.

RESULTS AND DISCUSSION

Figure C-1 shows an unfiltered EC-STM image of a Pd(111)-(3 × 3)-Q adlayer formed spontaneously when a Pd(111) electrode surface is exposed to a dilute aqueous solution of hydroquinone at 0.5 V [C9]. It was proposed that the molecules are adsorbed parallel to the surface, albeit at a slight tilt, and with the C_2 axis rotated 30^o from the hexagonal close-packed [110] direction of the Pd(111) substrate. Two possible real-space structures of the adlayer were proposed as shown in Figures C-2A and C-2B. Unfortunately, differentiation between the two domains to identify the most likely structure could not be achieved from only the EC-STM images. Using a similar solution concentration, an HREEL spectrum was also obtained, Figure C-3 [C4]. It was proposed (Table C-1) that peaks 1, 2, 3, and 4 correspond to aromatic out-of-plane bending (γ(CH)), aromatic in-plane bending (δ(CH)) or stretch (ν(C=C)), carbonyl stretch (ν(CO)), and C–H stretch (ν(CH)) modes, respectively. The absence of a hydroxyl stretch (ν(OH)) peak at around 3600 cm^{-1} indicates the absence of a phenolic O–H functional group due to the oxidation of H_2Q to Q during chemisorption [C4]. In addition, if the molecule adopts a rigidly flat (η^6) adsorbed-aromatic orientation, the metal-surface dipole selection rule would render peaks 2, 3, and 4 HREELS-inactive [C22,C23]; thus, the presence of peaks 2 to 4 suggests that chemisorbed Q is not entirely oriented flat on the surface, but is tilted slightly.

Figure C-4 shows possible adsorbed-molecule structures of Q on Pd(111) based on the adsorption of a wide variety of aromatic compounds on Pt(111) and Pd(111) electrode surfaces [C11-C13]. Holl, Bri, and Atop represent adsorption centered on 3-

fold hollow, 2-fold bridge, and atop sites, respectively; 0 and 30 correspond to the angles between the molecule's C_2 axis (or peripheral C–H and C=O bonds) and the [110] direction of the metal substrate. In some of the adsorption structures, two positions exist at which the carbonyl oxygen can be located; these are labeled A and B to differentiate. It is important to note that the structures in Figures C-2A and C-2B correspond to Bri-30-A and Bri-30-B, respectively.

The adsorption energy of each structure is calculated and is presented in Table C-2. E_{ads} values for Bri-0-B, Atop-0, and Atop-30 were not calculated since no stable geometries were obtained for these structures after geometry optimization. It shows that Bri-30-B, which is one of the structures proposed from EC-STM results, has the most negative adsorption energy (-1.09 eV) and may be interpreted as the most stable or probable structure. It is also important to mention that a significant difference in adsorption energy exists between the proposed Bri-30-A and Bri-30-B structures. Identification of the most likely structure based on a comparison of the adsorption energies at different adsorption sites has already been adopted in previous studies on benzoquinone sulfonate [C11] and benzene [C12,C13].

In an attempt to ascertain the actual structure, the frequencies of the different vibrational states in Bri-30-A and Bri-30-B, the two models proposed from EC-STM results, were calculated and are shown in Figure C-5. It can be observed that the most significant difference is the frequency of the C=O stretch; 1564 cm^{-1} for Bri-30-A while 1464 cm^{-1} for Bri-30-B. Since the experimental ν(CO) is 1466 cm^{-1} from HREELS

results (Table C-1), this may indicate that Figure C-2B or Bri-30-B may indeed most likely be the actual structure.

Figure C-6 shows Bri-30-B after geometry optimization. The peripheral C–H bonds of the quinone ring are evidently tilted away from the surface at an angle of approximately 20°; this is clearly different from the planar Q molecule shown in Figure C-7. Such deviation from planarity may explain why the in-plane C-H modes are HREELS-active in the specular direction. Similar behavior has been previously observed for benzoquinone sulfonate on Pd(111) [C11] and benzene on Pt(111) [C11-C13].

It is important to mention that the method of identifying the most probable adsorption structure by comparing the theoretical and experimental vibrational spectra has previously been used on the study of the adsorption of benzene on Pt(111), Pd(111), and Rh(111) [C13]. Furthermore, the computational method used in this work to obtain theoretical vibrational spectra has earlier been validated by comparing the spectra with those obtained experimentally and from well-known computational methods [C24-C28].

CONCLUSION

Previous studies on the chemisorption of hydroquinone (H_2Q) on well-defined Pd(111) surfaces based on electrochemistry, high-resolution electron energy loss spectroscopy, and *in situ* scanning tunneling microscopy revealed that H_2Q undergoes oxidative chemisorption to generate an adlayer of benzoquinone (Q) oriented parallel to the surface but with a slight tilt. Critical structural details, however, such as the actual adsorbate structure and the surface-coordination site could not be unambiguously

confirmed solely from the experimental measurements. Density functional theory was thus employed not only to calculate the total adsorption energies of the likely configurations but also to simulate their respective vibrational spectra. The results suggest that: (i) the flat-adsorbed quinone ring is centered on a bridge site in which the C_2 axis that points along the *para*-oxygen atoms is rotated 30^o from the [110] direction of the Pd(111) substrate; (ii) the *p*-oxygen atoms are located above two-fold sites; and (iii) quinonoid ring is slightly puckered with the C–H bonds tilted away from the surface, at an angle of approximately 20^o.

ACKNOWLEDGMENT

Acknowledgment is made to the Texas A&M University-CONACYT Collaborative Research Grant Program for partial financial support, to the Center for Electrochemical Systems and Hydrogen Research for equipment use, and to the Laboratory for Molecular Simulation (Dr. L. M. Perez) at Texas A&M University for the computational software and computer time.

REFERENCES

[C1] J. Lipkowski, P.N. Ross, Electrocatalysis, Wiley-VCH, New York, 1998.

[C2] A.T. Hubbard, Chem. Rev. 88 (1988) 633.

[C3] M.P. Soriaga, Prog. Surf. Sci. 39 (1992) 325.

[C4] J.E. Soto, Y.-G. Kim, M.P. Soriaga, Electrochem. Commun. 1 (1999) 135.

[C5] J. Soto, Y.-G. Kim, X. Chen, Y.-S. Park, M.P. Soriaga, J. Electroanal. Chem. 500 (2001) 374.

[C6] Y.-G. Kim, M.P. Soriaga, Phys. Chem. Chem. Phys. 3 (2001) 3303.

[C7] Y.-G. Kim, J.E. Soto, X. Chen, Y.S. Park, M.P. Soriaga, J. Electroanal. Chem. 554-555 (2003) 167.

[C8] X. Chen, J. Sanabria-Chinchilla, M.P. Soriaga, Electroanalysis 17 (2005) 2121.

[C9] Y.-G. Kim, J.H. Baricuatro, M.P. Soriaga, Langmuir 22 (2006) 10762.

[C10] J.E. Soto, D. Li, J. Sanabria-Chinchilla, X. Chen, M.P. Soriaga, J. Mol. Struc. 890 (2008) 298.

[C11] A. Javier, D. Li, P.B. Balbuena, M.P. Soriaga, Electrocatal. 1 (2010) 159.

[C12] C. Morin, D. Simon, P. Sautet, J. Phys. Chem. B 107 (2003) 2995.

[C13] C. Morin, D. Simon, P. Sautet, J. Phys. Chem. B 108 (2004) 5653.

[C14] P. Hohenberg, W. Kohn, Phys. Rev. B 136 (1964) 864.

[C15] M. Levy, Proc. Natl. Acad. Sci. U.S.A. 76 (1979) 6062.

[C16] W. Kohn, L.J. Sham, Phys. Rev. A 140 (1965) 1133.

[C17] S.J. Clark, M.D. Segall, C.J. Pickard, P.J. Hasnip, M.J. Probert, K. Refson, M.C. Payne, Z. Kristallogr. 220 (2005) 567.

[C18] J.P. Perdew, K. Burke, M. Ernzehof, Phys. Rev. Lett. 77 (1996) 3865.

[C19] J.P. Perdew, Y. Wang, Phys. Rev. B 45 (1992) 13244.

[C20] H.Q. Qian, H.Y. Mao, F. Song, S.Q. Shi, H.J. Zhang, H.Y. Li, P.M. He, S.N. Bao, Appl. Surf. Sci. 256 (2010) 2686.

[C21] E.B. Wilson, J.C. Decius, P.C. Cross, Molecular Vibrations, Dover, New York, 1955.

[C22] H. Ibach, D.A. Mills, Electron Energy Loss Spectroscopy, Academic Press, New York, 1982.

[C23] N.R. Avery, in: J.T. Yates, Jr, T.E. Madey (Eds.), Vibrational Spectroscopy of Molecules on Surfaces, Plenum Press, New York, 1987.

[C24] V. Milman, K. Refson, S.J. Clark, C.J. Pickard, J.R. Yates, S.-P. Gao, P.J. Hasnip, M.I.J. Probert, A. Perlov, M.D. Segall, J. Mol. Struct. (Theochem) 954 (2010) 22.

[C25] T. Lin, X. Liu, C. He, J. Phys. Chem. B 116 (2012) 1524.

[C26] P. Hermet, M. Goffinet, J. Kreisel, Ph. Ghosez, Phys. Rev. B 75 (2007) 220102.

[C27] E. Balan, A.M. Saitta, F. Mauri, G. Calas, Am. Mineral. 86 (2001) 1321.

[C28] S.F. Parker, K. Refson, K.P.J. Williams, D.A. Braden, B.S. Hudson, K. Yvon, Inorg. Chem. 45 (2006) 10951.

TABLES

Table C-1. Vibrational (HREELS) Frequencies of Adsorbed Benzoquinone on Pd(111) [C4]

Peak	Description	Frequency (cm^{-1})
1	Out-of-plane C–H bend	810
2	C–H bend	1230
3	C=O stretch	1466
4	C–H stretch	3007

Table C-2. Adsorption Energy (eV) of Benzoquinone at Various Adsorption Sites on Pd(111)[a]

Adsorption structure	Adsorption Energy (E_{ads})
Holl-0	– 0.64
Holl-30	– 0.83
Bri-0-A	– 0.39
Bri-0-B	No stable structure
Bri-30-A	– 0.66
Bri-30-B	– 1.09
Atop-0	No stable structure
Atop-30	No stable structure

[a] All calculations were performed using a 3 × 3 surface unit cell with a fixed cell volume equal to that of a bare Pd surface. The energy of the benzoquinone molecule was calculated separately in a 12 x 12 x 12 $Å^3$ cell.

FIGURES AND CAPTIONS

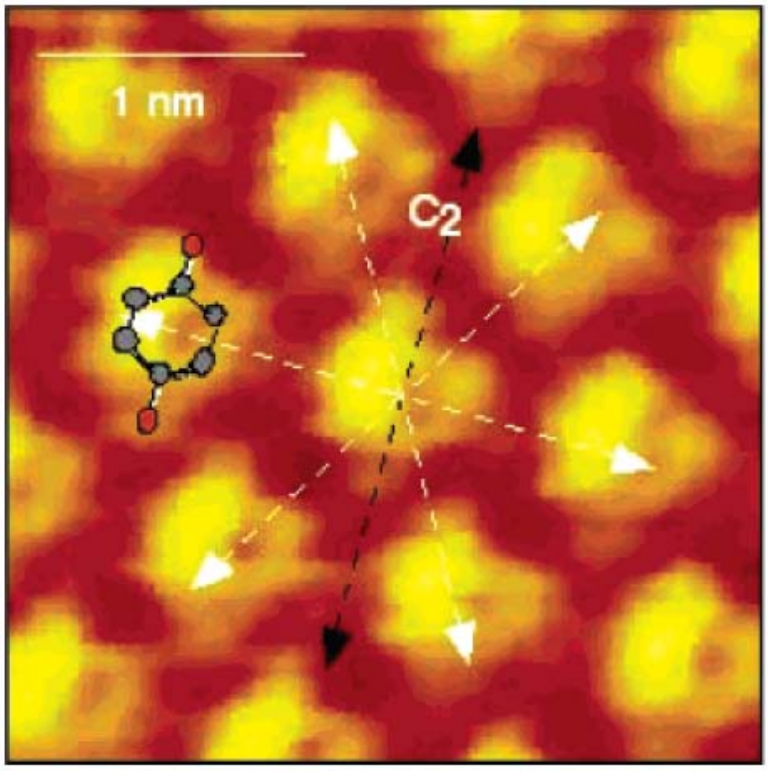

Figure C-1. Unfiltered high-resolution EC-STM image of the (3 x 3)-Q adlayer of the Pd(111) electrode surface immersed in a 0.1 m*M* solution of Q in 0.05 M H_2SO_4 at 0.5 V. Bias voltage, 120 mV; tunneling current, 30 nA [C9]. This figure is reproduced with permission from Y.-G. Kim, J.H. Baricuatro, M.P. Soriaga, Langmuir 22 (2006) 10762. Copyright American Chemical Society.

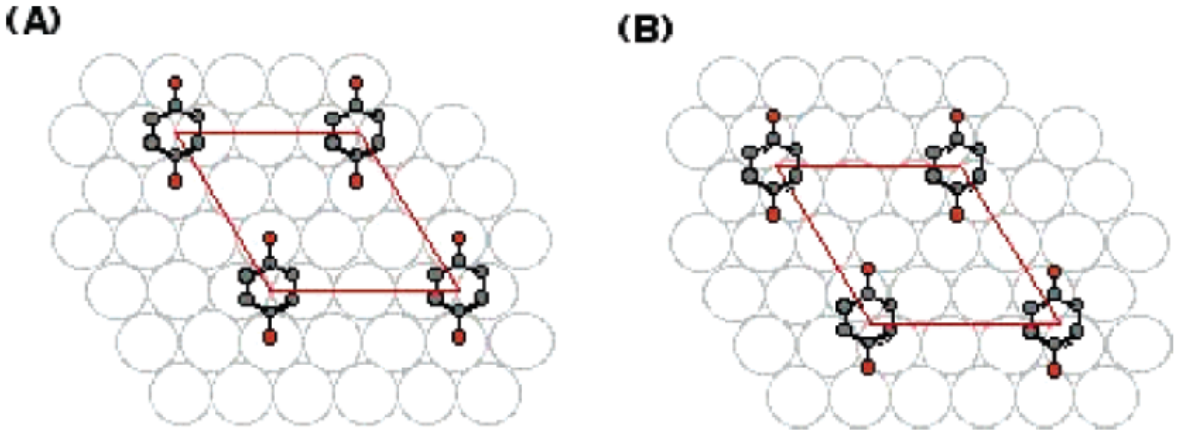

Figure C-2. Possible real-space structures of Pd(111)-(3 x 3)-Q from EC-STM results. The oxygen atoms are located above atop sites in structure A but occupy bridge sites in B [C9]. This figure is reproduced with permission from Y.-G. Kim, J.H. Baricuatro, M.P. Soriaga, Langmuir 22 (2006) 10762. Copyright American Chemical Society.

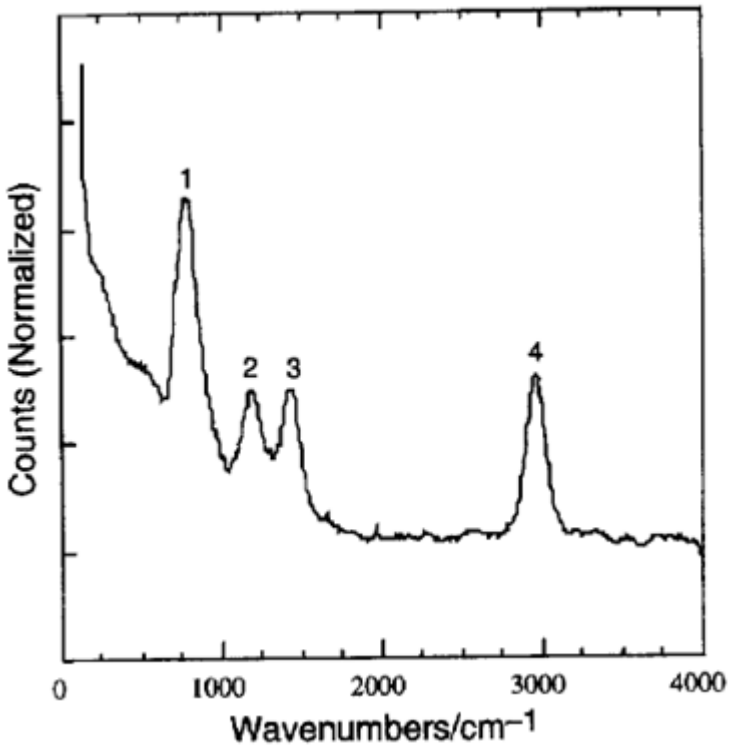

Figure C-3. HREEL spectrum of a Pd(111) surface after emersion from a 0.1 m*M* aqueous solution of Q in 1 m*M* TFA. Peaks 1, 2, 3, and 4 correspond to aromatic γ(CH), aromatic δ(CH), ν(C=O), and ν(CH) modes, respectively [C4]. This figure is reproduced with permission from J.E. Soto, Y.-G. Kim, M.P. Soriaga, Electrochem. Commun. 1 (1999) 135. Copyright Elsevier.

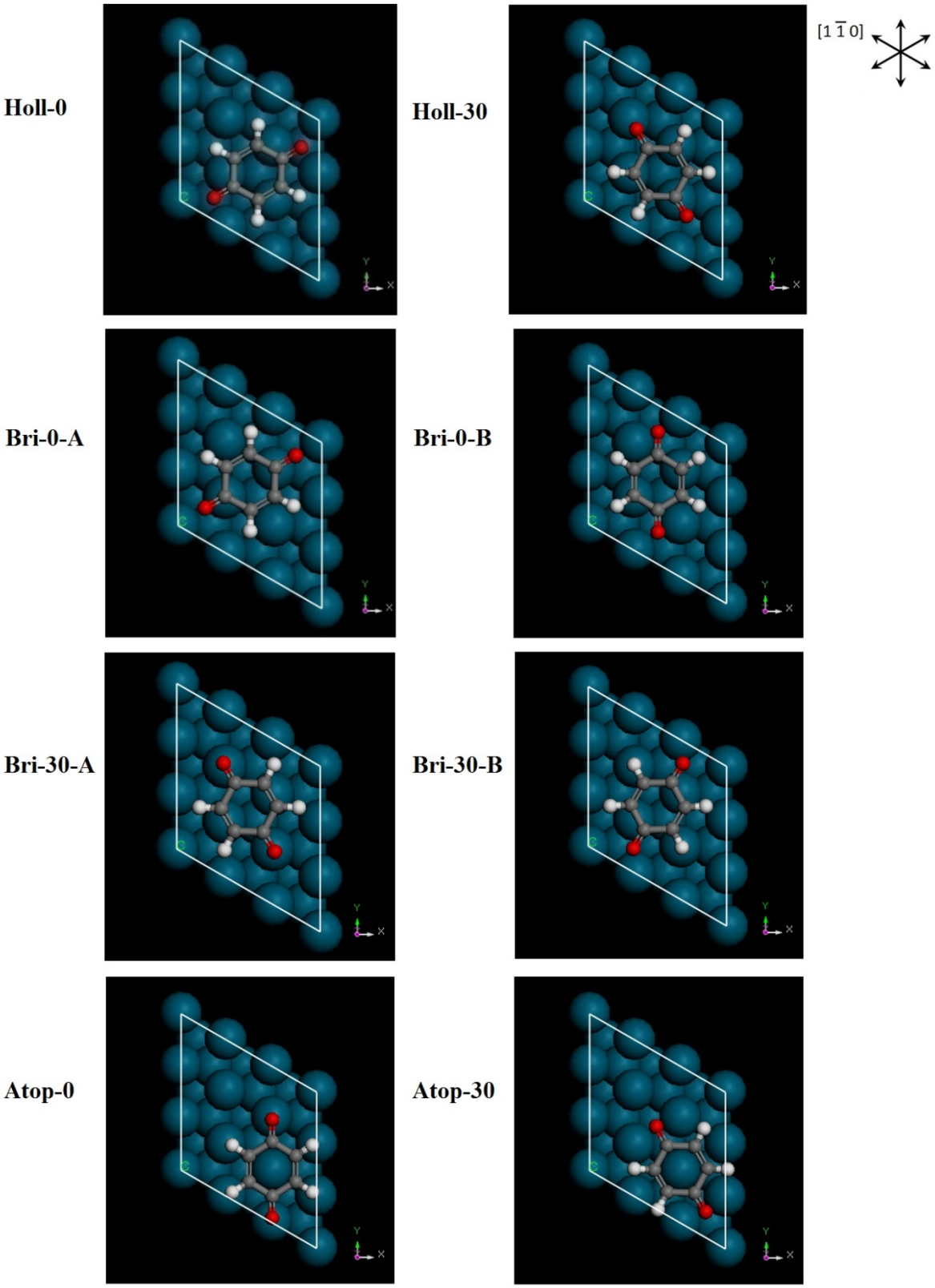

Figure C-4. Possible adsorption structures of benzoquinone on a Pd(111) surface.

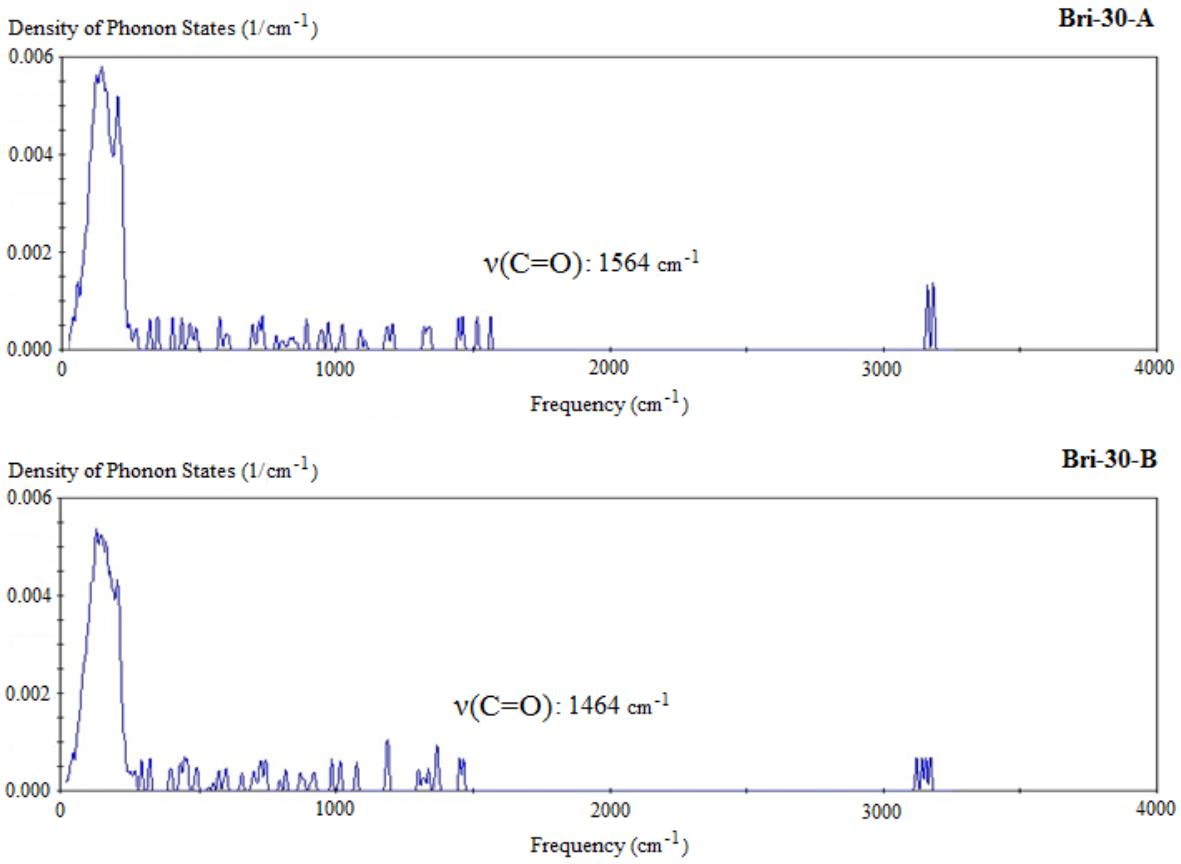

Figure C-5. Calculated vibrational frequencies of various vibrational states in Bri-30-A and Bri-30-B.

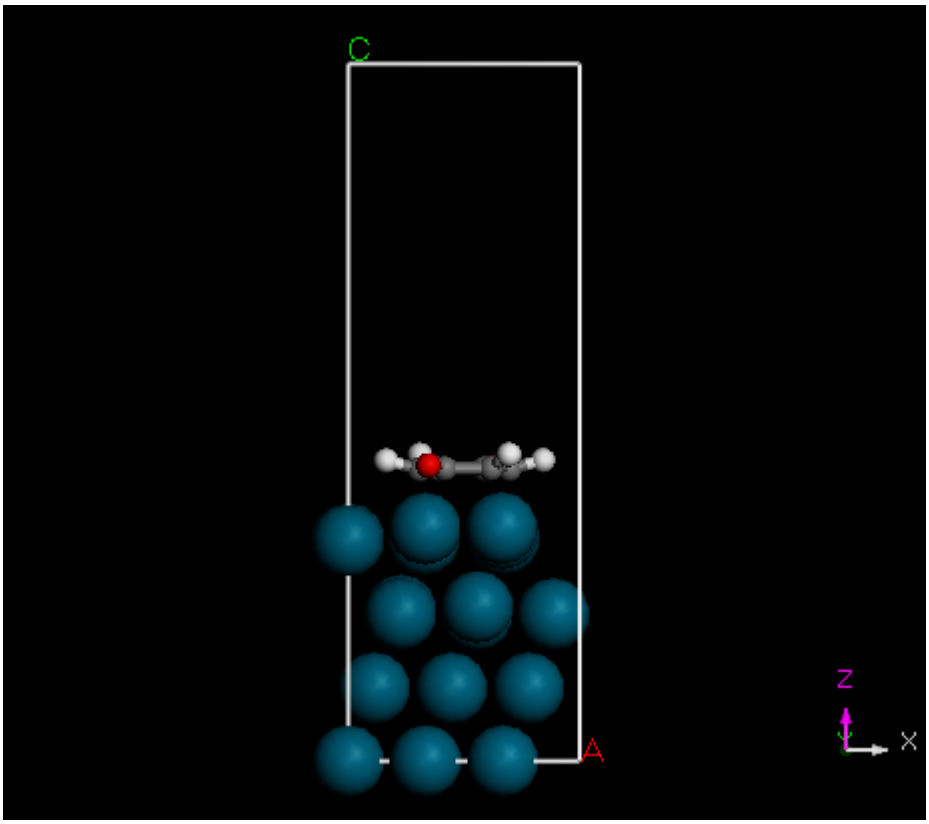

Figure C-6. Side view of the optimized adsorption structure of Bri-30-B.

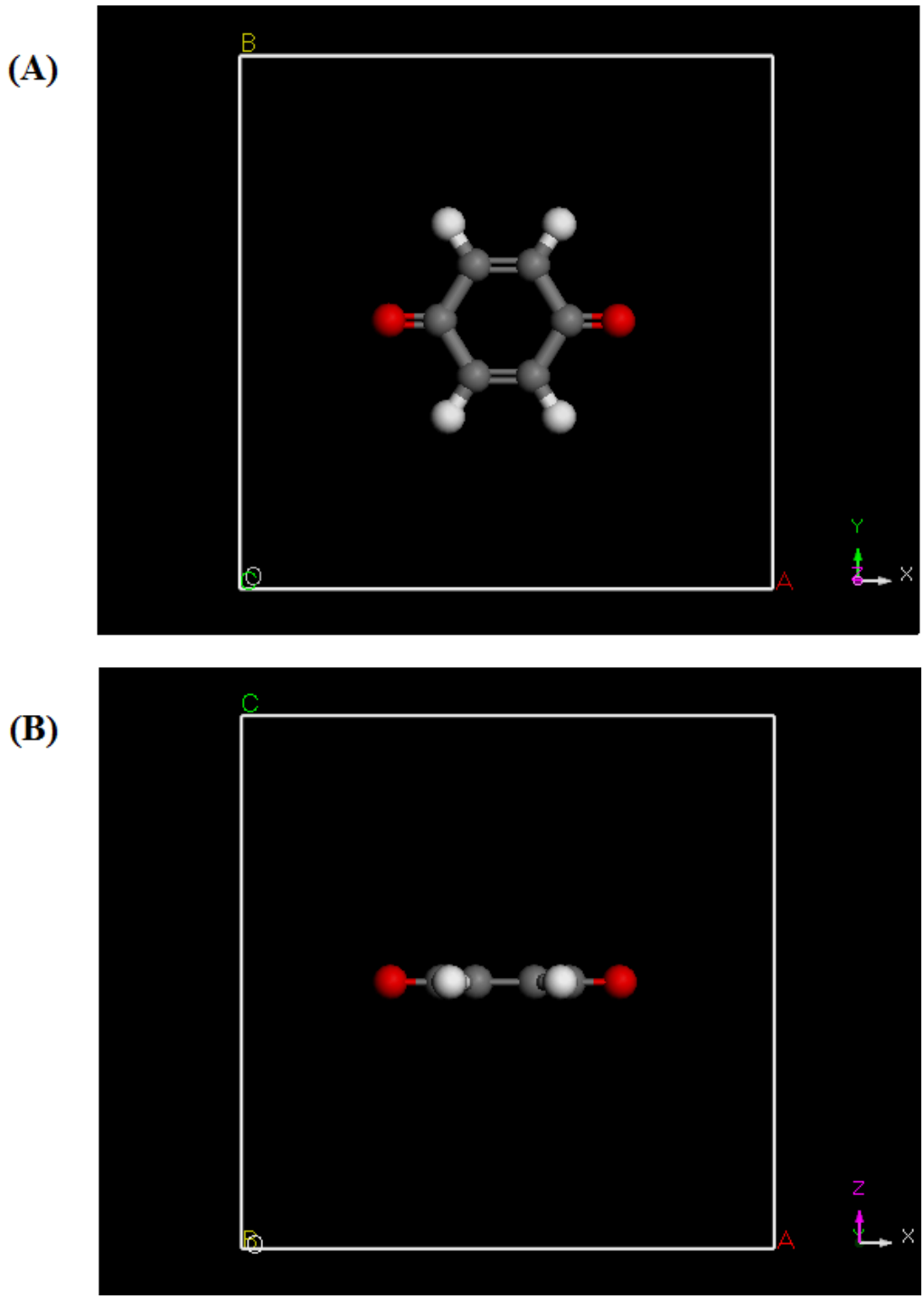

Figure C-7. Optimized geometry of an isolated benzoquinone molecule: (A) top view and (B) side view.

APPENDIX D

Simulation of Scanning Tunneling Microscope Image of Benzene Chemisorbed on a Pd(111) Electrode Surface by Density Functional Theory

Alnald Javier[1], Ding Li[1], Perla B. Balbuena[2], and Manuel P. Soriaga[1*]

[1]Department of Chemistry

[2]Department of Chemical Engineering

Texas A&M University

College Station, Texas 77843

Published: Reports in Electrochemistry, Dove Press, January 16, 2013

A. Javier, D. Li, P.B. Balbuena, M.P. Soriaga, Reports in Electrochemistry 3 (2013) 1.

The final publication is available at **www.dovepress.com**

[*]Corresponding author

Phone: (979) 845-1846. Fax: (979) 845- 3523. E-mail: m-soriaga@tamu.edu

ABSTRACT

A computational method based on density functional theory was used to simulate the scanning tunneling microscopy (STM) image of benzene chemisorbed on a Pd(111) electrode in order to confirm the adsorption site of the aromatic molecule on the metal surface held at a certain applied potential. The simulated STM images on various adsorption sites were obtained and compared to the experimental electrochemical STM images. The simulation results indicate that, when the potential of the Pd electrode is held at 0.3 V, benzene is chemisorbed on a 3-fold hollow site; at 0.55 V, the molecule is adsorbed on a position between a 3-fold and a 2-fold bridge site. These findings corroborate previously published experimental EC-STM results.

Keywords:

Density functional theory

Scanning tunneling microscopy

STM simulation

Benzene chemisorption

Pd(111) surface

INTRODUCTION

In the field of electrochemical surface science, it is of fundamental importance to determine the structure of molecular species chemisorbed on electrocatalyst surfaces. A surface-sensitive technique that can be used for this purpose is electrochemical scanning tunneling microscopy (EC-STM). However, interpretation of molecular STM images is not straightforward since they do not always unambiguously reveal the actual positions of the atoms; instead, the electronic states of the interface near the substrate Fermi energy level are shown [D1]. Fortunately, STM profiles can be simulated by computational methods such as those based on density functional theory (DFT). By comparison of experimental and theoretical STM results, elucidation and confirmation of certain structural features such as adsorbate orientations and adsorption sites can be achieved.

The chemisorption of aromatic molecules such as benzene on Pt(111) surfaces has been studied by STM. It has been observed that the STM images of benzene molecules on metal surfaces are dependent on the molecular adsorption site [D2]. With the aid of STM images simulated based on the electron scattering quantum chemical (ESQC) method, the following results were obtained: (i) when benzene is chemisorbed parallel to the surface at a 3-fold hollow site, the molecule appears triangular with three lobes at each vertex of the triangle; (ii) if the molecule is on a 2-fold bridge site, the molecular images appears to be a single elongated bump; and (iii) a ring-like structure with six lobes is observed only when the molecule is on a top site [D1,D3,D4].

Simulation of STM images of benzene adsorbed on Pd(111) surfaces has also been carried out [D5]. In that theoretical investigation, extended Hückel molecular orbital theory (EHT) was employed in the computations. The results were similar to those obtained with Pt(111) [D1,D3,D4].

In an earlier report, several EC-STM images were described of benzene adsorbed, at certain potentials, on Pd(111) electrode surfaces [D6]. The images suggested that, when the potential of the Pd electrode is held at 0.3 V, benzene is chemisorbed on a 3-fold site in a Pd(111)-(3×3)-C_6H_6 adlattice. However, at 0.55 V, the molecule is located on a spot between a 3-fold and a 2-fold site as a Pd(111)-c$(2\sqrt{3} \times 3)$-*rect*-C_6H_6 adlayer. To validate those scenarios, we present here DFT-based simulated STM profiles of benzene at various adsorption sites on a Pd(111) surface; the computed results are then compared with the experimental images [D6].

COMPUTATIONAL DETAILS

The Cambridge Sequential Total Energy Package (CASTEP) code was used in the calculations [D7]. This DFT-based module is incorporated in Material Studio 5.0 of Accelrys Inc., employs Vanderbilt-type ultrasoft pseudopotentials that allow calculations to be performed at a lower cutoff energy, and solves the Kohn-Sham equations using a plane-wave basis set.

Geometry optimization and energy calculations were performed utilizing a 3 x 3 x 1 Monkhorst-Pack grid, a cutoff energy of 300 eV, and a Fermi smearing of 0.1 eV. Earlier studies showed that these conditions are adequate enough in obtaining acceptable

energy values [D8,D9]. The generalized gradient approximation (GGA) [D10] and the Perdew-Wang exchange-correlation functional (PW91) [D11] were used to address exchange and correlation effects.

The calculations employed a 3 x 3 supercell to minimize lateral interactions between the molecule and its neighboring periodic images [D8,D12] and to simulate low adsorbate coverage conditions as seen in the actual EC-STM experiments performed before [D6]. In this structure, the surface was created as a metal slab containing four layers of Pd atoms with the upper two layers allowed to relax. The cell was also built in such a way that the slab was separated from its periodic images with a vertical vacuum space of ~15 Å [D8,D9,D12].

The STM profiles were obtained using DFT to determine the energy levels of the Pd-benzene system and the Tersoff-Hamann method [D13] to display a two-dimensional plot of the surface local density of states (LDOS) or the electron density isosurface produced by electronic states at a certain energy away from the Fermi energy level. In actual STM experiments, the precise energy difference from the Fermi level is determined by the applied bias on the STM tip. With CASTEP and in this simulation, a hypothetical tip potential can be set to view the LDOS and thus simulate the STM image. A theoretical tip voltage of 0.100 V was used in this study to emulate the conditions used in the previous EC-STM experiments [D6].

Geometry optimization was performed on the structures before simulated STM images were obtained. This implies that the molecule's most favorable adsorption structure and distance to the surface were determined and the resulting geometry was

used for STM image simulation. Optimizing the structure using this DFT method takes into account all possible interactions within the aromatic compound, on the surface, and between the molecule and the surface. It is also important to note that this method of simulating STM images was also used in studying the adsorption of sulfate anions on Pd(111) surfaces [D14].

RESULTS AND DISCUSSION

Unlike the ESQC method, which calculates the actual tunneling current obtained from the scattering matrix for the electrons on the tunnel gap [D3], or the EHT-based approach, which uses the semi-empirical Hückel method in calculating the energy levels [D5], the STM-simulation method adopted in this research relies on DFT to calculate and determine the energy levels of various electronic states, and the Tersoff-Hamann [D13] method to display the electron density isosurface as the STM profile.

Figure D-1a shows the adsorption geometry of benzene chemisorbed on a 3-fold hollow site on a Pd(111) surface. The corresponding simulated STM image is displayed in Figure D-1b. Based from the simulated profile, it is apparent that benzene in this adsorption site adopts a triangular shape with three humps at each vertex of the triangle. These humps are believed to correspond to the three bright spots observed in the ESQC-based and EHT-based simulated STM images of benzene adsorbed on the hollow sites of Pt(111) [D1] and Pd(111) [D5] surfaces, respectively.

Figure D-2a displays a Pd(111) surface with benzene on a 2-fold bridge site and its simulated STM profile is presented in Figure D-2b. In this image and in this

adsorption site, benzene conforms an oval-shaped figure, which is quite similar to the form observed in the ESQC-based [D1] and EHT-based [D5] STM simulations.

The adsorption configuration of benzene chemisorbed on a top site on a Pd(111) surface is shown in Figure D-3a. Based on its DFT-based STM profile as presented in Figure D-3b, six humps or protrusions can be observed on the ring. This corresponds perfectly well with the six bright spots or lobes observed in the simulation on the Pt(111) surface using a similar adsorption structure [D3].

The dependence of the molecular STM image on the adsorption site originates from the specific interactions between the electronic states of the adsorbed molecule and those of the surface metal atoms directly below it. Individual adsorbate molecular orbitals will have varying contributions to the perturbation of the surface electronic structure at different adsorption sites since the symmetries of the orbitals and of the sites are different [D3].

The difference in the simulated STM profiles of benzene on various adsorption sites on a Pd(111) surface may be utilized to identify the molecule's site of adsorption on several experimental EC-STM images of Pd(111) single-crystal electrodes immersed in dilute solutions of benzene. Figure D-4 shows the EC-STM image of benzene on a Pd(111) electrode surface at an applied potential of 0.3 V. It is apparent that the molecule is composed of three spots since the fourth and faintest spot is considered to be due to a co-adsorbed water molecule [D6,D15]. Upon comparison of this STM image with those in Figures D-1-D-3, it is clear that at 0.3 V, benzene is chemisorbed on a 3-

fold hollow site as shown in Figure D-1a. This confirms the previous findings obtained earlier [D6].

Figure D-5 shows the EC-STM image of benzene on a Pd(111) surface held at 0.55 V. It is significant to note that in this STM image, the benzene molecule can be perceived as composed of two spots with one spot larger than the other to form a semi-triangular shape. Obviously, this does not correspond to any of the STM images in Figures D-1-D-3. However, when benzene is on a position between a 3-fold hollow and a 2-fold bridge site as shown in Figure D-6a, an STM profile that shows a wide and a narrow hill or lobe is obtained (Figure D-6b). This simulated STM profile clearly resembles the adsorbate images in Figure D-5. This validates the results proposed previously [D6].

CONCLUSION

Density functional theory was employed to simulate the STM images of benzene chemisorbed on various adsorption sites on a Pd(111) surface. The simulated profiles were compared with the experimental EC-STM images in order to verify the adsorption site of the aromatic molecule on the Pd(111) electrode surface at a certain applied potential. Theoretical results suggest that, at 0.3 V applied potential, benzene is chemisorbed on a 3-fold hollow site. At 0.55 V, the center of the ring lies on a location between a 3-fold hollow and a 2-fold bridge site. Results from this theoretical study confirm the interpretations made in an earlier published study.

ACKNOWLEDGMENT

The authors would like to express their gratitude to the Welch Foundation for financial support and to Dr. Lisa Perez and the Laboratory for Molecular Simulation (LMS) at Texas A&M University for the computational software.

REFERENCES

[D1] P. Sautet, M.-L. Bocquet, Phys. Rev. B 53 (1996) 4910.

[D2] P.S. Weiss, D.M. Eigler, Phys. Rev. Lett. 71 (1993) 3139.

[D3] P. Sautet, M.-L. Bocquet, Surf. Sci. 304 (1994) L445.

[D4] P. Sautet, Chem. Rev. 97 (1997) 1097.

[D5] D.N. Futaba, S. Chiang, Jpn. J. Appl. Phys. 38 (1999) 3809.

[D6] Y.-G. Kim, J.E. Soto, X. Chen, Y.S. Park, M.P. Soriaga, J. Electroanal. Chem. 554-555 (2003) 167.

[D7] S.J. Clark, M.D. Segall, C.J. Pickard, P.J. Hasnip, M.J. Probert, K. Refson, M.C. Payne, Z. Kristallogr. 220 (2005) 567.

[D8] C. Morin, D. Simon, P. Sautet, J. Phys. Chem. B 107 (2003) 2995.

[D9] A. Javier, D. Li, P.B. Balbuena, M.P. Soriaga, Electrocatal. 1 (2010) 159.

[D10] J.P. Perdew, K. Burke, M. Ernzehof, Phys. Rev. Lett. 77 (1996) 3865.

[D11] J.P. Perdew, Y. Wang, Phys. Rev. B 45 (1992) 13244.

[D12] C. Morin, D. Simon, P. Sautet, J. Phys. Chem. B 108 (2004) 5653.

[D13] J. Tersoff, D.R. Hamann, Phys. Rev. B 31 (1985) 805.

[D14] A.C. Javier, Y.-G. Kim, J.B. Soriaga, P.B. Balbuena, M.P. Soriaga, Phil. Sci. Letters 4 (2011) 18.

[D15] S.-L. Yau, Y.-G. Kim, K. Itaya, J. Am. Chem. Soc. 118 (1996) 7795.

FIGURES AND CAPTIONS

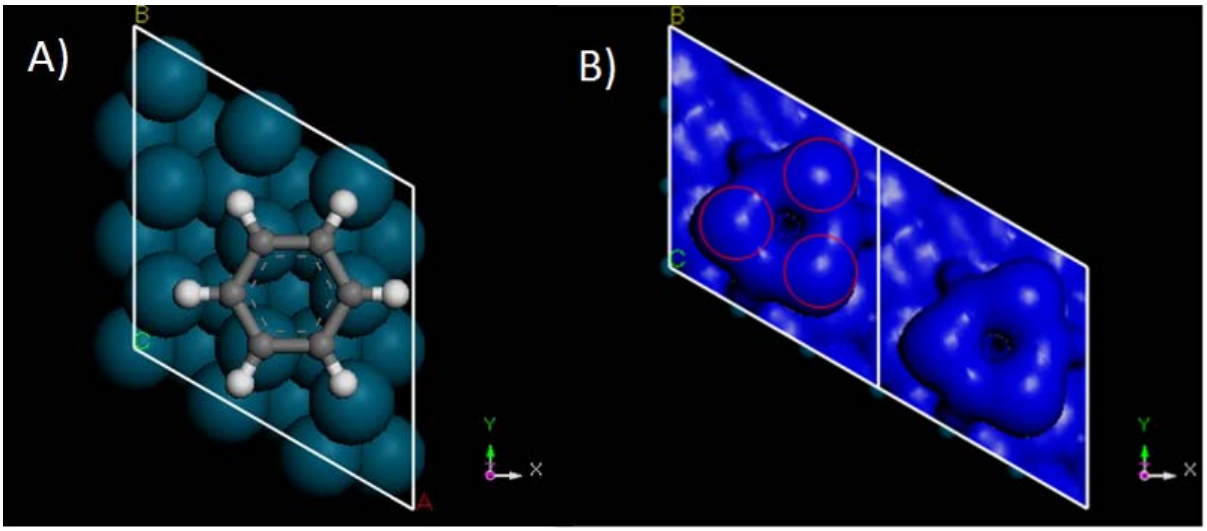

Figure D-1. (A) Adsorption geometry of benzene adsorbed on a 3-fold hollow site on a Pd(111) surface. (B) Simulated STM images of the surface in (A).

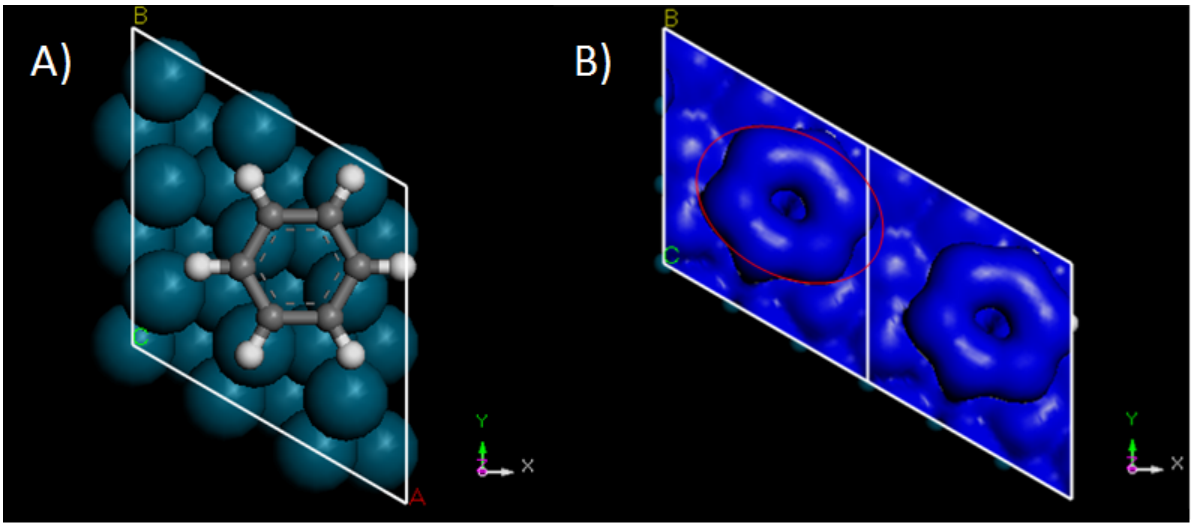

Figure D-2. (A) Adsorption geometry and (B) simulated STM images of benzene chemisorbed on a 2-fold bridge site on a Pd(111) surface.

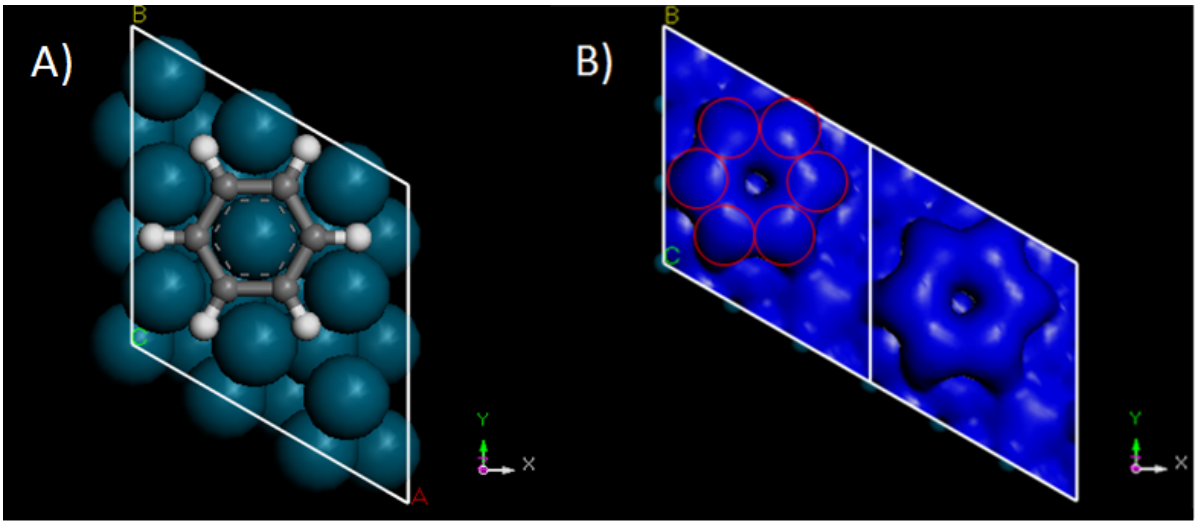

Figure D-3. (A) Adsorption configuration of benzene adsorbed on a top site on a Pd(111) surface. (B) Simulated STM images of the Pd(111) surface with benzene on a top site.

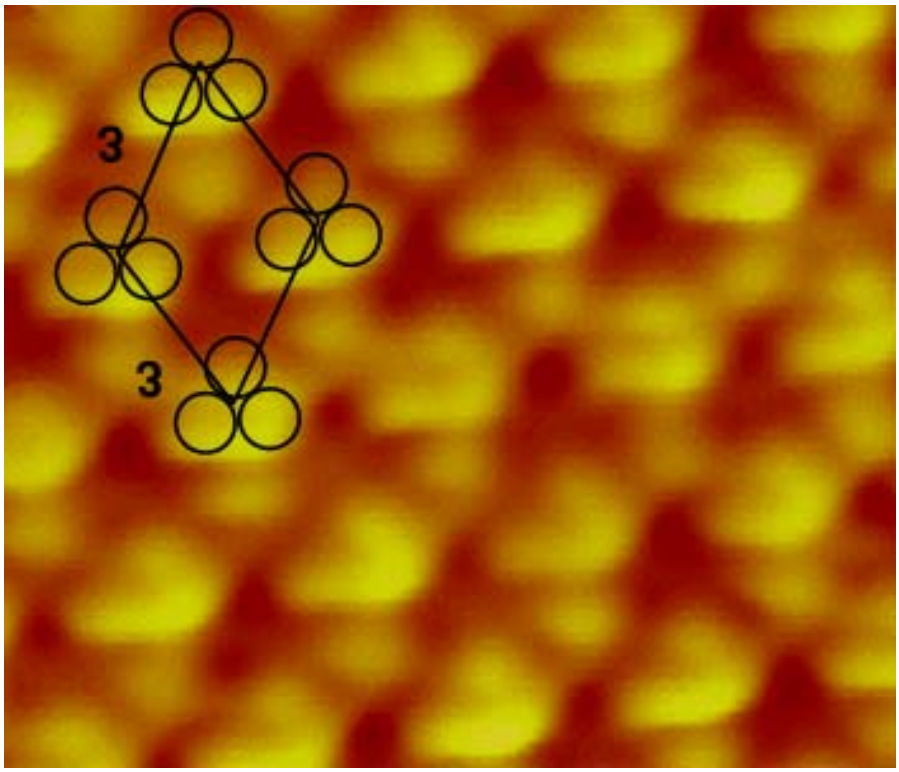

Figure D-4. High-resolution EC-STM image of the Pd(111)-(3 x 3)-C_6H_6 adlayer at 0.3 V. Bias voltage: 100 mV; tunneling current: 30 nA.

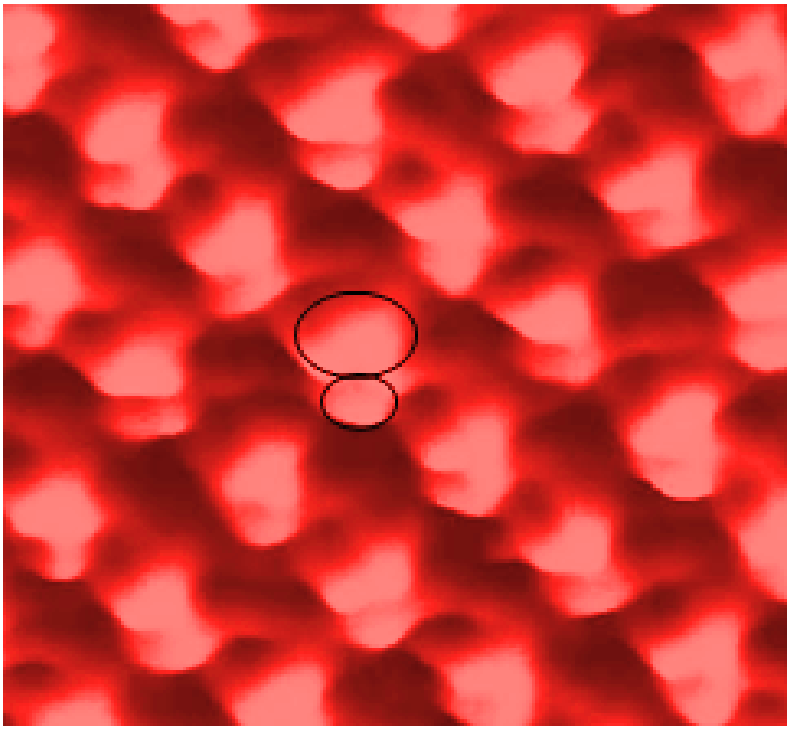

Figure D-5. High-resolution EC-STM image of the Pd(111)-c(2√3 x 3)-*rect*-C_6H_6 adlattice at 0.55 V. Bias voltage: 120 mV; tunneling current: 30 nA.

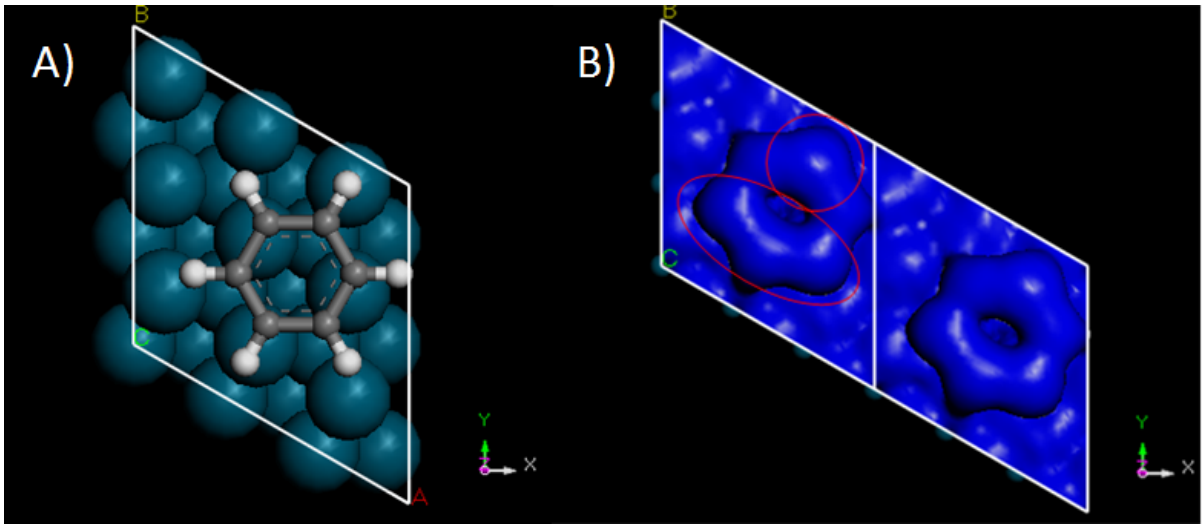

Figure D-6. (A) Adsorption geometry and (B) simulated STM images of benzene chemisorbed on a site between a 3-fold hollow and a 2-fold bridge site on a Pd(111) surface.